Journal of Materials Chemistry A

ROYAL SOCIETY OF CHEMISTRY

REVIEW

View Article Online
View Journal

Cite this: DOI: 10.1039/d6ta01248e

Direct recycling of lithium-ion battery materials: separation and regeneration

Jingjing Liu, Ruixin Wu, Junxiang Liu and Chengcheng Fang *

The rapid development of lithium-ion batteries (LIBs) has led to an urgent need for efficient recycling. Among current recycling strategies, direct recycling emerges as a promising alternative to conventional pyrometallurgy and hydrometallurgy, restoring valuable electrode materials while preserving the original crystal structure and minimizing energy consumption. However, direct recycling remains technically immature and faces challenges in practical cost, material purity, scalability, and process integration. This review summarizes recent advances in direct recycling of LIB active materials, following the workflow of disassembly, separation and regeneration, along with material degradation mechanisms. Various thermal, mechanical, and solvent-based separation methods are discussed in terms of their product size, efficiency, material compatibility, and cost. Regeneration methods, including solid-state sintering, solution-based, and molten salt regeneration, are discussed from their relithiation kinetics, processing conditions, upcycling strategies and electrochemical performance of restored materials. Finally, future perspectives are proposed to address current limitations towards scalable and cost-effective direct recycling technologies for sustainable LIB development.

Received 9th February 2026
Accepted 17th April 2026

DOI: 10.1039/d6ta01248e

rsc.li/materials-a

1 Introduction

The application of lithium-ion batteries (LIBs) has seen rapid growth in recent years. Global demand for LIBs is projected to rise from ~300 GWh in 2020 to ~2400 GWh by 2030, corresponding to an estimated production volume of 3 to 24 million tons (assuming 1 kWh ≈ 10 kg battery) (Fig. 1a).[1] Among them, ~12% of the batteries will reach the end-of-life (EOL) between 2025 and 2040, highlighting the urgent need for spent battery recycling.[2,3] With efficient recycling, cost savings could reach $2–15 per kg (of battery). While recycling can reduce greenhouse gas (GHG) emissions by over 50% overall, its benefits are strongly chemistry-dependent, with clear GHG reductions for Ni/Co-rich cathodes but little or no advantage for LFP (Fig. 1b).[1,4,5] However, the actual benefits are highly dependent

Department of Chemical Engineering and Materials Science, Michigan State University, East Lansing, Michigan, USA. E-mail: cfang@msu.edu

Jingjing Liu

Jingjing Liu is a PhD candidate in Materials Science and Engineering at Michigan State University, supervised by Dr Chengcheng Fang. She received her B.E. from Nanjing Tech University in 2019 and her M.E. from Southeast University in 2022. Her research focuses on advanced electrochemical energy systems, including energy storage materials, lithium-ion/metal batteries, fuel cells and advanced characterization techniques.

Ruixin Wu

Ruixin Wu is a PhD candidate in the Department of Mechanical, Aerospace, and Nuclear Engineering at Rensselaer Polytechnic Institute in Troy, USA. He previously worked as a research assistant at Michigan State University in East Lansing, USA, under the supervision of Prof. Chengcheng Fang. He received his M.Sc. in 2022 from the Hong Kong University of Science and Technology, Hong Kong, China. His research focuses on lithium metal anodes for solid-state batteries, interlayer design for anode-free solid-state batteries, solution-based synthesis of sulfide solid-state electrolytes, and the synthesis of sodium-ion battery cathode materials.

on recycling techniques and waste management during the recycling process. Maximizing both economic and environmental gains requires optimizing material recovery, reducing energy consumption, and controlling pollutants throughout the recycling workflow.

Various recycling techniques have been applied to restore battery materials, including pyrometallurgy, hydrometallurgy, and direct recycling.[6,7] Among them, hydrometallurgy and pyrometallurgy are the most widely commercialized. Hydrometallurgy soaks the electrode sheets in acid (sulfuric acid (H_2SO_4), hydrogen chloride (HCl)) and leaches the metal ions into soluble phase. The obtained solution undergoes several chemical precipitation reactions and sintering to restore the active materials.[8] Hydrometallurgical recycling can achieve a high yield ratio and product purity, but it generates substantial wastewater, necessitating additional treatment steps that increase overall processing costs.[9] Pyrometallurgy utilizes high temperature sintering to directly convert the entire electrode sheets into metallic alloys, which are then processed through hydrometallurgy to re-synthesize the materials. During the sintering, polymer binder and conductive agent decompose into gas, simplifying the operation of pyrometallurgical recycling but at the expense of high energy consumption, secondary pollution, and significant lithium (Li) loss.[10] In contrast, direct recycling recovers the incumbent materials while preserving the crystal structure,[11] thereby increasing recovery efficiency for both Li and transition metal (TM) (Fig. 1c). Furthermore, less energy is consumed compared with pyrometallurgy and hydrometallurgy, providing a promising direction to expand the manufacturing recycling market.

Direct recycling involves multiple steps (Fig. 1d) from EOL battery to recovered battery materials. The spent batteries are first fully discharged and dismantled to separate components such as shells, separators, cathodes, and anodes (electrolytes attached to these parts). Strong binder-induced adhesion between active materials and current collectors greatly hinders peeling efficiency and reduces material purity. Therefore, effective separation, including solid-state, mechanical, or chemical methods, is essential for deactivating these bonds and liberating active materials for subsequent regeneration. Among the active materials, cathodes are the most valuable component to regenerate due to the precious elements, including TM such as nickel (Ni), cobalt (Co), and manganese (Mn), as well as Li, which is particularly important in lithium iron phosphate ($LiFePO_4$, LFP). However, the complexity of cathode materials, resulted from their diverse compositions,[12] surface chemistries,[13,14] multi-scale degradation mechanisms,[15,16] poses significant challenges for recovering the crystal structure and crystallinity.[17] Thus, effective regeneration of spent cathode materials must address degradation across three distinct scales without sacrificing the original crystal structure: (1) atomic scale, involving issues such as cation mixing, anti-site defects, ion loss, and oxygen (O_2) evolution; (2) nanoscale, characterized by phase transitions, lattice distortions, and resistive interphases; (3) microscale, where mechanical degradation manifests as cracking, pulverization, and delamination. Overcoming these multiscale challenges requires regeneration strategies with thermodynamic-driven relithiation and cracked grain boundary migration, including solid-state sintering, solution-based and molten salt regeneration. During regeneration, lost ions are reintroduced into the lattice to repair atomic vacancies, while targeted thermal treatment promotes the migration and healing of cracked grain boundaries, thereby enhancing structural homogeneity and reducing interfacial resistance.

However, the commercialization of direct recycling remains challenging due to high costs, time-consuming manual dismantling, cathode heterogeneity, and low recovery yields

Junxiang Liu

Dr Junxiang Liu is a postdoctoral researcher in Argonne National Laboratory. He previously worked as a postdoctoral researcher at Michigan State University, under the supervision of Prof. Chengcheng Fang. He received his PhD from Nankai University and specializes in gaining a fundamental understanding of failure mechanisms and the rational design of electrode–electrolyte interfaces and interphases in rechargeable batteries. He is a recipient of the 2024 Argonne Impact Award and 2025 Outstanding Postdoctoral Performance Award.

Chengcheng Fang

Prof. Chengcheng Fang is an Assistant Professor in the Department of Chemical Engineering and Materials Science at Michigan State University. She received her PhD in Materials Science and Engineering from the University of California San Diego. Her research focuses on next-generation electrochemical energy storage, integrating advanced materials design, scalable manufacturing, and multiscale quantitative characterization across lithium/ sodium-based batteries, solid-state systems, liquid electrolytes, interfaces, and sustainable manufacturing. She is a recipient of the MIT Technology Review Innovators Under 35, the MSU Corporate Connector Award, and the Rising Star of Advanced Materials, recognizing her pioneering contributions and translational impact in battery technology.

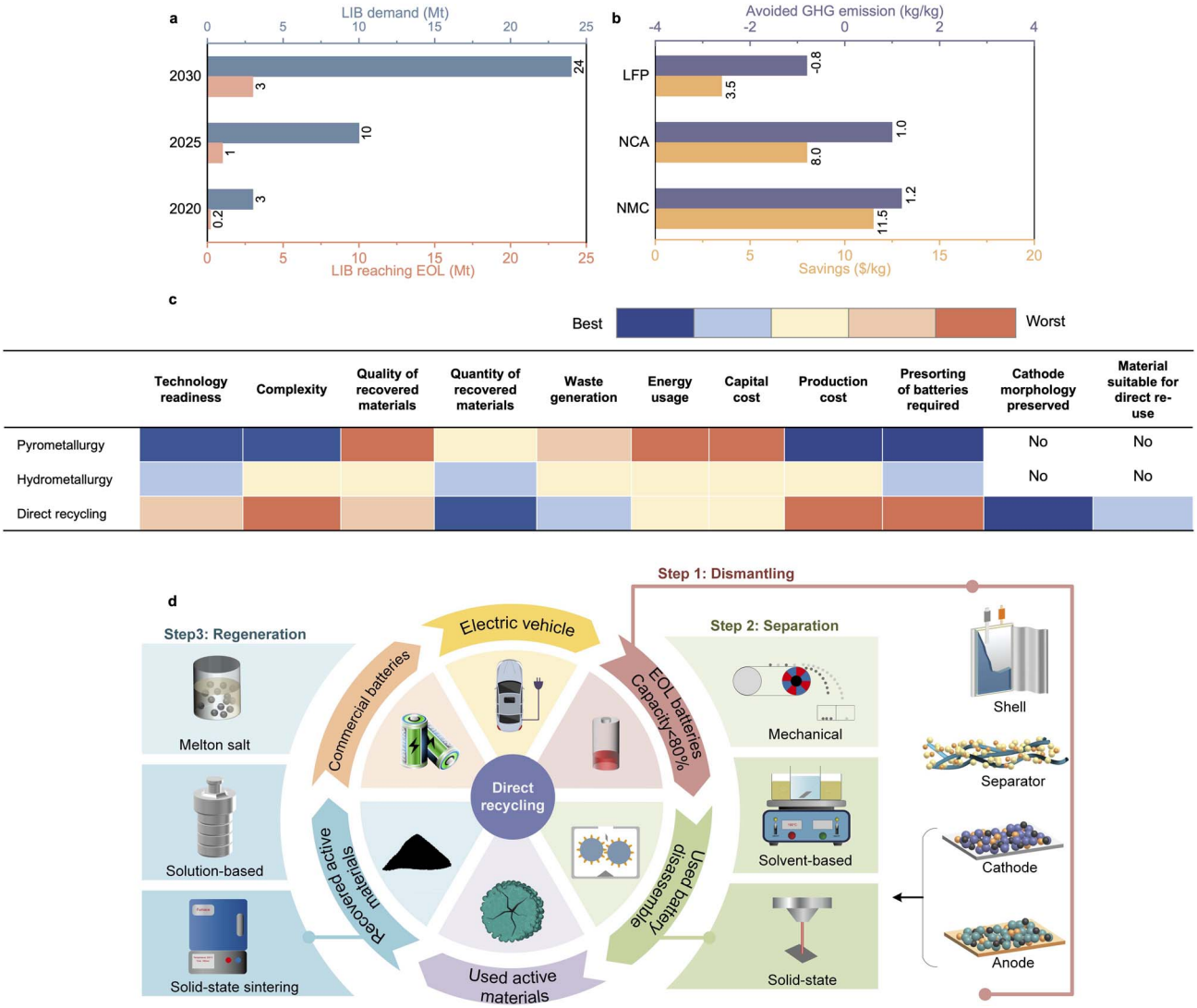

Fig. 1 (a) The projected LIB demand (Mt) and predicted LIB reaching EOL from 2020 to 2030.[1–3] (b) Savings ($ per kg) and avoided GHG emissions (kg kg^{-1}) by recycling NMC, nickel cobalt aluminum oxide (NCA), and LFP.[1,4,5] (c) The comparison among pyrometallurgy, hydrometallurgy, and direct cycling. Adapted from ref. 5. Copyright 2019 Springer Nature. (d) Illustration of the direct recycling workflow.

relative to material demand. In this review, we focus on recent advances in direct recycling following the workflow of direct recycling (Fig. 1d). We first systematically discuss separation methods based on their underlying mechanisms and evaluate them from peeling efficiency, separation rate, product purity, structural integrity, and cost. Next, we summarize various strategies for restoring the crystal structure of both cathode and anode materials. An in-depth analysis of failure mechanisms from a material perspective, covering lithium cobalt oxide ($LiCoO_2$, LCO), lithium nickel manganese cobalt oxides ($LiNi_xMn_yCo_{1-x-y}O_2$, $x+y+z=1$, NMC), and LFP, is performed, followed by a detailed study on their specific regeneration strategies, process optimization and upcycling approaches. Finally, we revisit the remaining challenges hindering the commercialization of direct recycling and provide an outlook to overcome them.

2 Active material separation

Efficient disassembly and separation are the foundation for a closed-loop, low-cost, and sustainable direct recycling, as they directly influence product purity, regeneration efficiency, and overall process cost. However, current separation processes are stepwise and heavily dependent on manual labor, resulting in low efficiency, reduced yield, and high operational costs.

Batteries at EOL will first be discharged for safety concerns and disassembled into four main parts: shell, separator, cathode, and anode.[18] Liquid electrolytes remain attached to these solid components and are then removed through volatilization at 0–200 °C.[19] Following electrolyte removal, the dried battery components are mechanically shredded and coarsely sorted by size to separate the electrode materials.[20] The mixture can contain diverse species due to the complex composition of electrode sheets, including active materials, conductive agents,

binders and current collectors. Conductive agents can enhance electronic conductivity while inducing additional impurities during recycling. Binders, typically polymer-based materials like polyvinylidene difluoride (PVDF), provide strong binder adhesion to firmly attach active materials to the current collector. This bonding yields an active material–aluminum (Al) interface shear strength nearly twice its tensile strength,[21] and the cathode–Al interfaces peel strength is about ten times that of anode–copper (Cu) interfaces.[22] Therefore, anode materials can easily be obtained by mechanical methods such as striking and pulverizing,[23,24] whereas cathode separation is far more challenging.[25] The crushed pieces are roughly categorized into three size ranges: fragments larger than 2 mm mainly consist of Al foils and separators; those between 0.5 mm and 2 mm include Al and Cu foils; particles smaller than 0.5 mm can be further milled, and those below 0.075 mm are considered as electrode materials containing metal oxides and graphite.[26,27] These fine particles undergo refined separation to improve material purity, which is critical for the further structural recovery of active materials.[28]

The process may remain impurities in the separated materials, such as electrolyte residues, conductive carbon, binder, current collector fragments, and mixed material phases, which hinder regeneration, introduce structural defects, and compromise the performance of recycled materials. The impact of impurities can be broadly categorized into three aspects. First, surface degradation, where impurities change the local reaction environment and disrupt surface stability. For example, residual graphite can create a reductive environment that counteracts the oxygen-rich conditions required for restoring layered cathodes (*e.g.*, LCO and NMC).[29] In LFP recovery, excess carbon may cause partial deoxygenation or dephosphatation, promoting Fe^0/Fe_2P secondary phases and lithium phosphate (Li_3PO_4) segregation.[30] In addition, PVDF decomposition may release hydrofluoric acid (HF), which further corrodes the cathode surface.[31] Second, compositional contamination, including Al/Cu fragments and cross-contamination between electrodes, can be incorporated into the lattice during high-temperature regeneration, inducing cation disorder and secondary phase formation. For example, Al impurities may form aluminum oxide (Al_2O_3), while Cu contamination above ~0.6 wt% can result in Li–Co–Cu–O phases and noticeable capacity degradation.[32,33] Third, non-uniform relithiation arises from residual electrolyte species and side reactions (*e.g.*, HF reacting with Li salts), which can form inorganic surface layers such as lithium fluoride (LiF). These layers impede Li^+ transport and lead to sluggish and spatially non-uniform relithiation.[34]

To address these challenges, effective impurity management is required throughout direct recycling, involving the coordinated strategies across three different stages. At the upstream stage, impurity introduction is minimized during disassembly and separation by improving delamination efficiency and limiting cross-contamination between cathode and anode materials. Advanced separation techniques, such as high-pressure water delamination, cryogenic treatment, and microwave-assisted processes, have been developed to achieve efficient material separation while reducing impurity incorporation.[35] At the midstream stage, purification treatments are often applied prior to regeneration to remove contaminants, including thermal pretreatment and solvent-based processes to decompose binders and eliminate residual organics, thereby improving material purity and accessibility for subsequent regeneration.[36] At the downstream stage, strategies are designed to tolerate or compensate for residual impurities during regeneration. For example, eutectic salt systems in molten salt regeneration can promote the *in situ* removal of Al impurities through selective dissolution or chemical conversion, thereby suppressing their incorporation into the cathode lattice.[37] The integration of stage-specific impurity management strategies is essential to balance impurity control, process complexity, and scalability in practical direct recycling. Among them, the effectiveness of separation processes becomes particularly critical, as they directly determine impurity levels and downstream regeneration outcomes.

Therefore, the primary goal of separation is to efficiently isolate high-value components while minimizing structural damage, manual handling, material loss, and processing cost. Numerous separation methods have been developed, yet a systematic summary remains limited. This section focuses on cathode separation techniques, categorized into solid-state, mechanical, and solvent-based methods based on their mechanisms (Fig. 2), and briefly evaluates each from peeling efficiency, separation rate, material purity, structural preservation, and cost.

2.1 Solid-state separation

Solid-state separation utilizes external intensive energy, such as heat and electrified field, to decompose or melt the PVDF. For thermal treatment, it is the most common and straightforward approach to deactivate PVDF, which has a melting point of 170–185 °C and decomposes above 350 °C. By sintering the pre-sorted powder at ~600 °C for 5 hours, PVDF and conductive carbon are decomposed and gasified,[38] leaving pure active material. However, under a long-time heat treatment, the cathode active material may have Li volatilization[39] and irreversible crystal structure distortion.[40,41] Moreover, PVDF may release HF gas during decomposition and react with hydroxyl on metal oxide surface,[31] inducing other impurities. Addressing these issues requires sintering aids to lower the reaction temperature and mitigate fluorine (F)-related impurities. For example, Wang *et al.*[42] employed calcium oxide (CaO) as the reaction medium to lower PVDF decomposition temperature to 300 °C. During sintering, CaO acted as a heat reservoir and neutralized acidic hydrogen atoms in PVDF, preventing *in situ* fluorination reactions. Thus, the formation of C–F bonds further facilitated PVDF decomposition at reduced temperatures. Ross *et al.*[43] reported that excess lithium hydroxide monohydrate ($LiOH \cdot H_2O$) as Li source can react with F released from PVDF to form stable phases such as LiF, thereby neutralizing harmful F-related byproducts and simultaneously relithiating the cathode material during sintering. Wang *et al.*[44] utilized aluminum chloride–sodium chloride ($AlCl_3$–NaCl) molten salt as the reaction medium which can achieve

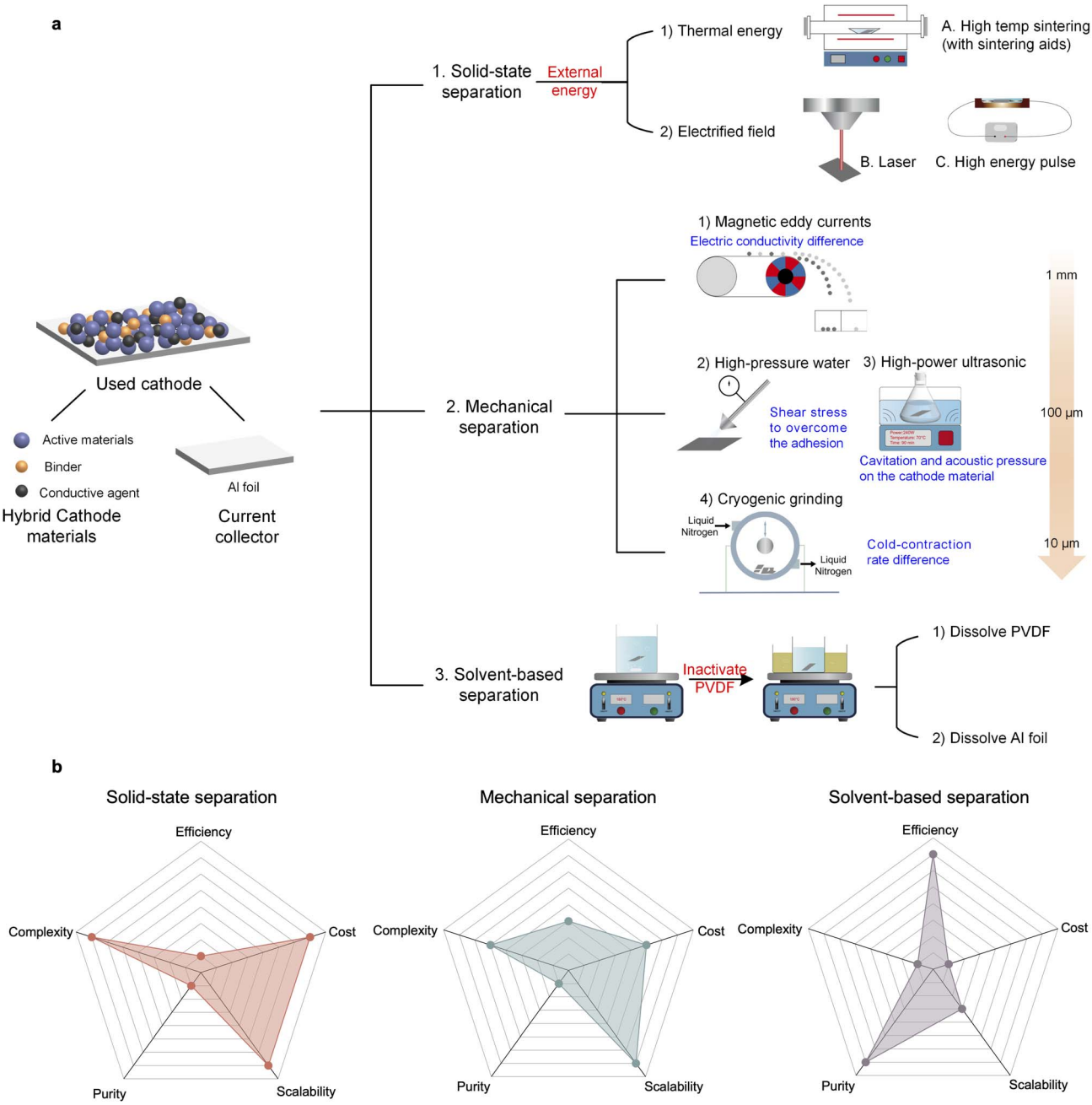

Fig. 2 Cathode material separation methods. (a) Used cathode consists of cathode materials and Al foil. The cathode materials need to be separated from Al foil before further regeneration. The cathode material separation methods can be classified into mechanical separation, solvent-based separation, and solid-state separation based on their working mechanism. (b) Comparison of the three separation methods in the metrics of efficiency, cost, scalability, purity and complexity.

a separation temperature as low as 160 °C, benefiting from high heat storage during phase transitions. Optimal peeling conditions at 160 °C for 20 minutes resulted in a 99.8 wt% removal of cathode materials. Currently, pyrolysis pretreatment is often the initial step in separation due to its convenience and effectiveness to disable PVDF, typically combined with other mechanical or chemical methods to enhance separation efficiency.[45]

For assistive electrified field, it can also provide intensive energy to delaminate the cathode materials. Gao *et al.*[46] demonstrated that a 15 watt laser can strip LCO cathodes by instantaneously decomposing or volatilizing PVDF and conductive carbon with a separation efficiency of 92.16%, resulting in high-purity regenerated cathode materials. However, it may induce severe Li loss and convert LCO into cobalt oxide (Co_3O_4) through localized heating, necessitating further relithiation. High-voltage pulsed discharge is another advanced technique. Tokoro *et al.*[47] applied pulsed energy to generate high-temperature plasma and shock waves that

decomposed PVDF and reduced adhesion *via* Joule heating of the Al foil at 19.0 kA and 25 kV, achieving a 93.9% separation efficiency. A limitation of this method is localized melting of Al, causing at least 2.95% Al contamination.

Most solid-state separation techniques can effectively decompose PVDF and conductive carbon, achieving high separation efficiencies. They are relatively simple to operate without advanced equipment. Nonetheless, the complete removal of PVDF and conductive carbon from cathodes remains challenging, limiting material purity. Furthermore, precise control of reaction conditions is essential, as excessive energy input can damage the cathode crystal structure or cause additional Li loss.

2.2 Mechanical separation

Mechanical separation first uses mechanical force to split cathode materials from the current collector and then separates PVDF and active materials according to their intrinsic properties, such as density, strain, and electronic conductivity.[48] The traditional method of grinding the cathodes into small pieces is typically followed by separation techniques such as magnetic eddy currents or forth flotation,[26,49] particularly in large-scale recycling. For the magnetic eddy current method, it works based on the electrical conductivity differences between organic binders and various nonferrous metals (mainly Al foils and electrode material).[50] As metallic particles move along a conveyor through a time-varying magnetic field, eddy currents are induced within them. The magnitude of these currents depends on the conductivity of each material[51] and force particles to move in different trajectories, which can be influenced by factors such as detachment angle, feed rate, and the speed of the magnetic roller.[52,53] Magnetic eddy current method offers a high separation rate and low cost for fragments smaller than 0.25 mm. However, it achieves a relatively modest separation efficiency of ~90%, with material purity remaining ~85%.[54]

Froth flotation is usually used to remove the graphite phase from coarsely separated materials.[55,56] After grinding, a fine fraction (−0.075 mm) of the mixed LIB particles enables high-purity graphite and cathode active materials.[26,27] Froth flotation can be subsequently applied to separate these components based on their differences in hydrophobicity.[57] The bubbles generated by flotation agents act as carriers to absorb hydrophobic graphite particles at the solid–liquid–gas interface, separating them from the more hydrophilic cathode materials. Although froth flotation achieves high separation efficiency, it is typically combined with other separation techniques due to limitations to separable species. Moreover, binders can hinder flotation by causing partial floatability of cathode materials thus decreasing the purity,[56] which can be improved by a pyrolysis pretreatment prior to flotation. For example, Li *et al.*[57] introduced a roasting flotation to enrich the metal content in the concentrate. Roasting at 500 °C for 1 hour optimally increased the enrichment ratio while preventing graphite oxidation. Besides the roasting flotation,[58] other strategies like Fenton reagent-assisted flotation[59,60] and grinding flotation[61–63] can also robust the separation efficiency. Despite its low cost and recent advancements achieving separation efficiencies over 95%, froth flotation inherently suffers from fine particle entrainment by bubbles, which remains a limiting factor for further improvement.[64]

Low-temperature treatments can also accelerate the exfoliation process. Immersing the grinded cathode in liquid nitrogen (N_2) can induce cracks due to different cold-contraction rates between cathode materials and Al foil. Moreover, PVDF exhibits significant stiffening at around −40 °C,[65,66] resulting in brittle behavior and weakening the bonding between cathode materials and the Al foil. Cryogenic grinding has demonstrated impressive peel-off rates. Wang *et al.*[67] pretreated cathode materials in liquid N_2 for 5 minutes, followed by cryogenic ball milling, achieving a peel-off efficiency of 87.29% within just 30 seconds of grinding. To further enhance separation efficiency, Liu *et al.*[66,68] combined cryogenic grinding with froth flotation, achieving a separation efficiency of 89.83% after 9 minutes of grinding. Cryogenic grinding clearly enables rapid and efficient separation, while the high cost of maintaining the low operating temperature (~235 K) poses a significant barrier to large-scale application.[69]

The separation methods discussed above all involve grinding and blending of spent electrode sheets, leading to the destruction of Al foil and impurities into the cathode material. To maximize the purity of recycled cathode materials, emerging techniques focus on binder deactivation while preserving the integrity of the Al foil. For example, Ji *et al.*[70] introduced a pressure washing system without involving chemical reagents or heat treatment, in which high-pressure water delivered through a nozzle generated significant shear stress that can break PVDF adhesion and achieve efficient separation in a short processing time (~74 min m^{-3}) with peel-off efficiency exceeding 90%. The process produces no secondary waste solution, but the high-pressure water can penetrate and damage the Al current collector, thereby increasing the risk of Al impurity.[69] Instead of intense mechanical force, ultrasonic treatment offers a mild approach that avoids Al foil chipping. He *et al.*[71] demonstrated that high-power ultrasound induced cavitation and acoustic pressure on the cathode surface. During the rarefaction stage, negative pressure in the solvent generated numerous microbubbles, facilitating the detachment of cathode material. Under the control of suitable temperature, solution, ultrasonic power, ultrasonic time, the peel-off efficiency can be up to ~99%. However, the separation efficiency significantly decreased below 90% at less than 70 °C or short ultra-sonic duration.

Mechanical separation methods can achieve efficient separation within a relatively short time. Most mechanical methods generate minor secondary pollution, and they are low-cost and easy to operate. Therefore, mechanical separation is a highly promising approach for large-scale recycling and mass production. However, a major limitation is the relatively lower purity of recovered materials, as Al foil fragments and anode active materials can mix with the cathode active materials.

2.3 Solvent-based separation

Solvent-based separation has been widely employed to separate cathode active materials by dissolving either the binder or the current collector in a suitable solvent without damaging cathode active materials. *N*-Methyl-2-pyrrolidone (NMP) is the commonly used solvent for binder removal, which is chemically stable with PVDF and allows reuse due to its strong dissolving capacity.[72] However, the separation efficiency is only ~90%, which is still insufficient for large-scale applications. To improve the separation efficiency of NMP, He *et al.*[71] introduced ultrasonic agitation and heating to the NMP dissolving process, generating bubbles that peel off cathode materials, raising the separation efficiency to ~99%. Another major issue of NMP remains its intrinsic toxicity,[73] making it less environmentally friendly. Ethylene glycol (EG), a widely used chemical in anti-freeze and polymer precursor,[74,75] has been used as a green and mild solvent for PVDF. EG can overcome the strong van der Waals forces of PVDF and efficiently disrupt the hydrogen bonds between PVDF and Al foil.[76] However, the peeling-off rate is limited by the low solubility and the high viscosity of EG, requiring longer treatment times or elevated temperatures to enable rapid exfoliation.[77,78] Besides NMP and EG, other organic solvents have been developed to achieve efficient separation,[79] such as *N*,*N*-dimethylacetamide (DMAC),[80] *N*,*N*-dimethylformamide (DMF),[81] dimethyl sulfoxide (DMSO)[82] and ethanol.[83] Among them, DMAC has demonstrated the highest efficiency in dissolving PVDF.[84] Although most organic solvents are green and non-toxic, their costs are much higher than inorganic solutions. Furthermore, additional reducing agents or external assistance, such as high-temperature treatment or mechanochemical activation, are often required to ensure high separation efficiency and peeling rates.[85,86]

In hydrometallurgical processes, deep eutectic solvents (DES) are gradually replacing the traditional leaching acid of a mixture of H_2SO_4 and hydrogen peroxide (H_2O_2) for safer, cleaner, and more controlled recycling processes.[75,87,88] DES are homogeneous systems formed by mixing a hydrogen bond donor (HBD) with a hydrogen bond acceptor (HBA),[89] combining the advantages of both organic and inorganic solvents. A commonly used DES is a mixture of choline chloride (ChCl) as HBA and EG as the HBD, which simultaneously dissolves metal ions and binders, necessitating subsequent active material re-synthesis *via* precipitation or electrodeposition.[90–93] Recent studies highlight the potential to optimize the composition, mole ratio and leaching conditions of the DES for selectively deactivating PVDF without attacking the active materials.[90,94,95] For example, Wang *et al.*[95] achieved a peeling efficiency of ~99.86% using a DES composed of ChCl and glycerol (molar ratio 2.3 : 1) at 190 °C for 15 minutes. The DES generates multiple hydrogen bonds that stabilize the solvent, while $[Cl]^-$ and other hydrogen-donating groups interact with the $-CH_2$ and $-CF_2$ groups of PVDF. These interactions weaken the C–F bonds, promoting their oxidation into hydroxyl or carbonyl groups, thereby deactivating PVDF and facilitating efficient material separation. Also, X-ray diffraction (XRD) showed no significant changes in the NMC crystal structure before and after DES treatment, confirming that the DES did not damage the cathode material. Optimized DES can selectively deactivate PVDF, enabling efficient separation of cathode materials from Al foil under mild and environmentally friendly conditions. However, achieving high selectivity without dissolving TM oxides remains challenging, requiring precise control of DES composition and process parameters.

Besides dissolving PVDF, dissolving Al foil is another approach to liberate cathode materials as Al foil readily dissolves in strong alkali.[96–98] Senćanski *et al.*[96] demonstrated that boiled 5 M sodium hydroxide (NaOH) solution can dissolve the Al current collector within 30 minutes, achieving a peeling-off rate twice that of NMP leaching and a yield ratio of ~100%. Also, the byproduct sodium aluminate ($NaAlO_2$) in the NaOH solution can be further processed to recover Al metal through precipitation. Kong *et al.*[99] investigated the effects of operating conditions on the dissolution rate and found that ultrasonic power (288 W) significantly reduced the required NaOH concentration to 10 wt% at 30 °C. However, an additional sintering step is necessary to completely remove residual PVDF and conductive carbon from the solid residue.

The solvent-based separation method is relatively simple and mild with high separation efficiency. Most solvents can operate separation under room-temperature (RT), reducing energy consumption, and can be reused across multiple cycles without complex equipment, making the process economical. Moreover, most solvents can directly deactivate PVDF, preventing HF generation and F diffusion into cathode active materials during subsequent regeneration. However, solvent-based separation may cause secondary pollution and organic solvent residue even after multiple washing.[28]

Overall, solid-state, mechanical, and solvent-based separation differ in efficiency, cost, and scalability (Fig. 2b). Solid-state methods are simple and scalable but limited in efficiency and impurity control. Mechanical methods are cost-effective and suitable for large-scale processing but often require additional purification. Solvent-based approaches provide higher selectivity and purity but involve higher cost and more complex processing. In practice, different methods are often combined and applied at different stages of the separation to optimize the process.

3 Cathode active material regeneration

Cathode active materials degrade across multiscale during electrochemical cycling. Therefore, cathode active material regeneration is the pivotal step in direct recycling to replenish ion disorder (atomic level), recover phases (nm level) and repair morphology (μm level). In this context, three commonly used terms in battery recycling literature refer to distinct processes. Relithiation refers to the replenishment of Li loss during cycling, aiming to restore the Li stoichiometry. Reconstruction describes the recovery towards the original crystal structure by reversing phase transitions or disorder. Regeneration represents a broader concept that encompasses the recovery of overall electrochemical performance by addressing degradation

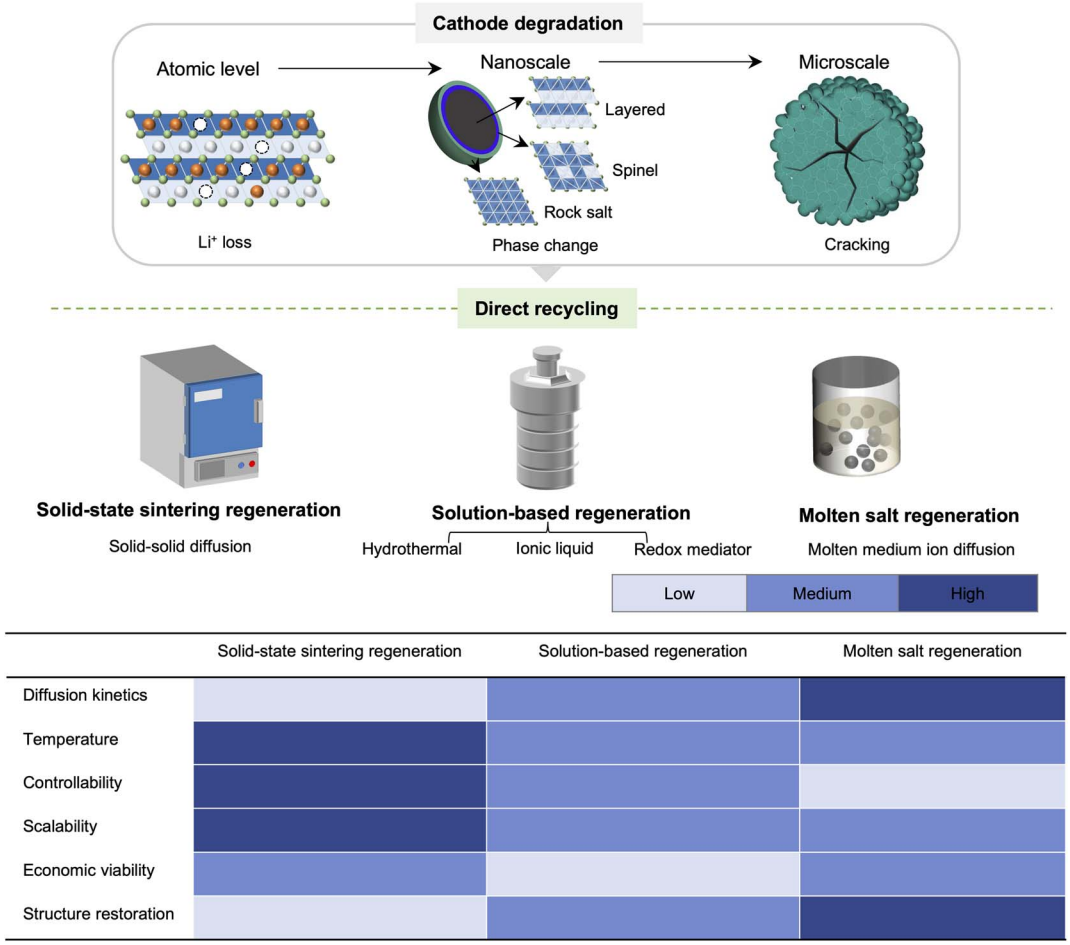

Fig. 3 Multiscale degradation of cathode materials and direct recycling strategies for regeneration. Cathode active materials degrade through structural and chemical changes at atomic, nano, and micron scales over cycling. To restore electrochemical performance, direct recycling approaches aim to replenish the Li loss, reconstruct the crystal structure and repair the morphology. Three regeneration approaches, solid-state sintering, solution-based, and molten salt, are compared based on key metrics including diffusion kinetics, temperature, controllability, scalability, economic viability, and structure restoration.

across multiple scales, including relithiation and reconstruction.

Solid-state sintering, solution-based and molten salt regeneration are three main strategies for cathode materials direct recycling (Fig. 3). This section focuses on LCO, NMC, and LFP, covering their failure mechanisms, regeneration mechanisms, condition optimization, upcycling approaches, as well as their respective advantages, limitations, and future outlooks.

3.1 Cathode failure mechanisms

3.1.1 $LiCoO_2$. LCO is one of the most widely used cathode materials in LIBs since it was proposed in 1981.[100,101] LCO crystallizes in an α-$NaFeO_2$-type layered structure (space group $R3m$), where Li and Co atoms are coordinated with oxygen to form edge-sharing LiO_6 and CoO_6 octahedra, providing a theoretical capacity of 274 mAh g^{-1}.[102] However, its practical capacity is limited to ~140 mAh g^{-1} due to the charging voltage constraint required to suppress Co dissolution.[103] The overall electrochemical reaction of LCO is described in (eqn (1)). During charging, Li^+ is progressively extracted from the lithium layers, inducing phase transformation from the initial hexagonal structure through H1, H2, M1 (monoclinic), H3, M2, and finally to the O1 (orthorhombic) phase.[104]

$$LiCoO_2 \rightleftharpoons Li_{1-x}CoO_2 + xLi^+ + xe^- \quad (1)$$

LCO has an anisotropic lattice contraction along the c-axis during delithiation, with charge compensation by the Co^{3+}/Co^{4+} redox couple.[105] The increased electronic repulsion between adjacent Co layers distorts the CoO_6 octahedra, reducing the thermodynamic stability of the lattice and weakening Co–O bonds.[106] Under high voltage (>4.4 V), further oxidation of Co beyond Co^{4+} becomes thermodynamically unfavorable, leading to partial oxidation of lattice oxygen (O) into O_2 and further destabilization of the structure.[107] Simultaneously, the local structural rearrangements, O deficiency, and interfacial side reactions can reduce nearby Co^{4+} into Co^{2+}, facilitating lattice gliding and migration into Li layers. This Li/Co cation mixing further promotes the formation of Co_3O_4-type spinel phase,

which imposes a higher energy barrier for Li^+ diffusion, hindering its reinsertion and resulting in Li loss.[108]

Such irreversible Li loss during cycling can lead to the overlap of Co t_{2g} and O 2p energy levels, promoting cathode electrolyte interphase (CEI) formation through electrolyte decomposition driven by surface Co^{2+}.[109] The electrolyte further reacts with the cathode surface, particularly at high voltages, forming a resistive CEI layer that consumes Li^+. Also, electrolyte oxidation at high voltages can generate HF, accelerating Co dissolution.[110]

The anisotropic lattice strain induced by CoO_6 octahedra distortion leads to particle fracture and microcrack formation,[105] exposing fresh LCO surfaces to the electrolyte, enhancing parasitic reactions and increasing interfacial impedance.[111] Furthermore, crack propagation causes loss of electronic contact and disrupts Li^+ transport pathways within particles, ultimately degrading material.

To enable effective direct recycling of LCO, regeneration strategies should focus on restoring Li stoichiometry, repairing structural distortions, and suppressing Co dissolution. Relithiation, oxygen replenishment, and surface reconstruction coatings can help recover lattice integrity and mitigate CEI-related resistance.

3.1.2 $LiNi_xMn_yCo_{1-x-y}O_2$. Even though NMC has the same O3-type crystal structure as LCO, it is more complex due to multiple redox pairs of Ni, Mn and Co. The reaction formula is shown in (eqn (2)). The Co is partially substituted with other TM, composing common compositions of $LiNi_{0.33}Mn_{0.33}Co_{0.33}O_2$ (NCM111), $LiNi_{0.5}Mn_{0.3}Co_{0.2}O_2$ (NMC532), $LiNi_{0.6}Mn_{0.2}Co_{0.2}O_2$ (NMC622), and $LiNi_{0.8}Mn_{0.1}Co_{0.1}O_2$ (NMC811).[112] Increasing the Ni content enhances the specific capacity and energy density due to the more Ni^{2+}/Ni^{4+} redox couples. However, higher Ni concentrations reduce structural and thermal stability,[113] as Ni-rich materials are more prone to cation mixing (Li/Ni disorder), O_2 release and microcracking under high-voltage operation.

$$LiTMO_2 \rightleftharpoons Li_{1-x}TMO_2 + xLi^+ + xe^- \quad (2)$$

NMC is a layered structure with Li layers in 3a sites and TM layers in 3b sites stack-up.[114] Multiple TM redox reactions are involved during delithiation, resulting in heterogeneous phase transitions from the initial H1 phase to intermediate hexagonal phases with different oxygen arrangements (H2 and H3), and eventually to a non-layered M phase.[115] These transitions induce anisotropic lattice shrinkage, leading to the accumulation of microstrain.[116] A higher Ni content further amplifies lattice volume changes during cycling, generating increased internal stress that eventually promotes crack formation.[113] Moreover, Ni^{4+}–O bonds are thermodynamically unstable and tend to undergo reduction to the more stable Ni^{2+} state, accompanied by lattice O_2 release.[117] The resultant Ni^{2+} can easily migrate from the crystallographic TM layer (3b sites) into the Li^+ layer (3a sites) due to the similar atomic radius of Ni^{2+} (0.69 Å) and Li^+ (0.76 Å),[118] leading to cation mixing.

The cation mixing causes irreversible Li loss, reduces the Li^+ mobility, and leads to the crystal structure collapse from layer to spinel and ultimately to a completely disordered rock-salt phase.[119,120] Meanwhile, Ni-rich cathodes exhibit poor surface stability due to their electronic structure. The t_{2g} orbitals of Ni and Mn lie closer in energy to the O 2p band than those of Co, resulting in stronger TM–O orbital hybridization and higher covalency.[121] This facilitates the generation of reactive O species, which readily react with electrolyte and result in the formation of a resistive CEI, gas evolution, and dissolution of TM.[122]

Compared to single crystal LCO cathodes with micron level particles, polycrystal NMC consists of secondary particles formed from nanosized primary crystallites. Heterogeneous phases and anisotropic microstrain make NMC more susceptible to mechanical degradation. The accumulated strain initiates microcracks in the core of primary crystallites, and then propagates across neighboring particles, leading to secondary particle cracking, particularly at high voltage.[115] Also, the higher surface area of polycrystalline NMC increases its exposure to the electrolyte and promotes parasitic reactions. Consequently, single-crystalline NMC with long-range, ordered atomic arrangement, has emerged as a more favorable cathode material in recent research.[123]

Direct recycling of NMC should target the recovery of Li content, minimization of cation mixing, and reconstruction of the layered structure degraded by Ni migration and O loss. Controlled relithiation, high-temperature phase healing, surface re-coating and morphology upcycling are essential to restore electrochemical activity and long-term cycling stability.

3.1.3 $LiFePO_4$. LFP was first introduced in 1996 and is widely used for its excellent thermal stability, long cycle life, and safety.[124] LFP has an orthorhombic crystal structure composed of alternating layers of FeO_6 octahedra and PO_4 tetrahedra, featuring a 1D pathway for Li^+ diffusion along the [010] direction. During delithiation, the Fe^{2+}/Fe^{3+} redox is triggered with single phase transition to iron phosphate ($FePO_4$), leading to a volume change of ~7% due to the same olivine structure of LFP and $FePO_4$. The reaction is:

$$LiFePO_4 \rightleftharpoons Li_{1-x}FePO_4 + xLi^+ + xe^- \quad (3)$$

The two-phase reaction between LFP and $FePO_4$ induces spatially anisotropic phase transformations, generating local lattice strain and transient Li vacancies during cycling. Thus, Fe^{2+} from adjacent FeO_6 octahedra can migrate into the vacant Li sites within the 1D diffusion channels, owing to similar ionic radius of Fe^{2+} (0.76 Å) and Li^+ (0.74 Å).[125] This cation migration is thermodynamically favorable as accumulated structural defects and non-uniform local phase lower the energy barrier for Li–iron (Fe) site exchange (~0.7 eV).[126] The resulting Li–Fe antisite defects partially obstruct Li^+ diffusion pathways, reduce Li^+ mobility, distort the crystal structure and progressively degrade the electrochemical performance of the cathode.

Simultaneously, HF produced from parasitic electrolyte decomposition reactions can dissolve Fe^{2+} into the electrolyte. The dissolved Fe^{2+} can migrate toward the anode, destabilizing the solid electrolyte interphase (SEI) and further depleting reversible Li. At the microscale, heterogeneous phase transition

of LFP and $FePO_4$ accumulate mechanical stress despite the small volume change during cycling, eventually leading to particle cracking, decreased interfacial kinetics, and disrupted Li^+ migration.[127]

Therefore, direct recycling of LFP should address Li–Fe antisite defect removal, Li replenishment, and reactivation of isolated particles caused by Fe migration and mechanical cracking. Thermal or chemical treatments in reductive atmosphere combined with surface modifications can repair Li^+ diffusion channels and restore electronic percolation for improved LFP performance.

3.2 Cathode material regeneration

3.2.1 Solid-state sintering regeneration. Solid-state sintering regeneration is a straightforward method to recycle spent cathode materials through intensive thermal energy. The degraded cathode materials are homogenously mixed with Li sources such as LiOH, lithium carbonate (Li_2CO_3), and the mixture is treated at high temperatures under a controlled atmosphere to compensate for the Li loss, recover the crystal structure, and repair surface cracks. However, this method is relatively coarse and difficult to precisely control the chemical stoichiometry and particle morphology.

3.2.1.1 Process optimization. Numerous studies have been conducted to optimize the solid-state sintering process, aiming to enhance lithiation efficiency, achieve more precise control over the particle properties, eventually improve the electrochemical performance of regenerated cathodes.

3.2.1.1.1 LCO. Nie *et al.*[128] investigated the effects of sintering temperature on the crystal structure of LCO. They found that regeneration at 800–950 °C eliminated Co_3O_4 impurities in spent LCO and facilitated the LCO layered structure, improving Li^+ intercalation and electrochemical properties as I_{003}/I_{104} increased. 900 °C was identified as the optimized sintering temperature since it showed the lowest cation mixing level. However, the crystal structure deteriorated when the regeneration temperature was further raised to 950 °C due to the Li dissolution. Chen *et al.*[32] studied the impacts of Li source amount on recycled LCO structure and cell performance. They revealed that the Co_3O_4 impurities disappeared until the Li/Co ratio was beyond 1.0, and the optimized ratio was 1.0–1.2. The possible reason is that when the Li/Co ratio is below 1, insufficient Li hinders the complete reaction with Co_3O_4 to produce LCO; conversely, when the ratio exceeds 1.2, excess Li remains as inactive residue in the cathode material, compromising the electrochemical performance. Additionally, they examined the effects of Al and Cu contamination and identified the critical concentration of Cu < 0.6 wt% and Al < 0.4 wt% to ensure an optimized cycling performance.

3.2.1.1.2 NMC. Meng *et al.*[129] regenerated NMC111 with a mechanochemical activation process before the solid-state sintering. 20% excessive Li_2CO_3 was mixed with spent NMC111 and then put into intensive ball milling. Ball milling at 500 rpm for 4 hours effectively reduced the particle size, shortened the diffusion path, and facilitated Li^+ diffusion during the sintering at 800 °C. This process resulted in a smaller Li/TM mixing ratio and a more ordered layered crystal structure (Fig. 4a). Montoya *et al.*[130] proposed a two-step sintering approach for NMC111 recycling, enabling Li source activation while mitigating insufficient sintering time or temperature. The cathode was regenerated through a two-step lithiation process at 350 °C for 4 hours followed by 650 °C for 4 hours, demonstrating an improved discharge capacity compared to a single-step annealing process at 650 °C for 8 hours. They claimed that single-step heating led to inadequate relithiation or structural degradation, while multi-stage processes enhance material homogeneity by optimizing Li activation and integration. The two-step annealing NMC111 exhibited a discharge capacity of 154 mAh g^{-1} at C/3, which was higher than that of the one-step annealing sample and comparable to the pristine NMC111. For Ni-rich layered structure recovery, oxygen partial pressure plays a crucial role in restoring the crystal structure. Shi *et al.*[131] demonstrated that the NMC111 samples recycled in air and pure oxygen had similar Li/Ni cation mixing. However, for NMC532, the sample sintered in air had higher cation mixing than that in oxygen, indicating that low oxygen partial pressure hindered the conversion of the rock-salt and spinel phase to the layered structure, preventing effective lithiation and promoting TM migration.

3.2.1.1.3 LFP. Song *et al.*[132] recovered LFP from the mixture with fresh LFP. The impurities of $FePO_4$, iron oxides (FeO and Fe_3O_4) were detected from the spent LFP, and they disappeared when sintering temperature increased to 700 °C. However, when the temperature increased to 800 °C, LiF peaks appeared alongside the main LFP phase, primarily due to the generation of HF from the incomplete decomposition of PVDF during separation. Also, excessive fresh LFP can improve the crystallization of $FePO_4$ and ferric oxide (Fe_2O_3), eliminating impurity phases and inhibiting PVDF decomposition. Except for sintering temperature control, another method to prevent HF is to completely pyrolyze PVDF before the Li supplementary. Liang *et al.*[133] applied the preheat on spent LFP at 450 °C for 2 hours before regeneration. The Fourier transform infrared spectroscopy (FTIR) revealed that the peaks corresponded to the CF_2 stretching vibration of PVDF disappeared after heat treatment, while the main peaks of LFP were stable, indicating successful pyrolysis of PVDF and preservation of LFP olivine structure.

3.2.1.2 Single crystal. For particle size control, single crystal materials have become a prominent focus of current research. Conventional polycrystalline cathodes are prone to structural degradation and cracking as charged to high voltage, leading to capacity fading and reduced battery lifespan.[134] Single crystal cathodes, characterized by the absence of grain boundaries, exhibit enhanced structural integrity and improved cycling stability. Thus, more studies focus on single crystal cathodes recycling for high-voltage application.

The direct recycling of single crystal cathode materials presents several challenges, primarily due to Li^+ diffusion kinetic limitations, structural degradation, and phase instability. Thus, it requires larger force to overcome diffusion barrier while maintaining the crystal structure. In solid-state

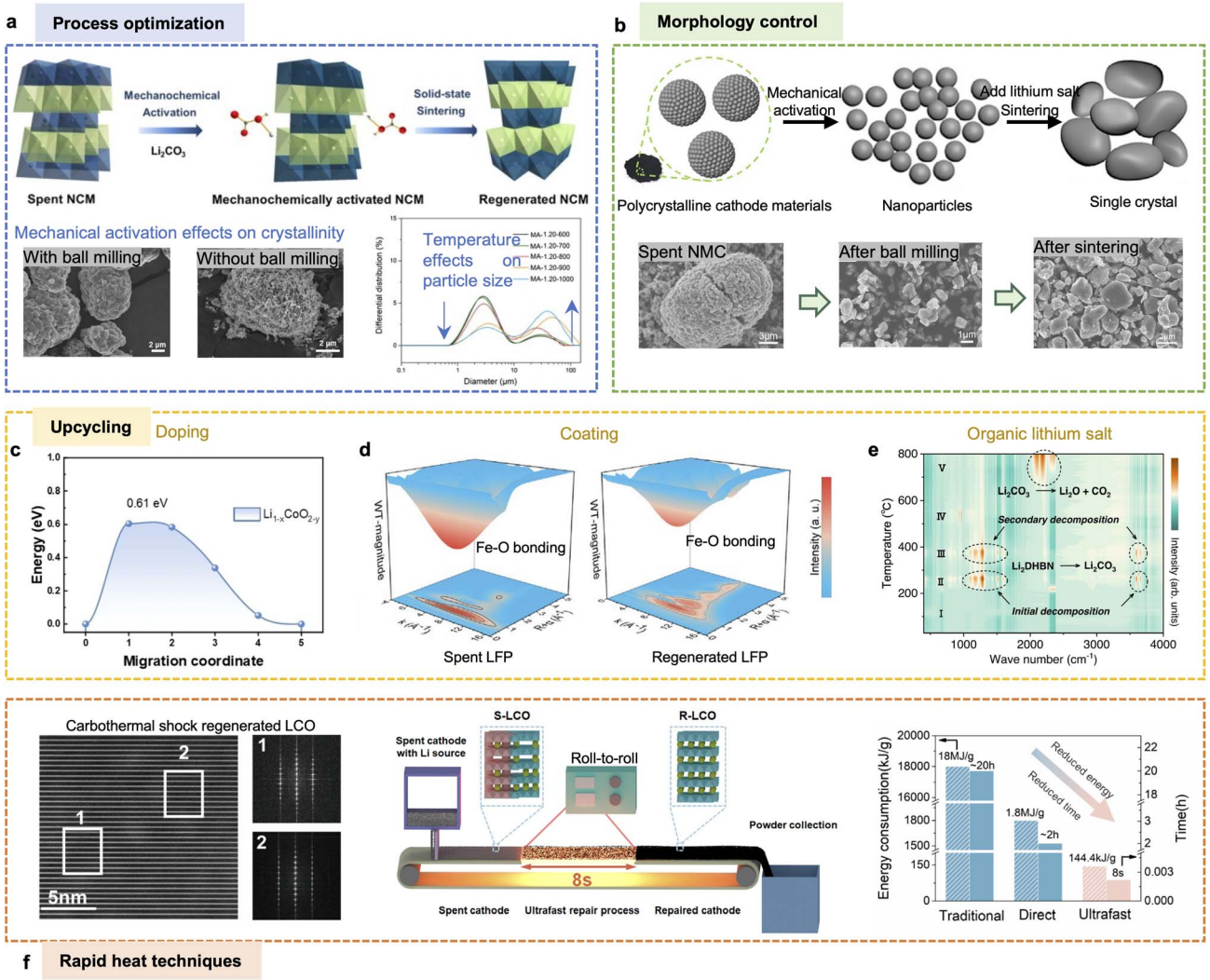

Fig. 4 Progress on solid-state regeneration. (a) Process optimization. Ball milling of spent NMC and lithium salt before sintering can mechanochemically activate NMC and increase the crystallinity, while the sintering temperature can modify particle size. Reprinted with permission from ref. 129. Copyright 2019 Elsevier. (b) Morphology control. Secondary agglomerate NMC can be broken down into nanoparticles after ball milling activation and further upgraded into single crystal after sintering. Reprinted with permission from ref. 136. Copyright 2022 American Chemical Society. (c–e) Upcycling. (c) Diffusion energy barrier of F in bulk spent-LCO. Reprinted with permission from ref. 138. Copyright 2024 Wiley. (d) Wavelet-transform EXAFS results of spent LFP and regenerated LFP. Reprinted with permission from ref. 140. Copyright 2024 Wiley. (e) Infrared spectroscopy (IR) map of the organic lithium salt Li_2DHBN from thermogravimetry (TG)-IR coupling measurements. Reprinted with permission from ref. 141. Copyright 2023 Springer Nature. (f) RHT techniques. High-angle annular dark-field scanning transmission electron microscopy (HAADF-STEM) image and corresponding fast Fourier transform (FFT) pattern of the RHT-regenerated LCO. Also shown are a schematic of the roll-to-roll ultrafast cathode repair method and a comparison of energy consumption and operation time among different regeneration methods. Reprinted with permission from ref. 144. Copyright 2023 American Chemical Society.

sintering regeneration, controlling temperature, duration, and Li source are crucial for uniform relithiation. Guan *et al.*[135] mixed single crystal NMC631 with Li_2CO_3 in Li/TM = 1.05 and sintered at 950 °C for 11 hours. The regeneration process for single crystal cathodes is similar to that of conventional polycrystalline cathodes, but they require significantly higher temperatures and longer sintering times due to the longer Li^+ diffusion paths in single crystals. A recent approach involves upcycling polycrystals into single crystals by adding additional mechanical force. Dong *et al.*[136] combined ball mailing, a mechanical activation process, with solid-stating sintering and achieved single crystal NMC532. As shown in Fig. 4b, secondary polycrystalline particles were broken down into smaller primary particles during the mechanical activation process. Subsequent sintering at 500 °C for 5 hours yielded single crystal NMC532 particles, with the pretreatment step facilitating their formation by lowering both the necessary sintering temperature and time. They further applied a lithium aluminate ($LiAlO_2$) coating on the surface of the recycled cathode, increasing the discharge capacity from 121.96 mAh g^{-1} to 132.52 mAh g^{-1} at 5C.

While single crystal cathodes offer superior structural stability and cycling performance compared to their polycrystalline counterparts, their direct recycling poses significant

challenges due to limited Li^+ diffusion and structural rigidity. Overcoming these barriers requires additional energy to promote the grain boundary migration during solid-state sintering. Thus, the direct recycling of single crystal particles is not achieved solely through conventional methods but often involves elements of upcycling to enhance material performance and restore functionality.

3.2.1.3 Upcycling. Solid-state sintering involves high temperature reactions and ion diffusion. The structure reconstruction can be used for synchronous material modification to further improve the cathode material properties and electrochemical performance.

3.2.1.3.1 Doping. Doping is commonly utilized towards increasing crystal structure stability and enhancing high-voltage performance. Wang *et al.*[137] reported magnesium (Mg) and Al co-doping into spent LCO, acting as 'pillars' between the CoO_6 layers and improving its structural stability. High-resolution transmission electron microscopy (HRTEM) revealed the occupation of Mg and Al mainly in the Li sites and the induced lattice disorder. The intercalation of Mg/Al atoms expanded the interlayer spacing between Co layers from 0.256 to 0.295 nm, mitigating the lattice contraction by H1-3 phase transition as charging to high voltage over 4.55 V. The regenerated LCO achieved 220.4 mAh g^{-1} at C/5 with 79.7% capacity retention after 300 cycles. Besides cation doping, halogens[138] and large molecular groups[139] are also employed during the solid-state sintering. Lei *et al.*[138] created gradient F-doped subsurface in LCO. Existing oxygen vacancies in spent LCO decrease the diffusion energy barrier of F from 1.73 eV to 0.61 eV (Fig. 4c) and promote rigid CoO_5F phase in CoO_6 octahedra, which enhances the structural stability of F-gradient LCO. The regenerated LCO with 0.2 wt% F dopant achieves 154.4 mAh g^{-1} at 5C with 88.3% capacity retention after 500 cycles (3–4.5 V). Fan *et al.*[139] introduced stoichiometric ratio metal source and ammonium dihydrogen phosphate ($NH_4H_2PO_4$) into spent NMC532. They reported that the doping of large molecular groups PO_4^{3-} enlarged the interlayer spacing of NMC532, thus increasing the electrostatic repulsion between TMO_6 octahedrons, stabilizing the crystal structure and facilitating Li^+ transport. The optimized dopant NMC532 with 0.02 M PO_4^{3-} reached 170.7 mAh g^{-1} at 1C and maintained 83.2% capacity retention after 300 cycles.

3.2.1.3.2 Coating. Coating is an efficient way to improve structure stability and inhibit side reactions. Cao *et al.*[140] used tannic acid to form a compact coating layer with abundant functional groups, creating a mildly acidic environment to reduce Fe^{3+} and recover the anti-sites vacancies. Another additive thiourea provided nitrogen (N) and sulfur (S) source as dopant in the carbon coater to enhance electronic conductivity. The extended X-ray absorption fine structure (EXAFS) results showed that the regenerated LFP had a shorter Fe–O bonds length than the spent LFP, indicating a stronger Fe–O bonding strength and more stable structure (Fig. 4d). The regenerated LFP reached 141.3 mAh g^{-1} at 1C and delivered 500 cycles with 85% capacity retention, surpassing the commercial LFP.

3.2.1.3.3 Multifunction Li source. Multifunctional Li salts have emerged as a more cost-effective and efficient alternative to monofunctional Li sources or additives in direct recycling. Ji *et al.*[141] developed a multifunctional organic lithium salt 3,4-dihydroxybenzonitrile dilithium (Li_2DHBN) to regenerate spent LFP cathodes, which can effectively replenish Li vacancies and create a reductive atmosphere to prevent Fe^{3+} formation. The salt decomposed into two inorganic salts to replenish Li loss (Fig. 4e): the initial decomposition occurs at ~200 °C, transforming Li_2DHBN into Li_2CO_3. At temperatures above 700 °C, the salt further decomposed and formed lithium oxide (Li_2O). Such decomposition also created a conductive carbon layer on the surface, enhancing Li^+ and electron transport. The restored LFP showed excellent cyclability at high charging rate and fast redox kinetics in low temperature (−20 °C), enabling 110 mAh g^{-1} at 5C with a high retention of 88% after 400 cycles.

3.2.1.4 Rapid heat treatment (RHT). Conventional solid-state sintering spans several hours to recover cathode materials. Therefore, RHT techniques, such as high temperature shock (HTS), flash Joule heating (FJH), carbothermal shock (CTS) have been employed in direct recycling to expedite regeneration, significantly reducing processing time, minimizing energy consumption, and improving material properties. RHT applies abrupt high-temperature pulse, including laser heating, Joule heating, plasma or microwave heating, to deliver substantial energy within seconds to overcome Li^+ migration barriers.[142] It has been demonstrated that controlled RHT processes can effectively restore the crystal structure of NMC, LCO and LFP cathodes, achieving near-original electrochemical properties.[125,143,144] Their key features comparison is shown in Table 1.

HTS heats materials indirectly using a preheated surface to induce a rapid thermal shock, such as hot metal plate or plasma. Guo *et al.*[125] reported that HTS enabled rapid atomic-scale Li–Fe reordering in LFP, restoring structure and enhancing electrochemical performance for sustainable battery regeneration. Simulation results revealed that the Li and Fe diffusion energy barriers depended on the concentration of Li vacancies: at low vacancy levels, Fe reordering occurred readily

Table 1 Comparison between three RHT recycling methods

Feature	High-temperature shock	Flash Joule heating	Carbothermal shock
Energy source	Preheated surface	Joule heating	Carbon-based reducing agent + thermal shock
Peak temperature	1500–2500 °C	2500–3000 °C	1500–3000 °C
Duration	Seconds to minutes	Milliseconds to seconds	Milliseconds to seconds
Atmosphere	Inert gas or vacuum		
Scalability	More scalable	Small samples	Moderate

Table 2 Summary of the solid-state sintering method for cathodes direct recycling

Recycling method	Cathode material	Recycling process	Electrochemical performance	Ref.
Solid-state sintering	LCO	Mixed with Li_2CO_3 (Li/Co = 1.05), 900 °C, 12 h, air	• 152.4 mAh g^{-1}@30 mA g^{-1}, 3–4.3 V • 80 cycles@98.35% capacity retention	128
Solid-state sintering	LCO	Mixed with Li_2CO_3 (Li/Co = 1.0), 850 °C, 10 h	• 150.3 mAh g^{-1}@C/10, 3–4.3 V • 100 cycles@93.21% capacity retention	32
Solid-state sintering	NMC333	(1) Ball milling, 500 rpm, 4 h, mechanochemical activation (2) Mixed with 20% Li_2CO_3, 800 °C, 4 h	• 165 mAh g^{-1}@C/5, 2.5–4.3 V • 100 cycles@80% capacity retention	129
Solid-state sintering	NMC333	(1) Mixed with $LiOH \cdot H_2O$, 350 °C, 4 h (2) 650 °C, 4 h	• 188 mAh g^{-1}@C/3, 3–4.3 V • 50 cycles@96% capacity retention	130
Solid-state sintering	NMC111	Mixed with 5% Li_2CO_3, 850 °C, 12 h, air	• 153.3 mAh g^{-1}@1C, 3–4.3 V • 100 cycles@81.8% capacity retention	131
Solid-state sintering	NMC532	Mixed with 5% Li_2CO_3, 850 °C, 12 h, O_2	• 153.3 mAh g^{-1}@1C, 3–4.3 V • 100 cycles@84.93% capacity retention	131
Solid-state sintering	LFP	Mixed with 10% fresh LFP, 700 °C, 8 h	• 142 mAh g^{-1}@C/10, 2.5–4.1 V • 100 cycles@95.07% capacity retention	132
Solid-state sintering	LFP	(1) 450 °C, 2 h (2) Mixed with Li, Fe, phosphate (P) salts, 650 °C, 10 h, N_2	• 139 mAh g^{-1} at C/5, 2.0–4.3 V • 100 cycles@94.96% capacity retention	133
Solid-state sintering	LFP	(1) 450 °C, 2 h, Ar (2) Mixed with Li_2CO_3, $C_6H_{12}O_6$, C_2H_6O, ball mill at 200 rpm, 2 h (3) 700 °C, 6 h, Ar/H_2	• 147 mAh g^{-1} at 1C, 2.5–4.3 V • 500 cycles@90% capacity retention	145
Solid-state sintering	LFP	(1) Mixed with lithium stearate, and creatine, 250 °C, 3h; 700 °C, 5 h	• 146.2 mAh g^{-1} at 1C, 2.5–4.3 V • 200 cycles@95.83% capacity retention	146
Solid-state sintering	Single crystal NMC631	(1) Mixed with 5% Li_2CO_3 (2) 950 °C, 11 h	• 184.6 mAh g^{-1} at 1C, 3–4.4 V • 200 cycles@95.12% capacity retention	135
Solid-state sintering	Single crystal NMC532	(1) Ball milling, 450 rpm, 6 h (2) Mixed with 15% Li_2CO_3, 950 °C, 10 h, air	• 167.5 mAh g^{-1} at 1C, 3–4.5 V • 100 cycles@99.7% capacity retention	136
Solid-state sintering	Mg/Ti doped, Al-coated LCO	(1) Mixed with 1% magnesium oxide (MgO), 1% titanium dioxide (TiO_2), 3%Li_2CO_3, ball milling, 200 rpm, 1 h; 100 °C, 15 h; press into pellet, 1000 °C, 10 h, air (2) Ultrasonic treatment of 0.25 wt% aluminum isopropoxide ($C_9H_{21}AlO_3$) in 50 mL ethanol, 30 min; stir with deionized (DI) water (4 : 1 v/v) and 4 g precursor from last step, 6 h (3) Water bath, 80 °C, stirred, 10 h (4) 650 °C, 3 h	• 174.29 mAh g^{-1} at 1C, 3–4.5 V • 200 cycles@96.77% capacity retention	147
Solid-state sintering	F doped LCO	Mixed with 10% Li_2CO_3 and 0.2% ammonium fluoride (NH_4F), ball milling, 400 rpm, 2 h; 450 °C, 5 h, 900 °C, 8 h, air	• 154.4 mAh g^{-1} at 5C, 3–4.5 V • 500 cycles@88.3% capacity retention	138
Solid-state sintering	PO_4^{3-} doped NMC532	(1) Mixed with stoichiometric LiOH, nickel oxide (NiO), manganese oxide (MnO_2) and 0.02 M $NH_4H_2PO_4$, 450 °C, 5 h, O_2 (2) 850 °C, 15 h, O_2	• 170.7 mAh g^{-1} at 1C, 2.7–4.3 V • 300 cycles@83.2% capacity retention	139
Solid-state sintering	F-doped carbon layer LFP	Mixed with 5% Li_2CO_3 and 2.5 wt% PVDF, 650 °C, 2 h, N_2	• 141.5 mAh g^{-1} at 1C, 2.5–4.2 V • 100 cycles@99.6% capacity retention	148
Solid-state sintering	N/S-doped carbon layer LFP	(1) Mixed with thiourea, tannic acid and DI water, stir, 2 h then heat 140 °C, 7 h (2) Centrifuged, collected, 80 °C dried (3) Mixed with glucose and ethyl alcohol, grind, 2 h (4) 600 °C, 5 h, hydrogen (H_2)/argon (Ar)	• 141.3 mAh g^{-1} at 1C, 2.5–4.3 V • 500 cycles@85% capacity retention	140
Solid-state sintering	Carbon coated-LFP	Mixed with 5 wt% Li_2DHBN, 800 °C, 6 h, H_2/Ar	• 110 mAh g^{-1} at 5C, 2.5–4.3 V• 400 cycles@88% capacity retention	141

Table 2 (*Contd.*)

Recycling method	Cathode material	Recycling process	Electrochemical performance	Ref.
Solid-state sintering	Na/S-doped LCO	Mixed with lithium lignosulfonate, 850 °C, 6 h, air	• 150 mAh g^{-1} at 10C, 3–4.6 V • 300 cycles@89.72% capacity retention	149
High temperature shock	F-doped carbon layer LFP	(1) React with 0.08 M LiOH solution, 45 °C, 0.5 h (2) Mixed with DI water and 1% wt Li_2CO_3 (Li : Fe : P = 1.02 : 1 : 1), 500 rpm (3) Dry at 80 °C, 12 h (4) HTS, 720 °C, 20 s (100 V/72 A), Ar	• 142 mAh g^{-1} at 1C, 2.5–3.7 V • 300 cycles@97.56% capacity retention	125
Flash Joule heating	LCO	(1) Mixed with conductive agents (2) Loaded into a quartz tube (graphite rods and copper wool as the electrodes and spacers) (3) Flash Joule, ~2850 K, 300 ms (120 V), Ar	• 132.09 mAh g^{-1} at C/5, 3–4.2 V • 100 cycles@96.9% capacity retention	143
Carbothermal shock	LCO	(1) Mixed with excessive Li_2CO_3 and alcohol, 6 h (2) Pressed into pellet after drying at 80 °C (3) Rapid Joule heating, 1440 K, 8 s, Ar (4) Washing and dry	• 123.9 mAh g^{-1} at C/5, 3–4.3 V • 300 cycles@80.71% capacity retention	144

with a lower energy barrier (0.19 eV), whereas high vacancy concentrations induced severe lattice distortion due to Fe^{3+} formation, raising the energy barrier to 1.12 eV. Thus, the pre-lithiation before HTS promoted defect repair and Li–Fe reordering by lowering migration barriers. Rapid heating supplied sufficient kinetic energy to overcome the energy barrier for Li–Fe antisite defect reordering within seconds while minimizing undesired side effects, such as impurity diffusion and phase degradation. The 1.6 Ah pouch cells made of the HTS-regenerated LFP remained 97.56% capacity retention after 300 cycles at 1C cycling.

FJH applies direct electrical current to a conductive material, rapidly increasing its temperature through Joule heating. Chen *et al.*[143] reported a FJH method combined with magnetic separation to recover fresh cathode materials from spent electrodes, followed by solid-state relithiation. The FJH rapidly removed the binder, CEI, conductive carbon, and metal impurities while largely preserving the cathode crystal structures and hierarchical morphologies, enabling their further reconstruction into new electrodes. The FJH process achieved a high metal recovery yield of ~98% within only milliseconds. This approach has been demonstrated to be feasible for layered LCO, NMC, and graphite materials, with the regenerated cathodes exhibiting cycling performance and capacities comparable to those of commercial counterparts.

CTS utilizes a carbon source as the conductive agent in a high-temperature shock process to transport direct current. Yin *et al.*[144] demonstrated one-step regeneration of spent LCO cathodes by CTS within 8 seconds. The TEM images revealed a heterogeneous mixture of $Li_{1-x}CoO_2$ and Co_3O_4 in the spent LCO (Fig. 4f), whereas the spinel Co_3O_4 phase was fully converted into an ordered LCO layered structure after ultrafast CTS treatment. The recovered LCO delivered 123.9 mAh g^{-1} at C/5, remaining 80% capacity after 300 cycles. They further proposed a roll-to-roll concept for large-scale cathode recycling (Fig. 4f), in which a mixed precursor comprising spent cathode material and Li source undergoes high-temperature treatment within a heating zone, rapidly restoring the crystalline structure and electrochemical performance. Enabled by RHT, this approach offers strong compatibility with existing industrial protocols and shows great potential for ultrafast, continuous roll-to-roll regeneration of cathode materials.

3.2.1.5 Summary. Solid-state sintering is a scalable direct recycling method for restoring cathode structures but requires high temperatures, long processing times, and precise parameter control. Key challenges for industrial adoption include process optimization, cost reduction, and consistent material quality. Advanced RHT enables replenishment within seconds but risks structural uncontrollability, oxygen deficiency, and irreversible cation mixing. While defective engineering can benefit materials like LFP, it is less suitable for layered cathodes unless delicate precursor design. Electrochemical performance reported across different studies is evaluated under varying materials, voltage windows, C-rates, cell configurations, and testing protocols, which limit direct quantitative comparability. Accordingly, the data summarized in Tables 2 and 4–6 are intended to highlight general trends and underlying mechanisms rather than provide strict quantitative benchmarks. To enhance transparency, the corresponding testing conditions are provided alongside the reported performance metrics. Ongoing research should integrate complementary techniques to simultaneously enhance product quality and lower costs.

3.2.2 Solution-based regeneration. Solution-based regeneration is a cost-effective method for recovering spent cathode materials.[150] Unlike hydrometallurgy, it barely emits toxic gases or requires prolonged high-temperature sintering. Instead, it

Table 3 Differences between three solution-based regeneration methods

	Hydrothermal	Ionic liquid	Redox mediator
Lithiation mechanism	Direct chemical lithiation *via* Li^+ in aqueous solution	Direct lithiation in non-aqueous ionic liquid	Indirect lithiation *via* redox couple mediator and electron shuttles
Solvent	Water	Ionic liquid	Organic or inorganic solvent with redox-active species
Temperature	140–200 °C	25–150 °C	25–100 °C
Post-treatment	Wash and post-annealing		
Cost	Low	High	Moderate

treats the degraded cathode materials in Li-containing solution to replenish Li. The process typically consists of two main steps: relithiation, which supplies lost Li, followed by post-annealing to restore the crystal structure. Hydrothermal, ionic liquid (IL), and redox mediator (RM) regeneration are all classified as solution-based regeneration. Their differences are compared in Table 3. These techniques enable precise control over particle size and morphology by tuning various parameters, such as solution temperature, pressure, reaction time, solution pH, solvent, concentration, and additives. However, the scalability of solution-based regeneration remains limited by its inherently batch-based nature, which poses challenges for continuous, large-scale production.[151]

3.2.2.1 Hydrothermal regeneration. The hydrothermal method is a conventional solution-based synthesis technique that facilitates chemical reactions in aqueous solutions, typically conducted in a sealed vessel such as an autoclave at 120–200 °C. In direct recycling of cathode materials, hydrothermal methods regenerate spent cathodes through controlled dissolution, ion exchange, and subsequent recrystallization. This method enables efficient microstructure restoration and fast relithiation due to high ion diffusivity in solution.

3.2.2.1.1 LCO. Kim *et al.*[152] first applied a hydrothermal method to renovate LCO in a concentrated LiOH solution. The relithiation process was conducted in polytetrafluoroethylene (PTFE) vessels placed inside an autoclave, where vapor pressure was generated during the reaction. The hydrothermal treatment was carried out in a 5.0 M LiOH solution at 200 °C for 20 hours. The resulting precipitate was thoroughly washed and dried, yielding well-crystallized particles of ~20 μm composed of nano-sized, aggregated grains (Fig. 5a), formed through a "dissolution–precipitation" mechanism. Raman spectroscopy and X-ray absorption near edge structure (XANES) analyses confirmed that the recovered LCO successfully replenished Li content and restored the transition metal valence state. Zhang *et al.*[153] investigated the effects of temperature, reaction time, and ultrasonic irradiation on the recovery. Spent LCO was placed in a 2 M LiOH solution and subjected to ultrasonic irradiation and stirring under varying temperatures and durations. XRD results revealed that hydrothermal relithiation at 120 °C for 6 hours yielded the most well-defined crystal structure, delivering 132.8 mAh g^{-1} at C/5 with 96.61% capacity retention after 40 cycles. However, hydrothermal treatment alone is insufficient to fully restore the crystal microstructure and crystallinity; post-annealing is more effective in refining structural and surface. Shi *et al.*[154] added a short post-annealing after the wet-chemical process. LCO powders were hydrothermally treated in 4 M LiOH or a 1 M LiOH + 1.5 M lithium sulfate (Li_2SO_4) solution at 220 °C for 4 hours. The powders were further annealed at 800 °C for 4 hours. The Co_3O_4 impurities have been totally removed after wet processing, but it displayed poor cycling stability due to severe cation mixing (Fig. 5b). After sintering, the particle surface became smoother and distributed evenly. The recovered LCO with short annealing showed 148.2 mAh g^{-1} at 1C and achieved 91.2% capacity retention after 100 cycles. To further shorten the reaction time, microwave was combined with hydrothermal.

The upcycling of LCO during hydrothermal regeneration is also preferable to improve electrochemical performance. Wang *et al.*[155] applied interface engineering to enhance the high-voltage performance of regenerated LCO. After hydrothermal relithiation, the sample was mechanically mixed with 2% lithium aluminum titanium phosphate ($Li_{1.4}Al_{0.4}Ti_{1.6}(PO_4)_3$, LATP) and sintered at 800 °C for 4 hours. At temperatures above 700 °C, LCO reacted with LATP to form composite surface phases, including Co_3O_4/cobalt aluminate (Co_2AlO_4), cobalt titanium oxide ($CoTiO_3$), and Li_3PO_4, acting as protective layers to suppress side reactions and enhance structural stability under high voltage. The regenerated LCO delivered superior performance at 4.4 V, achieving a discharge capacity of 166 mAh g^{-1} and retaining 93.0% of its capacity after 100 cycles at 1C.

3.2.2.1.2 NMC. NMC cathode regeneration is complicated by TM non-stoichiometry and cation mixing with the formation of surface rock-salt and spinel phases. The surface heterogeneity hinders Li^+ transport, making the reverse to the layered structure thermodynamically and kinetically challenging. Hydrothermal synthesis effectively produces uniform, highly ordered NMC layered oxides with controlled, rapid reaction kinetics driven by the high Li^+ diffusivity in solution environment, enabling efficient relithiation with lower energy use.[156] However, post-annealing is required to fully incorporate adsorbed Li^+ into the lattice. Chan *et al.*[157] studied the hydrothermal relithiation mechanism based on simulation. The pseudo-second-order fit indicated that hydrothermal relithiation is governed by chemisorption *via* electron sharing or exchange (Fig. 5c). Monolayer adsorption, consistent with the Langmuir model (Fig. 5d), suggested each Li^+-deficient site accommodates one Li^+, requiring high Li^+ concentration for

Table 4 Summary of the solution-based regeneration for cathodes direct recycling

Recycling method	Cathode material	Recycling process	Electrochemical performance	Ref.
Hydrothermal	LCO	(1) 5.0 M LiOH solution, vapor pressure, ~3.0 °C min^{-1}, 200 °C, 20 h (2) Wash, dried at 80 °C, 10 h	• 144.0 mAh g^{-1}@C/5, 3–4.3 V • 40 cycles@92.2% capacity retention	152
Hydrothermal	LCO	(1) 2 M LiOH solution, ultrasonic (work 5 s, stop 2 s), 120 °C, 6 h (2) Wash, dried at 80 °C	• 132.8 mAh g^{-1}@C/5, 2.7–4.3 V • 40 cycles@96.61% capacity retention	153
Hydrothermal	LCO	(1) 4 M LiOH or a 1 M LiOH + 1.5 M Li_2SO_4 solution, 200 °C, 4 h, wash, dry (2) 850 °C, 5 °C min^{-1}, 4 h	• 148.2 mAh g^{-1}@1C, 3–4.3 V • 100 cycles@91.2% capacity retention	154
Hydrothermal	LCO	(1) 4 M LiOH solution, microwave-assistance, 220 °C, 45 min, centrifugation, wash, dry (2) 800 °C, 5 °C min^{-1}, 4 h	• 151.5 mAh g^{-1}@1C, 3–4.3 V • 100 cycles@94.5% capacity retention	172
Hydrothermal	$Li_{1.4}Al_{0.4}Ti_{1.6}(PO_4)_3$-coated LCO	(1) 4 M LiOH solution, 220 °C, 4 h, wash, dry (2) Mixed with LATP, ball milling (3) 800 °C, 5 °C min^{-1}, 4 h	• 166 mAh g^{-1}@1C, 3–4.4 V • 100 cylces@93.0% capacity retention	155
Hydrothermal	Ni–Mn co-doping LCO	(1) 1 g LCO mixed with 0.51 mmol of nickel and manganese acetates (Mn : Ni = 3 : 1) in 10 mL DI water (2) Add 1.275 mmol of urea as precipitation agent (3) Mix, 30 min (4) Mixed with 20 mL solution containing 3.0 M LiOH and 3.0 M KOH, 190 °C, 16 h (5) Centrifugation, 900 °C, 4 h, air	• 160.23 mAh g^{-1}@1C, 3–4.35 V • 100 cylces@91% capacity retention	173
Hydrothermal	$LiNi_{0.15}Mn_{0.15}Co_{0.7}O_2$	(1) 4 M LiOH solution, 220 °C, 2 h, stir at 300 rpm, wash, dried at 80 °C, 24 h (2) 850 °C, 4 h, air	• 150.7 mAh g^{-1}@C/3, 2.8–4.4 V • 50 cylces@91.2% capacity retention	157
Hydrothermal	NMC111	(1) 4 M LiOH solution, 220 °C, 4 h, wash (2) Mixed with 5% Li_2CO_3, 850 °C, 5 °C min^{-1}, 4 h, O_2	• 158.4 mAh g^{-1}@1C, 3–4.3 V • 100 cylces@77.4% capacity retention	131
Hydrothermal	NMC532	(1) 4 M LiOH solution, 220 °C, 4 h, wash (2) Mixed with 5% Li_2CO_3, 850 °C, 5 °C min^{-1}, 4 h, O_2	• ~155 mAh g^{-1}@1C, 3–4.3 V • 100 cylces@82.8% capacity retention	131
Hydrothermal	NMC532	(1) 4 M Li^+ solution, 225 °C, 8 h, wash, dry at 120 °C in vacuum (2) 800 °C, 5 °C min^{-1}, 3 h, air	• 157 mAh g^{-1}@C/10, 3–4.2 V • 1500 cylces@80% capacity retention (C/2, 8 Ah pouch cell)	174
Hydrothermal	NMC622	(1) 2 g of harvested material, 75 mL of concentrated 4 M LiOH and 4 mL of 30% H_2O_2, 125 °C, 30 min, dry at 120 °C in vacuum (2) 800 °C, 5 °C min^{-1}, 3 h, O_2	• 175 mAh g^{-1}@C/10, 3–4.2 V	174
Hydrothermal	NMC111	(1) 0.1 M LiOH + 3.9 M KOH solution, 220 °C, 2 h, wash, dried at 120 °C, vacuum (2) Mixed with 5% LiOH, 750 °C, 4 h	• 150.5 mAh g^{-1}@C/3, 3–4.3 V • 50 cylces@93.3% capacity retention	159
Hydrothermal	NMC532	(1) 3 M LiOH solution, dry at 150 °C, 4 h (2) 810 °C, 5 °C min^{-1}, 3 h	• 136.7 mAh g^{-1}@1C, 2.8–4.25 V • 100 cylces@90% capacity retention	175
Hydrothermal	NMC532	(1) 200 mg of spent NMC532, 20 mL DI water, 8 mL ammonium hydroxide, 180 °C, 6 h, wash, dry at 60 °C in vacuum (2) Mix with LiOH, 500 °C, 5 °C min^{-1}, 2 h; 850 °C, 5 °C min^{-1}, 10 h, air	• 152 mAh g^{-1}@C/2, 2.5–4.3 V • 100 cylces@90% capacity retention, 200 cylces@76% capacity retention	158

Table 4 (*Contd.*)

Recycling method	Cathode material	Recycling process	Electrochemical performance	Ref.
Hydrothermal	NMC622	(1) 200 mg of spent NMC532, 20 mL DI water, 8 mL ammonium hydroxide, 180 °C, 6 h, wash, dry at 60 °C in vacuum (2) Mix with LiOH, 500 °C, 5 °C min^{-1}, 2 h; 800 °C, 5 °C min^{-1}, 10 h, air	• 167 mAh g^{-1}@C/2, 2.5–4.3 V • 100 cylces@90% capacity retention, 250 cylces@75% capacity retention	158
Hydrothermal	Nb-doped NMC532	(1) 4.83 g of spent NMC532, 60 mL of 2 M LiOH, 150 °C, 12 h, wash, dry (2) Ball mill in anhydrous ethanol with Li_2CO_3 and Nb_2O_5 at 400 rpm, 6 h (3) 500 °C, 8 h, air	• 150 mAh g^{-1}@C/5, 2.5–4.3 V • 200 cylces@75.3% capacity retention	176
Hydrothermal	LFP	(1) 5 g of spent LFP, L/S = 6 mL g^{-1}, Li^+ (Li salt $Li_2SO_4 \cdot H_2O$) = 12 g L^{-1}, 1.0 mL of *hydrazine hydrate*, 200 °C, 3 h (2) Wash, dry at 80 °C, 10 h	• 141.9 mAh g^{-1}@1C, 2.2–4.2 V • 200 cylces@98.6% capacity retention	162
Hydrothermal	LFP	(1) 3 g of spent LFP mixed with 30 mL 0.08 M *tartaric acid*, 20 mL 0.2 M Li^+ (Li salt $LiOH \cdot H_2O$) solution, 200 °C, 3 h, wash, dry (2) Concentrated at 95 °C; saturated sodium carbonate (Na_2CO_3) was added to recover Li (3) 700 °C, 2 h, Ar	• 114.96 mAh g^{-1}@5C, 2.0–4.3 V • 200 cycles@94.7% capacity retention	163
Hydrothermal	LFP	(1) Mixed with 0.2 M LiOH and 0.08 M *citric acid* solution, 80 °C, 5 h, wash, dry (2) Mixed with excess 4% Li_2CO_3, 600 °C, 5 °C min^{-1}, 2 h, N_2	• 102 mAh g^{-1}@10C, 2.5–3.8 V • 300 cycles@~92% capacity retention	164
Hydrothermal	LFP	(1) 5 g of spent LFP, L/S = 6 mL g^{-1}, Li^+ (Li salt Li_2SO_4) = 9 g L^{-1}, 6 g of Na_2SO_3, 200 °C, 6 h (2) Wash, dry, 8 h	• 135.9 mAh g^{-1}@1C, 2.2–4.2 V • 100 cycles@>99% capacity retention	166
Hydrothermal	LFP	(1) 1 g of spent LFP, 1 mmol $Li_2C_2O_4$, 5 mL DI water, 100 °C, 4 h (2) Wash, dry, 80 °C, 12 h (LFP-Hydro) (3) 1 g of LFP-Hydro, 50 mg *tartaric acid* in 10 mL DI water, stir, 15 min, wash, dry, 80 °C, 12 h (4) 600 °C, 4 h, Ar	• 106 mAh g^{-1}@10C, 2.2–4.1 V • 400 cycles@79.34% capacity retention	177
Hydrothermal	Cu-doped LFP	(1) Mixed with 0.05 M LiOH, 0.025 M Na_2SO_3, 150 °C, 24 h, filter, wash, dry (2) Mixed with cupric nitrate ($Cu(NO_3)_2$) (3 wt%) and glucose (5 wt%), 600 °C, 4 h, N_2	• 130.03 mAh g^{-1}@C/5, 2.5–3.65 V • 100 cycles@92.36% capacity retention	165
Hydrothermal	N-doped carbon layer LFP	(1) Spent LFP (100 mg) mixed with PVP and filled with 15 mL *ethanol*, lithium acetate (CH_3COOLi) (15 mg) was added after stirring for 5 h (2) 180 °C, 5 h, centrifuged, collected, vacuum drying at 120 °C for 12 h (3) 700 °C, 5 °C min^{-1}, 5 h, Ar	• ~95 mAh g^{-1}@10C, 2.5–4.3 V • 1000 cycles@76.8% capacity retention	167

Table 4 (*Contd.*)

Recycling method	Cathode material	Recycling process	Electrochemical performance	Ref.
Hydrothermal	Lignin-chain zinc (Zn) complex composite LFP	(1) Mixed with LiOH solution according to Li loss (ICP Li : Fe : P = 1.05 : 1 : 1), stirred for 0.5 h at 25 °C (2) Mixed with glucose (10 wt%), washed and dried at 80 °C (3) 650 °C, 5 h, Ar	• ∼40 mAh g^{-1}@5C, 1.8–3.9 V (full cell with gr) • 1000 cycles@78.7% capacity retention	168
Hydrothermal	LFP/microwave-reduced graphene oxide (MWrGO)	(1) Graphite, freeze-dried overnight, placed in a microwave reactor, 3–5 s, 1000 W to get MWrGO (2) MWrGO (−) placed in 0.01 wt% poly(diallyldimethylammonium chloride) (PDDA), sonication (3) 5 wt% MWrGO (+) and spent LFP mixed with LiOH, *L-ascorbic acid* solution (molar ratio of 1 : 1 : 0.5), stir for 1 h, transferred into Teflon microwave reactors, 150 °C, 60 min	• 161.4 mAh g^{-1}@C/5, 2.5–4.2 V • 100 cycles@94.9% capacity retention	178
Hydrothermal	LFP/reduced graphene oxide (RGO)	(1) 1 g spent graphite and 0.5 g sodium nitrate ($NaNO_3$) added into a three-necked flask with 23 mL concentrated H_2SO_4 in ice-bath (2) Potassium permanganate ($KMnO_4$) was added slowly into the mixture, <3 °C, stir for 1 h (3) Three-necked flask was transferred to a water-bath, 38 °C, stir for 1 h (4) 46 mL DI water was added into mixture, 95 °C, stir for 0.5 h (5) 140 mL DI water of 40 °C and 15 mL 30% vol. H_2O_2 was added (6) The GO powder was washed, dispersed and dried (7) Spent LFP mixed with 30 mL LiOH, *AA (L-ascorbic acid)* and dodecyl benzene sulphonic acid sodium (SDBS, $C_{18}H_{29}SO_3Na$) solution with the molar ratio of 1 : 3 : 3 : 1, stirred for 0.5 h, mixed with 5% regenerated GO, transferred into Teflon microwave reactors, 160 °C, 6 h	• 150.4 mAh g^{-1}@C/2, 2.5–4.2 V • 300 cycles@∼100% capacity retention	179
Hydrothermal	$AlPO_4$/Li_3PO_4 coated-LFP	(1) 0.2 M LiOH and 0.08 M tea polyphenols solution, 120 °C, 10 h, wash, dry (2) Mixed with $Al(NO_3)_3$, $NH_4H_2PO_4$, and 2 wt% Li_2CO_3, stirred at 80 °C until dry (3) 600 °C, 5h, N_2	• 134.96 mAh g^{-1}@2C, 2.5–4.2 V • 400 cycles@92.1% capacity retention	180
Ionic liquid	NMC111	(1) Mixed 2.5 mmol degraded NMC111 and 2.5 mmol LiBr in 2.5 mL [C_2mim][NTf_2], 150 °C, 6 h (2) Filtration, washed, acetone, ethanol, dried at 100 °C, 2 h (3) 500 °C, 4 h	• 125 mAh g^{-1}@1C, 3–4.3 V • 100 cycles@∼88% capacity retention	169
Ionic liquid	LFP	(1) Mixed 0.5 g spent LFP and 0.3 g L-AA in 7 g [BMIM][BF_4], stirred for 10 min, 60 °C, 2 h, Ar (2) Added 0.1 g LiBr, 210 °C, 8 h, Ar (3) Centrifuged, washed, acetone, DI water, ethanol, dried at 80 °C for 6 h under vacuum (4) 700 °C, 2 h, Ar	• 138.5 mAh g^{-1}@1C, 2–4 V • 300 cycles@92.1% capacity retention	181

Table 4 (*Contd.*)

Recycling method	Cathode material	Recycling process	Electrochemical performance	Ref.
Redox mediator	NMC111	(1) Mixed 0.5 M DTBQ in DME, stirred overnight (2) Added Li^0 to electrolyte, stirred, removed Li^0 before next step (3) Mixed 7.5 mL lithiated DTBQ electrolyte with 5 g spent NMC111 (4) Sealed a Li^0 chip in Celgard separator and added in the mixture (5) Stirred for 60 min (5) Wash, DME (6) 850 °C, 5 °C min^{-1}, 4 h, air	• 157 mAh g^{-1}@C/10, 3–4.3 V	170
Redox mediator	LFP	(1) Mixed 4 mmol Li chip and 4 mmol Py in 20 mL DME, stirred for 1 h (2) Mixed 0.5 g degraded LFP (3.22 mmol) with 5.6 mL Py–Li (0.2 mol L^{-1}), stirred for 15 min (3) Centrifugation, dried at 80 °C overnight, air	• 160.1 mAh g^{-1}@C/2, 2.7–4.2 V • 100 cycles@~100% capacity retention	171

effective adsorption. Based on adsorption kinetics and redox behavior, the relithiation begins with Li^+ chemisorption on deficient sites, releasing water and oxygen (Fig. 5e). However, wet treatment alone cannot fully restore structure, as some Li^+ remain surface-adsorbed due to the spinel or rock-salt phases that hinder Li^+ penetration into bulk (Fig. 5f). Therefore, post-annealing is required to provide additional thermal energy for Li^+ to overcome barriers and integrate into lattice sites.

Shi *et al.*[131] supported this mechanism through a systematic comparison between LCO, NMC111 and NMC532 recovered by hydrothermal method and solid-state sintering. The inductively coupled plasma optical emission spectrometry (ICP) showed that both NMC111 and NMC532 had more sluggish Li^+ transport kinetics than LCO, requiring higher temperature during hydrothermal relithiation (NMC 220 °C *vs.* LCO 180 °C). Also, NMC recovered by hydrothermal treatment followed by post-annealing exhibited lower cation mixing than that recovered by solid-state sintering in pure O_2, with no rock-salt phase observed in HRTEM. To further overcome the high energy barriers from spinel and rock-salt phases of NMC, Jia *et al.*[158] developed a new strategy of using transition metal hydroxide ($TM(OH)_2$) as an intermediate. Simulations revealed that the 2-TM Li^+ transport channels (2.13 eV) from cation disorder have larger migration barrier than 1-TM transport channels in pristine NMC (1.37 eV), leading to inhomogeneous Li^+ transport during relithiation (Fig. 5g). Therefore, they added ammonium hydroxide in a hydrothermal process to convert the spinel and rock-salt phases into $TM(OH)_2$ first, which can be topotactically transformed into NMC due to their structural similarity. The depth profiling analysis of X-ray photoelectron spectroscopy (XPS) and HRTEM confirmed uniform Li^+ distribution and layered structure in topotactic hydrothermal transformed NMC throughout surface to bulk, unlike gradient profiles from solid-state sintering. NMC532 recovered from the hydroxide delivered 152 mAh g^{-1} at C/2, remaining 90% after 100 cycles and 76% after 200 cycles. This strategy can also be broadly applied to various layered cathode materials, including NMC532, NMC622, and LCO.

Although a high Li^+ concentration is required for effective hydrothermal relithiation, strategies exist to reduce raw material costs. Xu *et al.*[159] investigated the effects of various hydrothermal conditions on the cycling performance of NMC111, including temperature, duration, solution composition, Li source compensation, and post-annealing temperature. They identified the most cost-effective and optimized relithiation protocol as hydrothermal treatment at 220 °C for 2 hours in a solution containing 0.1 M LiOH and 3.9 M potassium hydroxide (KOH), followed by post-annealing with 5% excess LiOH at 750 °C for 4 hours. Replacing 4 M LiOH with 0.1 M LiOH + 3.9 M KOH remained compatible with NMC111 due to the preferential insertion of Li^+ over K^+, attributed to higher reduction potential and smaller ionic radius of Li^+.

3.2.2.1.3 LFP. Performance degradation in LFP cathodes is mainly due to Li vacancies and Li–Fe antisite defects.[160] A high activation energy of 1.4 eV is needed for Fe^{2+} to return to their original M2 sites due to strong electrostatic repulsion from

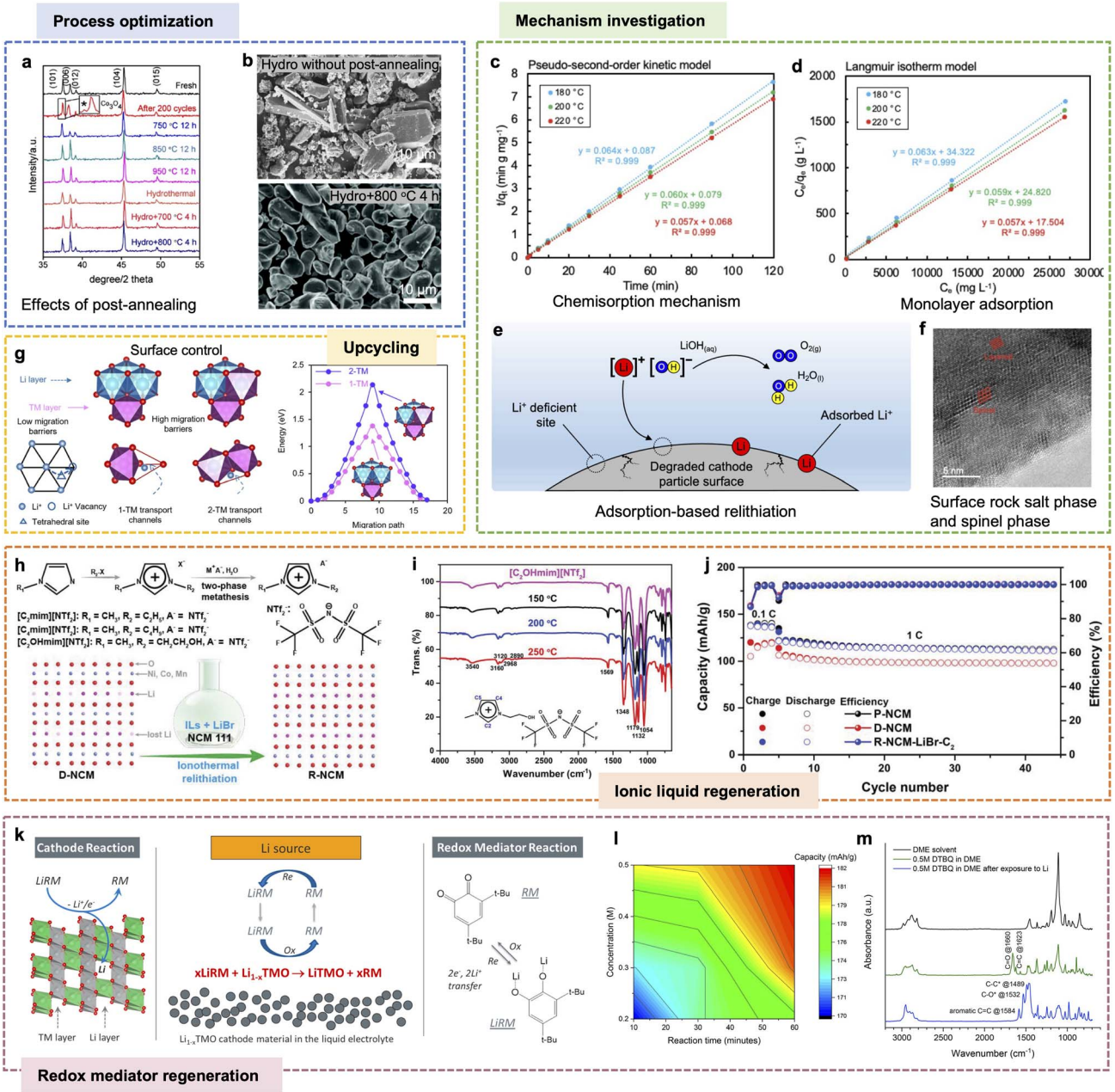

Fig. 5 Progress on solution-based regeneration. (a and b) Process optimization. The post-annealing after hydrothermal regeneration can refine the (a) crystal structure and (b) particle morphology. Reprinted with permission from ref. 152 and 154. Copyright 2004 Elsevier. Copyright 2018 Royal Society of Chemistry. (c–f) Mechanism investigation. (c) Pseudo-second-order kinetic model. (d) Langmuir isotherm model. (e) Schematic of the hydrothermal relithiation mechanism. (f) HRTEM image of the cathode particle regenerated *via* solid-state sintering, revealing the coexistence of layered and spinel phases, which may introduce additional barriers to Li^+ diffusion. Reprinted with permission from ref. 157. Copyright 2023 Elsevier. (g) Upcycling. Illustration of Li^+ diffusion pathways in NMC532. Reprinted with permission from ref. 158. Copyright 2023 American Chemical Society. (h–j) Ionic liquid regeneration. (h) Reaction mechanism, (i) FTIR of $[C_2OHmim][NTf_2]$ and (j) cycling performance of ionothermal regenerated NMC. Reprinted with permission from ref. 169. Copyright 2020 Wiley. (k–m) Redox mediator regeneration. (k) Reaction mechanism, (l) effects of solution concentration and reaction time on recycled NMC capacity, (m) FTIR spectra of a pure DME solvent and the 0.5 M DTBQ in DME before and after exposure to Li^0 chip. Reprinted with permission from ref. 170. Copyright 2021 American Chemical Society.

Fe^{3+}.[161] Thus, the reduction of Fe^{3+} is the core of LFP regeneration. Various reductive agents have been used in previous studies, including hydrazine hydrate,[162] tartaric acid,[163] citric acid,[164] sodium sulfite (Na_2SO_3),[165,166] ethanol[167] and glucose.[168] Most concerns are still the reductive agents' cost. Xu *et al.*[164] used citric acid as the reductive agent to spontaneously reduce Fe^{3+} and replenish Li^+ in spent LFP. Gibbs free energy calculations revealed that the reaction between $FePO_4$ and citric acid is thermodynamically favorable, significantly reducing the hydrothermal duration and cost. ICP analysis showed that lowering the solution temperature to 80 °C had minimal impact on the relithiation kinetics. Also, XRD confirmed full reduction

of Fe^{3+} within 5 hours. Highly crystalline LFP with further reduced anti-site defects was obtained after short annealing, delivering 102 mAh g^{-1} even at 10C with minor degradation after 300 cycles.

Surface coating is a common upgrading strategy to enhance the intrinsically low electrical conductivity of LFP while effectively utilizing organic additives. Jia *et al.*[167] used ethanol as a reducing agent, leveraging its electron-donating tendency upon oxidation. XPS confirmed effective Fe^{3+} reduction to Fe^{2+} at 180 °C for 5 hours, progressing from the surface into the bulk material. To further prevent the oxidation of Fe^{2+} during cycling, polyvinylpyrrolidone (PVP) was introduced to form a heterogeneous interface with N-doped carbon, modifying the d-band structure of recycled LFP. According to d-band center theory, shifting the d-band away from the Fermi level reduces antibonding state occupation, enhancing Fe–O bond strength and immobilizing Fe^{2+} to prevent Li–Fe antisite defects. DFT simulations confirmed a raised d-band center, strengthened Fe–O bonding, and reduced Li^+ diffusion barriers in the modified structure. Thus, the upcycled LFP exhibited faster Li^+ transport, minimal phase transformation, and enhanced performance, delivering over 90 mAh g^{-1} at 10C and retaining 76.8% capacity after 1000 cycles.

3.2.2.2 Ionic liquid regeneration. IL regeneration is a moderate-temperature chemical approach for restoring Li content in degraded battery cathode materials using Li-containing IL as both the solvent and Li source. IL is made of bulky, asymmetric organic cations and anions, allowing them to stay liquid at low temperatures. In a typical process, spent cathode powders are mixed with a Li salt dissolved in a stable ionic liquid, such as $[C_2mim][NTf_2]$, $[C_4mim][NTf_2]$, $[C_2OHmim][NTf_2]$,[169] $[BMIM][BF_4]$, and heated to moderate temperatures under an inert atmosphere. The high thermal and electrochemical stability of IL provides a non-volatile and highly ionic conductive medium. During relithiation, Li^+ from the IL intercalates into the cathode structure, driven by the chemical potential gradient and the inherent mobility of Li^+ in the IL. IL relithiation operates under mild reaction conditions without proton attack, but it suffers from relatively slow lithiation kinetics, potential contamination from IL residues, and the high cost or limited recyclability.

Wang *et al.*[169] introduced an ionothermal regeneration method for direct recycling of spent NCM111 cathodes, leveraging ILs and lithium halides as the reaction medium and Li source, respectively. The optimal relithiation was achieved using recyclable IL containing LiBr in $[C_2OHmim][NTf_2]$ at 150 °C for 6 h. After treatment, the cathode was separated, and ILs were recovered for subsequent cycles, demonstrating IL recyclability. The ionicity of the ionothermal medium enables Li^+ insertion into the TM oxide layer structure without compromising particle morphology (Fig. 5h). The hydrophilic hydroxide groups in $[C_2OHmim]$ improved Li salt solubility and interaction with degraded NMC, and lithium bromide (LiBr) was superior to lithium chloride (LiCl) due to its lower oxidation potential, allowing Br^- to be oxidized to Br_2 (1.065 V) more readily than Cl^- to Cl_2 (1.358 V). Moreover, FTIR confirmed that the $[C_2OHmim][NTf_2]$ remained chemically stable during the ionothermal relithiation process at 150–250 °C (Fig. 5i). All the key functional group peaks were preserved without any degradation, indicating excellent thermal stability and recyclability (98.7%) of the IL. The NMC111 relithiated by $[C_2mim][NTf_2]$ delivered a discharging capacity of 125 mAh g^{-1} at 1C, remaining ~88% retention after 100 cycles (Fig. 5j).

3.2.2.3 Redox mediation regeneration. RM regeneration is a direct recycling method that uses soluble redox-active species to shuttle electrons and Li^+ between a reductant (*e.g.*, Li^0) and degraded cathodes. RM is first reduced by the reductant, then oxidized by transferring Li^+ to cathode (Fig. 5k), enabling Li^+ reinsertion *via* repeated redox cycles. RM regeneration can be operated under ambient temperature and pressure, driving relithiation spontaneously by electrochemical potential without costing external energy. However, its efficiency is limited by redox potential constraints and sluggish kinetics. Also, chemical RMs can induce side reactions at higher potentials and promote the formation of passivation layers on the cathode surface, which may hinder further Li^+ insertion and reduce overall efficiency.

Park *et al.*[170] developed a mild RM regeneration for NMC111. They regenerated spent NMC111 through a spontaneous redox reaction using 3,5-di-*tert*-butyl-*o*-benzoquinone (DTBQ) as the RM in dimethoxyethane (DME) solvent, with Li^0 as the reductant. DTBQ was pre-reduced by Li^0 to form a lithiated DTBQ solution, after which the Li^0 strip was removed. The lithiated DTBQ solution was then mixed with spent NMC111 and another fresh Li^0 chip enclosed in a Celgard separator to prevent particle crossover while allowing ion transport. The mixture was stirred for 10–60 minutes at RT. Afterwards, the relithiated NMC111 powder was washed with DME and annealed in air at 850 °C for 4 hours. The DTBQ concentration and reaction time were tuned, with 0.5 M DTBQ and 60 minutes showing optimal results (Fig. 5l). FTIR showed that the C=O and C=C peaks of Li–DTBQ disappeared, while new peaks corresponding to C–O*, C–C* radicals, and aromatic C=C bonds emerged, indicating Li^+ coordination and electron transfer to the quinone ring (Fig. 5m). The Li–DTBQ complex then transferred Li^+ and electrons to the spent NMC111, enabling relithiation and reduction of TM ions. Redox potential is a key criterion in selecting RMs, as it governs both the driving force and selectivity of the relithiation reaction. The redox potential of RM should be positioned between the Li^0 potential (0 V *vs.* Li/Li^+) and the cathode operating potential (typically 3.5–4.5 V *vs.* Li/Li^+) to ensure efficient mass transfer from Li^0 to the cathode while minimizing parasitic reactions. Aromatic Li complexes such as biphenyl lithium (Biph-Li) and naphthalene lithium (Naph-Li) have low reduction potentials (<0.5 V *vs.* Li^+/Li), making them strong lithiation agents for Li compensation. However, their high reducing power risks overlithiation, causing irreversible crystal damage and interface degradation in cathode materials. Based on this RM design strategy, Wu *et al.*[171] screened controllable reductive polycyclic aromatic hydrocarbons (PAHs) and identified pyrene lithium complex (Py–Li) as suitable RM in DME. Py–Li provided sufficient driving force to insert Li^+ into delithiated LFP without triggering overlithiation or side reactions due to a suitable reduction potential

Table 5 Summary of the molten salt regeneration for cathodes direct recycling

Recycling method	Cathode material	Recycling process	Electrochemical performance	Ref.
Molten salt	LCO	(1) 50 g LiOH–KOH–Li_2CO_3 (salt molar ratio = 3 : 7 : 0.5) mixture, heat at 500 °C, 3 °C min^{-1} (2) 1 g degraded LCO added to molten salt, 8 h, under air (3) Wash, centrifuged, dried at 80 °C for 12 h	• 144.5 mAh g^{-1}@C/5, 2.75–4.5 V • 200 cycles@92.5% capacity retention	184
Molten salt	LCO	(1) The spent LCO was heated at 300 °C, 8 h and 500 °C, 16 h in LiOH–KOH with 0.05 mol $LiNO_3$, under air, 840 mL min^{-1} (2) Wash, centrifuged, dried at 80 °C for 12 h	• 149.1 mAh g^{-1}@C/5, 2.75–4.25 V • 100 cycles@93% capacity retention	195
Molten salt	LCO	(1) Spent LCO, potassium chloride (KCl), $LiNO_3$, and CaO (mass ratio of CaO : LCO = 0.015), mixed, 750 °C, 12 h, air (2) Wash, dried at 60 °C for 12 h	• 128.1 mAh g^{-1}@2C, 3–4.3 V • 300 cycles@79.7% capacity retention	185
Molten salt	NMC532	(1) Spent NMC532, $LiNO_3$, LiOH (salt molar ratio = 3 : 2), mixed, heat at 300 °C, 4 h (2) Wash, DI water (3) Mixed with 5% Li_2CO_3, 850 °C, 5 °C min^{-1}, 4 h, O_2	• 149.3 mAh g^{-1}@1C, 3–4.3 V • 100 cycles@90.15% capacity retention	192
Molten salt	NMC532	(1) Spent NMC532, KCl, potassium nitrate (KNO_3), $LiNO_3$ (molar ratio = 1 : 8 : 8 : 0.8), mixed, heat at 750 °C, 5 °C min^{-1}, 12 h, air (2) Wash, DI water, dried at 80 °C, 12 h	• 152.2 mAh g^{-1}@C/5, 2.75–4.25 V • 100 cycles@95.5% capacity retention	196
Molten salt	NMC532	(1) Spent NMC532, LiOH, Li_2CO_3 (molar ratio = 0.95 : 0.84 : 0.16), mixed, heat at 5 °C min^{-1}, 440 °C, 5 h; 850 °C, 12 h	• 146.3 mAh g^{-1}@1C, 2.8–4.3 V • 200 cycles@89% capacity retention	197
Molten salt	NMC532	(1) Spent NMC532, LiOH, Li_2CO_3 (molar ratio = 7 : 3), mixed, heat at 500 °C, 5 h; 800 °C, 6 h	• 152.92 mAh g^{-1}@C/2, 2.8–4.3 V • 100 cycles@96% capacity retention	198
Molten salt	From NMC532 to single crystal $LiNi_{0.665}Mn_{0.195}Co_{0.14}O_2$	(1) Spent NMC532, $Ni_{0.83}Mn_{0.09}Co_{0.08}(OH)_2$, LiOH, Li_2SO_4 (molar ratio = 1 : 1 : 2.5 : 0.5), mixed, heat at 10 °C min^{-1}, 900 °C, 5 h; 860 °C, 15 h, air; cooling, −2 °C min^{-1}, 300 °C; nature cooling (2) Wash, DI water, dried at 70 °C, air (3) 700 °C, 4 h, air	• 160 mAh g^{-1}@1C, 2.8–4.3 V, 30 °C • 200 cycles@95% capacity retention	190
Molten salt	From NMC532 to single crystal $LiNi_{0.8}Mn_{0.12}Co_{0.08}O_2$	(1) Spent NMC532, $Ni_{0.83}Mn_{0.09}Co_{0.08}(OH)_2$, LiOH, Li_2SO_4 (molar ratio = 1 : 1 : 2.5 : 0.5), mixed, heat at 10 °C min^{-1}, 780 °C (2) Wash, DI water, dried at 70 °C, air (3) 700 °C, 4 h, air	• 175 mAh g^{-1}@1C, 2.8–4.3 V, 30 °C • 200 cycles@85% capacity retention	190
Molten salt	NMC532	(1) Spent NMC532, $LiNO_3$, LiOH, CH_3COOLi (salt molar ratio = 9 : 6 : 10), mixed, heat at 400 °C, 4 h (2) Soak, DI water, ultrasonic 30 min (3) 5% Li_2CO_3, 850 °C, 6 h, O_2	• 160 mAh g^{-1}@C/2, 3–4.3 V • 100 cycles@93.7% capacity retention	199
Molten salt	From NMC111 to NMC622	(1) Spent NMC111, nickel nitrate hexahydrate ($Ni(NO_3)_2 \cdot 6H_2O$), LiCl, NaOH (mole ratio = 1 : 2.4 : 0.86 : 1.2), mixed, dried at 110 °C, vacuum; heat at 5 °C min^{-1}, 300 °C, 5 h; 800 °C, 5 h, air (2) Wash, dried at 110 °C, vacuum (3) 600 °C, 5 °C min^{-1}, 2 h, air	• 140 mAh g^{-1}@200 mA g^{-1}, 3–4.3 V • 100 cycles@92.8% capacity retention	200

Table 5 (*Contd.*)

Recycling method	Cathode material	Recycling process	Electrochemical performance	Ref.
Molten salt	From NMC111 to single crystal NMC622	(1) Spent NMC111, NiO, LiOH (mole ratio = 1 : 0.67 : 0.67), mixed, 20% excess LiOH and 10% excess Li_2SO_4 added to flux, heat at 10 °C min^{-1}, 900 °C, 10 h, O_2	• 125 mAh g^{-1}@5C, 2.5–4.3 V • 100 cycles@77.59% capacity retention	201
Molten salt	NMC532	(1) Spent NMC532, LiI, LiOH (mole ratio = 1 : 1.65 : 1.35), mixed, 5 wt% dicobalt trioxide (Co_2O_3), 5 wt% MnO_2 added, 200 °C, 4 h; 850 °C, 5 h	• 137 mAh g^{-1}@C/2, 2.5–4.3 V • 300 cycles@73.0% capacity retention	194
Molten salt	NMC532	(1) Spent NMC532, 3 wt% Al, $LiNO_3$, LiOH (salt molar ratio = 3 : 2), 300 °C, 4 h (2) Wash, dried at 60 °C (3) 5 wt% LiOH, 800 °C, 8 h	• 135.93 mAh g^{-1}@1C, 2.8–4.3 V • 200 cycles@89.6% capacity retention	202
Molten salt	NMC532	(1) Spent NMC532, LiOH, $LiNO_3$, lithium salicylate ($LiC_7H_5O_3$) (mole ratio = 10 : 2 : 3 : 5), 300 °C, 4 h (2) Wash, DI water, ethyl alcohol, dried at 70 °C, 10 h (3) 5% Li_2CO_3, 850 °C, 6 h	• 136.9 mAh g^{-1}@C/2, 2.5–4.3 V • 200 cycles@88.2% capacity retention	203
Molten salt	Single crystal NMC811	(1) Spent NMC811, $LiOH{\cdot}H_2O$, NaCl (mole ratio = 1 : 2 : 0.4), mixed, 850 °C, 15 h (2) Wash, DI water (3) 5 wt% LiOH, 800 °C, 10 h	• 155.8 mAh g^{-1}@1C, 3–4.3 V • 200 cycles@86.5% capacity retention	188
Molten salt	NMC532	(1) 0.2 g spent NMC532, 9.9 mg LiOH, 42.8 mg $LiNO_3$, 132.5 mg $LiC_7H_5O_2$, 5 °C min^{-1}, 300 °C, 4 h (2) Wash, centrifuge, dry for 12 h (3) 0.25% Li_2CO_3, 850 °C, 5 °C min^{-1}, 6 h	• 145.7 mAh g^{-1}@C/2, 2.5–4.3 V • 300 cycles@70.1% capacity retention	204
Molten salt	LFP	(1) Spent LFP, $LiNO_3$, ferrous oxalate (FeC_2O_4) (mole ratio = 1 : 0.5 : 0.1), mixed, 10 wt% of sucrose added, 300 °C, 2 h, Ar (2) Wash, DI water, 80 °C, 12 h (3) 650 °C, 6 h	• 145 mAh g^{-1}@C/2, 2.5–4.2 V • 100 cycles@90% capacity retention	191

of ~0.82 V *vs.* Li/Li^+. Nuclear magnetic resonance (NMR) supported that pyridine was successfully coordinated with Li^+, forming a soluble and labile complex that readily dissociated to release Li^+. As a result, Li^+ can rapidly intercalate into the cathode lattice, enabling regeneration of spent LFP within minutes.

3.2.2.4 Summary. Solution-based regeneration is cost-effective and efficient, but output stability is influenced by numerous factors. The required conditions and environments vary widely across materials, and diverse additives have been explored to improve regeneration performance. However, no clear standards or guidelines exist for their selection. Also, aqueous or organic media may damage surface-sensitive materials. Future research should theoretically decouple the roles of different compositions in the solution, elucidating and quantifying their effects and design rationality, thereby identifying optimal conditions based on performance and cost. Furthermore, the batch-to-batch nature of solution-based regeneration limits its applicability for rapid commercial use, underscoring the need for innovative designs that enable continuous production.

3.2.3 Molten salt regeneration. Although solution-based regeneration offers faster kinetics than solid-state methods, it can sometimes lead to undesirable side reactions such as TM leaching or structural degradation due to the aqueous environment and harsh conditions. Furthermore, solution-based relithiation can have fast surface kinetics in aqueous, pressurized environments, but this does not necessarily translate to effective bulk relithiation. The solution medium often has limitations to penetrate Li^+ deep into particle bulk due to its relatively low chemical potential (concentration), especially in degraded or dense materials.[182] In contrast, molten salt benefits from the proton-free and Li rich environment, enabling more controlled and efficient Li^+ transport into the bulk of cathode materials under air atmosphere. By immersing the cathode materials in a molten Li salt, such as LiCl, lithium nitrate ($LiNO_3$) at medium temperatures (typically 300–600 °C), Li^+ can quickly diffuse and penetrate the host crystal lattice.[183] The

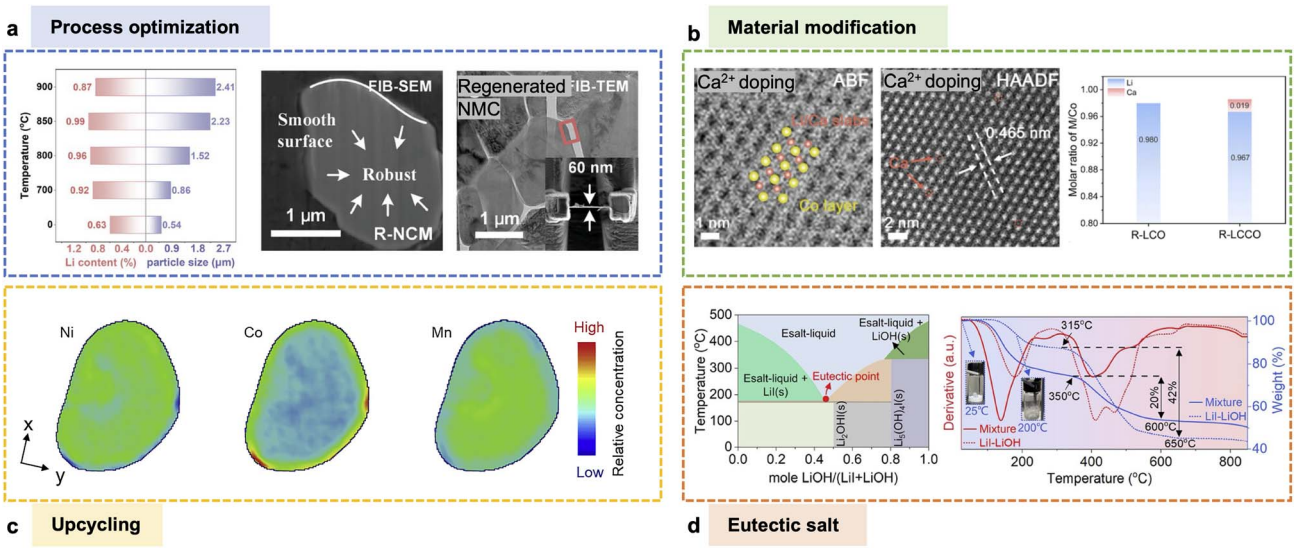

Fig. 6 Progress on molten salt regeneration. (a) Process optimization. Temperature effects on Li content and particle size. Reprinted with permission from ref. 188. Copyright 2024 Wiley. (b) Material modification. Annular bright-field (ABF)-STEM, HAADF-STEM, ICP result of Ca^{2+} doped LCO. Reprinted with permission from ref. 185. Copyright 2024 Elsevier. (c) Upcycling. Ni, Mn and Co relative concentrations distribution over a particle slice revealed by XRF. Reprinted with permission from ref. 190. Copyright 2022 Elsevier. (d) Eutectic salt. Phase diagram and TG-DTG curves of the LiI–LiOH eutectic salt system. Reprinted with permission from ref. 194. Copyright 2022 American Chemical Society.

proton-free, oxidative environment and fast kinetics of molten salt regeneration make it suitable for restoring layered oxide cathode materials, such as LCO, NMC.[112]

3.2.4 LCO. Yang *et al.*[184] chose LiOH–KOH–Li_2CO_3 mixture as the eutectic salt. A LiOH–KOH eutectic was the basic molten salt system, resulting in a lower melting point than the individual component. Li_2CO_3 was added as an additional Li source due to its higher reactivity compared to LiOH. The degraded LCO was added to the molten eutectic salt bath and maintained at 500 °C for 8 hours. The strong oxidative environment of LiOH–KOH–Li_2CO_3 effectively broke down residual carbon and organic binders through spontaneous reaction, while the Li-rich, uniform molten phase enhanced Li^+ transport, promoting relithiation. After regeneration, the cracks on LCO were repaired, and the particles became smooth, leading to a capacity improvement from 70 mAh g^{-1} to 150 mAh g^{-1}, which maintains 92.5% retention after 200 cycles at C/5.

To further improve the structure stability and crystallinity of LCO, Gao *et al.*[185] developed Ca^{2+}-assisted molten salt relithiation. Minor CaO was introduced into eutectic salts, followed by moderate heating at 750 °C. The addition of CaO expanded the metastable dissolution region of LCO and raised the relithiation temperature from 470 °C to 540 °C, promoting highly ordered crystal formation and improved Li^+ diffusion for structural repair. Differential scanning calorimetry (DSC) indicated that CaO facilitated Ostwald ripening, leading to the precipitation of isotropic crystals with uniform size and improved structural ordering. Moreover, HAADF-STEM revealed calcium (Ca) atoms within the Li intercalation layer, partially compensating for Li vacancies formed during cycling (Fig. 6b). Simulations indicated that Ca^{2+} doping modifies Li^+ pathways and enhances diffusivity by creating localized internal electric fields from charge imbalance and improving connectivity between adjacent Li sites.

3.2.5 NMC. Molten salt becomes disordered IL at medium temperatures, weakly solvating Li^+ that transports through vehicular diffusion and ion coordination mechanisms, diffusing rapidly into the Li slab of cathode lattice driven by the concentration gradient.[186] Also, the molten salt environment facilitates oxygen incorporation and TM reoxidation, further stabilizing the layered structure. Thus, it is preferable to solid-state sintering or solution-based regeneration of NMC.

Chen *et al.*[187] compared the molten salt and traditional solid-state sintering method for spent NMC. XPS revealed that molten salt recovered NMC exhibited homogenous surface with less Ni^{2+}, while traditional solid-state sintering remained F-related impurities from CEI decompose. Also, molten salt recovered NMC had larger grain size (~2 μm), indicating a secondary particle growth due to rapid ion diffusion and grain boundary migration. Qin *et al.*[188] reported that higher temperatures and longer duration promoted NMC811 grain coarsening in LiOH–NaCl molten salt. However, there was significant surface Li volatilization when the treatment temperature reached 900 °C. Additionally, focused ion beam (FIB)-TEM revealed fully connected secondary particles of recovered NMC811 (Fig. 6a). These observations suggested that NMC811 was completely relithiated and reconstructed into single crystal, driven by enhanced mass transport within LiOH–NaCl molten salt.

Beyond morphology control and grain growth, molten salt relithiation enables value-added upcycling. Low-Ni NMC compositions such as NMC111 and NMC532 dominate commercial use due to their structural stability and mature manufacturing processes but offer limited energy density.[189] In contrast, Ni-rich layered oxides like NMC622 and NMC811 are

Table 6 Summary of the anode material direct recycling

Recycling method	Recycling process	Electrochemical performance	Ref.
Flash Joule sintering recycling	(1) Heating the graphite *via* the flash system (T_{max} = 2850 K, 1 s, 120 V, 1.3 Ω) (2) Leach at 60 °C for 3 h in 0.1 M HCl	• Recycled graphite‖LFP • 131.1 mAh g^{-1} at C/5 • 400 cycles@77.3% capacity retention (C/2)	209
Pretreatment and catalytic graphitization	(1) Leach at 35 °C overnight in 2 M sulfuric acid (2) Stir acid-leached powder, cobalt nitrate, and alcohol mixture until alcohol evaporates (3) 900 °C, 4 h, N_2	• 358 mAh g^{-1} at C/10 • 500 cycles@245.4 mAh g^{-1} (1C)	210
Alkali etching	(1) Alkali roasting, 300 °C, 2 h, air (KOH : NaOH = 5 : 1) (2) Leach at 60 °C for 2 h with stirring in 2 M H_2SO_4 (60 mL) and H_2O_2 (40 mL, 30 wt% in H_2O) (3) 1100 °C, 2 h, N_2 (leached powder and pyrolytic)	• 336.9 mAh g^{-1} at C/10 • 100 cycles@99.7% capacity retention	211
Alkaline roasting	(1) Alkali roasting, 350 °C, 2 h, Ar (spent graphite : NaOH = 1 : 2) (2) Leach in DI water	• 361.2 mAh g^{-1} at 0.05A g^{-1} • 200 cycles@368.1 mAh g^{-1} (0.1 A g^{-1})	212
Microwave heating	(1) Microwave heating, 800 W, 20–30 s, N_2 (2) Graphite mixed with DI water (1 : 5), go through CO_2 (60 mL min^{-1}) with stirring (600 rpm) (3) Recover Li salt: heat and evaporate lithium solute	• 353.5 mAh g^{-1} at C/10 • 100 cycles@320 mAh g^{-1} (C/2)	213
Hydrometallurgical	(1) Leach in 5 M sulfate acid and 35 w/w% H_2O_2 (2) Alkali roasting, 500 °C, 40 min with NaOH	• 359.3 mAh g^{-1} at C/5 • 100 cycles@84.63% capacity retention	214
Boric acid leaching and short annealing	(1) Leach in 5 wt% boric acid solution (1 g graphite and 2 mL acid solution) (2) 1050 °C, 1 h, N_2	• 330 mAh g^{-1} at C/3 • 100 cycles@333 mAh g^{-1}	215
Solid-state sintering	(1) 750 °C, 5 h, Ar (2) Wash, dimethyl carbonate (DMC) (3) 750 °C, 5 h, Ar	• 310 mAh g^{-1} at C/2 • 1000 cycles@93% capacity retention	216
Electrolysis	(1) Graphite plate as positive electrode, spent graphite as negative electrode, Na_2SO_4 solution as electrolyte (2) 10 cm of inter-electrode distance, 1.5 g L^{-1} of electrolyte concentration and 30 V of voltage, separation for 25 min	• 353.5 mAh g^{-1} at C/10 • 100 cycles@320 mAh g^{-1} (C/2)	217
Leaching combined with sintering	(1) Used graphite, 98.3% H_2SO_4, 20% of total mass DI water, mixed, stir for 20 min (2) 200 °C, 24 h (3) Leaching in 200 g per L H_2SO_4 solution (4) Wash, DI water, washing until PH = 7 (5) 1500 °C, 2 h, Ar	• 349 mAh g^{-1} at C/10 • 50 cycles@98.9% capacity retention	218

preferred for future applications. As the retired low-Ni NMC increases alongside growing demand for high-Ni NMC, upcycling provides a critical pathway to bridge this gap. Qian *et al.*[190] introduced additional $TM(OH)_2$ into $LiOH–Li_2SO_4$ eutectic salts. The TM ions and Li^+ diffuse simultaneously into the NMC lattice at elevated temperature, transiting NMC111 into NMC622 or NMC811 depending on the feedstock stoichiometry. The recovered particles exhibited well-defined morphology, uniform crystallinity, and a homogeneous distribution of Ni, whereas X-ray fluorescence (XRF) tomography revealed inhomogeneous spatial distributions of Mn and Co (Fig. 6c). This may be attributed to differences in the solubility and diffusivity of Ni, Co, and Mn in the molten salt system of $LiOH–Li_2SO_4$, which affected the bulk mass transport and crystal growth kinetics. Despite this, ICP showed that the recovered NMC622 and NMC811 reached target TM content from electrode level to particle level, as well as good cycling performance in both half cells and pouch-type full cells.

3.2.6 LFP. While the oxidative atmosphere in molten salt offers benefits on layered oxide cathode recovery, it is detrimental for LFP, which requires reductive atmosphere to avoid Fe^{3+}. Thus, a reductive atmosphere must be coupled with molten salt to suppress the oxidation. For example, Liu *et al.*[191] used sucrose as a reducing agent during the $LiNO_3$-based molten salt relithiation of LFP to maintain its structural integrity. The recovered LFP delivered a specific capacity of 145 mAh g^{-1} at C/2, representing more than a 13% improvement compared to the spent LFP. However, the high cost of molten salt treatment makes it less practical for recycling LFP. Instead, LFP is suited for wet chemicals due to its lower processing cost and milder reaction conditions.

3.2.7 Molten salt system design. The Li salts used in molten salt regeneration typically have low melting points. For example, LiOH melts at ~462 °C, and $LiNO_3$ melts at ~255 °C.[192] However, single-component Li salts are rarely used in molten salt regeneration due to their limited Li^+ mobility, high viscosity, and poor thermal stability.[192] To achieve low melting points, high relithiation kinetics, and good thermal stability, binary or ternary eutectic salt systems have been developed.

In pure salt, cations and anions form a stable lattice with a characteristic melting point. Introducing other salts with different ionic radius or lattice parameters disrupts this lattice, lowering its stability and favoring liquid-phase formation at reduced temperatures due to lower Gibbs free energy.[193] For example, Ma *et al.*[194] proposed the eutectic lithium iodide (LiI)–LiOH salt, which crystallizes at the minimum melting point of ~176 °C, corresponding to the eutectic point at the intersection of the liquidus curves in the binary phase diagram (Fig. 6d). However, TG and derivative thermogravimetric (DTG) showed that the eutectic salt and NMC532 mixture mainly replenish Li and reconstruct surface lattice oxygen between 315–650 °C, which is still a high temperature for efficient regeneration (Fig. 6d). Additionally, the use of dual Li salts results in elevated costs that challenge commercialization.

To reduce costs and enhance Li^+ diffusivity, potassium (K) and sodium (Na) salts can partially substitute Li salts. Non-Li salts reduce molten salt viscosity to enhance Li^+ mobility and dissolve metals, facilitating simultaneous impurity removal. Also, K^+ and Na^+ are unlikely to be incorporated into the cathode lattice due to their larger ionic radius. For example, Yang *et al.*[195] demonstrated that LiOH–KOH eutectic salts with $LiNO_3$ and air as oxidants can effectively remove impurities, including graphite, carbon black, PVDF. Gibbs free energy calculations confirmed that reactions between the impurities and $LiNO_3/O_2$ are thermodynamically favorable, thereby suppressing side reactions with LCO. With increasing oxygen partial pressure, the impurity removal reactions were promoted. Therefore, the treated LCO exhibited a smooth surface with no impurity residues, delivering a discharge capacity of 149.1 mAh g^{-1} at C/5.

3.2.8 Summary. The molten-salt regeneration has highest relithiation kinetics and requires no specialized equipment, enabling practical implementation. However, excessive Li salt increases chemical costs, and residual deposits on the cathode surface can raise interfacial resistance, promote side reactions, and accelerate capacity fading, necessitating additional washing and post-annealing steps. Thus, commercialization of molten salt requires material innovations and salt reuse to reduce the eutectic salt cost, simplify the processing and avoid impurities.

4 Anode graphite direct recycling

Graphite is the most common anode material in LIB industry due to its low electrochemical potential, high theoretical capacity (372 mAh g^{-1}), good mechanical stability, strong thermal resistance, low cost and accessibility. So far, synthetic graphite boost production surpassing natural graphite and is preferable by LIB fabrication, attributing to its high purity and better thermal stability.[205] Despite the relatively higher prices, it's still affordable as it was priced at about $890 per metric ton.[206] Thus, less attention was given to graphite anode recycling. The anode fabrication cost is ~10% in LIBs,[207] so it's still significative to recycle spent graphite anode from economical and eco-friendly perspectives. Also, precious battery metal resources such as Li, Ni, Mn, Co still distribute from the spent graphite layered structure to the surface of SEI,[208,209] which is valuable to extract.

The successful recycling of graphite anode involves the deactivation of binders, the extraction of Li, the removal of SEI, trapped salt, and other impurities. Similar to cathode recycling, pyrometallurgy and hydrometallurgy are the mainstream for anode active material recycling. However, commercial interest has been limited due to the high cost of these processes and the relatively low market price of synthetic graphite. Recently, numerous advanced strategies have been developed to enable cost-effective anode recycling. Chen *et al.*[209] proposed a flash Joule heating method for recycling spent graphite anodes, which applied a high current to the spent anode, generating rapid Joule heating to above 2000 K in less than 1 s due to the high resistivity of residual impurities (Fig. 7a). In contrast, the low-resistivity graphite remained at a significantly lower temperature, in accordance with Joule's law. Under such high temperatures, surface impurities such as SEI components, Li

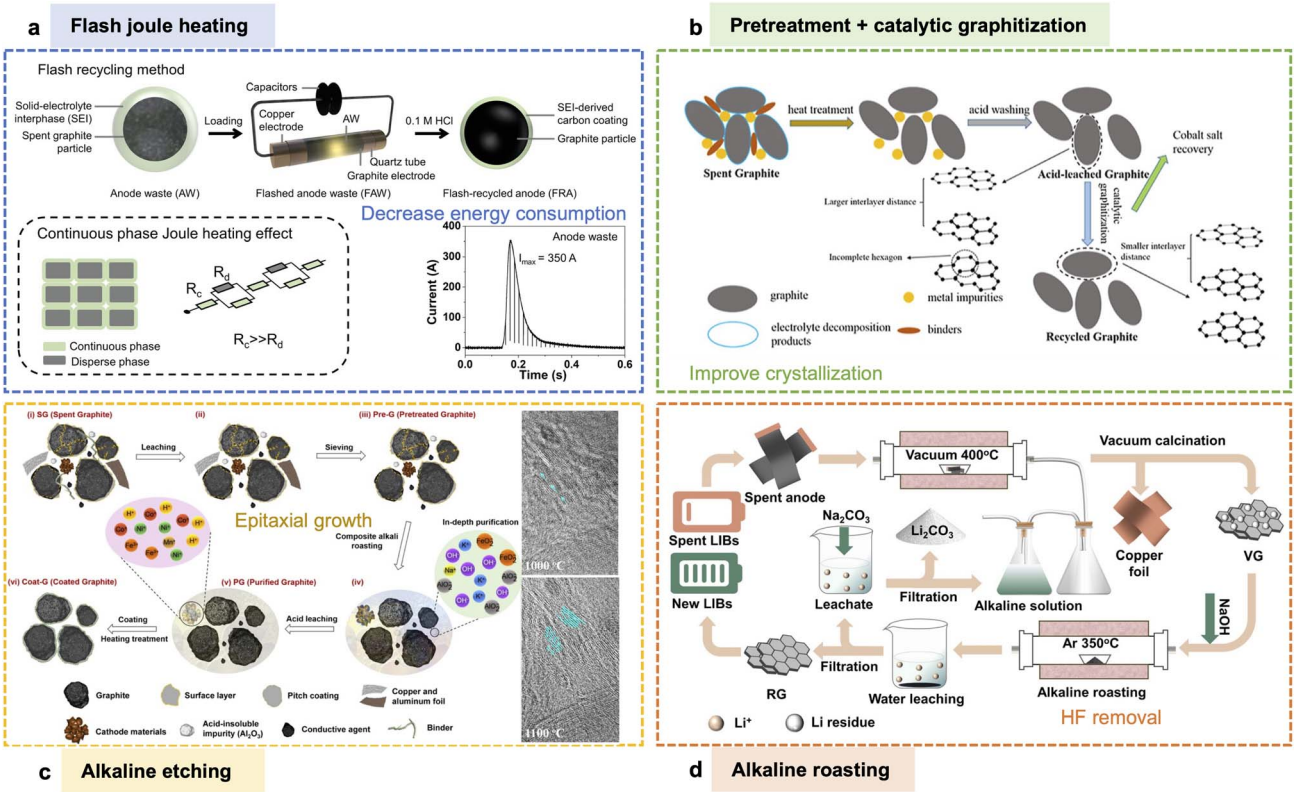

Fig. 7 Progress on graphite anode regeneration. Workflow and mechanism of (a) flash Joule heating. Reprinted with permission from ref. 209. Copyright 2022 Wiley. (b) Pretreatment + catalytic graphitization. Reprinted with permission from ref. 210. Copyright 2022 Elsevier. (c) Alkaline etching. Reprinted with permission from ref. 211. Copyright 2021 American Chemical Society. (d) Alkaline roasting. Reprinted with permission from ref. 212. Copyright 2022 American Chemical Society.

salts, and other volatile compounds were gasified, leaving behind graphite and transition metals (higher boiling points above 3000 K). A subsequent acid-leaching removed residual transition metals, enabling a clean, reusable graphite anode. Chen *et al.*[210] introduced a two-stage strategy that combined pretreatment with catalytic graphitization to regenerate graphite (Fig. 7b). First, spent graphite was annealed at high temperature followed by acid leaching using H_2SO_4 to eliminate impurities, preparing it for structural restoration. Then, the mixture of Co salt and graphite was further catalytically graphitized, with the Co ions acting as catalysts to promote reformation of crystalline graphite by repairing defects. The Co-catalyzed graphite exhibited significantly enhanced electrochemical performance, achieving ~207.3 mAh g^{-1} at 1C and 245.8 mAh g^{-1} after 500 cycles. Da *et al.*[211] introduced alkaline etching to regenerate spent graphite. The spent graphite was etched by KOH–NaOH at 180–300 °C, which can effectively remove acid-insoluble impurities embedded in the graphite matrix. After purification, the clean graphite was coated by pitch to rebuild graphitic crystallinity and grow epitaxially on the underlying graphite surface during a subsequent short, low-temperature annealing. TEM revealed that this epitaxial growth not only refined the graphitic layer but also reconstructed Li^+ transport channels between the regenerated surface layers and the original graphite bulk (Fig. 7c). Liu *et al.*[212] replaced hazardous acid-based roasting with an alkaline source NaOH, avoiding toxic HF emissions by chemically transforming LiF into sodium fluoride (NaF) and LiOH at moderate temperatures (Fig. 7d). Following the roasting, Li was further recovered *via* simple water leaching, producing nearly quantitative yields without harsh acids. The graphite left behind maintained excellent electrochemical performance of 370.8 mAh g^{-1} at 0.05 A g^{-1}, paving the way for scalable, eco-friendly anode recycling with high resource efficiency.

In addition, microwave heating,[213] hydrometallurgical,[214] boric acid leaching,[215] and solid-state sintering[216] all paved the way to achieve anode recycling. Recent progress of graphite anode recycling is summarized in Table 6. However, artificial graphite itself is inexpensive, so the key to anode direct recycling is keeping the overall cost lower than producing new graphite while delivering clear industrial benefits. The process must balance cost, performance, and sustainability to be commercially viable.

5 Conclusions and outlook

In this review, we discussed recent progress in the direct recycling of LIBs. Following the typical workflow of direct recycling, we first introduced various separation methods to obtain active materials from spent batteries. We then discussed degradation

mechanisms and regeneration techniques for cathode materials (LCO, NMC, LFP), highlighting process optimization, relithiation mechanism and upcycling strategies. Additionally, we summarized direct recycling approaches for graphite anodes, emphasizing the challenges and opportunities in morphology control and yield efficiency.

Direct recycling is considered as a promising approach for recovering active materials in LIBs without sacrificing original crystal structure, requiring lower energy and chemical input than pyrometallurgy and hydrometallurgy. However, direct recycling is still constrained at laboratory or pilot scale due to both technical and cost limitations. Research efforts should be devoted toward the following aspects in the future:

(1) Cost reduction: separation and sorting are crucial to ensure the effectiveness of further regeneration, however, they involve extensive manual labor and are highly time-consuming, particularly when transitioning from battery pack to active material level. Battery packs incorporate complex circuitry, and their designs vary significantly across manufacturers due to differing priorities in maximizing energy density and ensuring operational safety. Moreover, spent LIBs typically retain residual energy, necessitating pretreatment to fully discharge and ensure safe disassembly before manual disassembly-further contributing to overall costs. Addressing these issues requires innovations in battery pack design to facilitate EOL processing (such as tool-free disassembly), reduce labor intensity and improve recycling efficiency. Furthermore, with the rapid development of artificial intelligence (AI), intelligent systems capable of integrating residual energy detection, automative discharging and disassembly have significant potential to enhance both the safety and cost-effectiveness of LIB direct recycling.

(2) Product quality: the separation process may still overlook certain impurities, and the regeneration feedstock often contains a mixture of coating layers, dopants, binders, and electrolyte decomposition fragments. Thus, achieving high product purity remains challenging. The impurities are often introduced during collection, storage, and disassembly, and are difficult to remove without compromising the target product. In addition, the heterogeneous nature of spent LIBs, which varies in chemistry, aging state, and manufacturer design, further complicates the purification process. Therefore, ensuring product quality at the industrial scale requires rigorous control of upstream processes, which increases operational complexity and cost. Overcoming these purity challenges demands the development of efficient separation technologies and real-time monitoring systems. Specifically, process-integrated purification strategies and closed-loop feedback mechanisms could improve material quality consistency.

(3) Upcycling: a key challenge in direct recycling lies in the material mismatch between cathodes currently in use and those required to meet future energy density demands. This discrepancy creates a gap between future applications and existing battery waste streams. Therefore, strategies for upcycling, transforming lower-performance recycled cathodes into high-value materials, are essential for maximizing the economic potential for direct recycling. For example, adding $TM(OH)_2$ into the feedstock enables the upcycling of low-nickel NMC into high-nickel NMC.[190] However, the inhomogeneous diffusivity and solubility of TM from the surface to the bulk has led to uneven stoichiometry, concentration gradients, and internal particle strain, ultimately undermining structural integrity. Thus, detecting micron-level particle integrity in real time and controlling diffusivity of different ions over varying grain sizes and morphology are critical. AI-driven models can analyze sensor data from spectroscopy or tomography in real time and dynamically adjust processing parameters to maintain material quality. Furthermore, closed-loop control systems can automatically adjust temperature, atmosphere, and precursor feeding based on detected deviations, enhancing the consistency and scalability of direct recycling processes.

(4) Life cycle assessment (LCA) and techno-economic analysis (TEA): LCA and TEA are critical in guiding the optimization and practical implementation of direct recycling. While lab-scale studies focus on material recovery and electrochemical performance, LCA provides a system-level evaluation of the environmental impacts, including energy consumption, GHG emissions, and resource utilization across the entire process chain.[219] Meanwhile, TEA assesses economic feasibility by quantifying process costs, capital investment, and operational efficiency.[220] They optimize the process by identifying steps with the highest energy demand and cost within the recycling workflow, thereby redirecting efforts toward the most impactful stages. For example, intensive thermal or solvent-based processes may improve material recovery but increase energy demand and environmental burden. Integrating LCA and TEA into protocol design enables trade-off analysis and comprehensive decision-making, ensuring environmental and economic viability as well as technical performance. Future efforts should couple LCA and TEA with process design in a closed-loop framework to enable data-driven optimization.

To bridge the gap between lab-scale studies and industrial implementation, a general roadmap toward direct recycling industrialization can be outlined. First, safe and automative pretreatment is required, including battery discharge, diagnostic sorting, and efficient disassembly to reduce labor intensity and handle diverse material feedstocks. Second, scalable separation and regeneration processes should be coupled with impurity control, green processing strategies, and real-time monitoring to ensure robust product quality. Third, industrialization requires continuous and closed-loop process design, including standardized evaluation metrics, pilot-scale validation, and LCA/TEA. In the long term, transparent and automated recycling systems, supported by battery passports and AI-driven robotics, will further enable a sustainable recycling ecosystem.[221]

Building on this roadmap, the goal of direct recycling is successful scale-up, which requires process optimization and precise control of key parameters through industrial-grade equipment. Cost-effective and automative pretreatment of the spent batteries is essential to manage diverse cell designs, while innovations in cell designs and intelligence systems can reduce labor demands. A comprehensive assessment of direct recycling and advanced upcycling is necessary from the perspective of technical, economic, environmental impacts, validating the feasibility of large-scale production. In addition, establishing

standardized evaluation metrics is critical to quantitatively compare and benchmark different direct recycling strategies. Key indicators, such as material recovery efficiency, energy consumption, process cost, and product quality, should be systematically defined and reported to guide technical optimization and support the transition from lab-scale demonstrations to industrial implementation. Finally, establishing pilot plants is crucial to demonstrate process stability and economic viability, while robust supply chains and policy compliance support smooth scaling-up.

Conflicts of interest

There are no conflicts to declare.

Data availability

No primary research results, software or code have been included and no new data were generated or analysed as part of this review.

Acknowledgements

The authors acknowledge the financial support from Michigan State University.

References

1 M. L. Machala, X. Chen, S. P. Bunke, G. Forbes, A. Yegizbay, J. A. de Chalendar, I. L. Azevedo, S. Benson and W. A. Tarpeh, Life cycle comparison of industrial-scale lithium-ion battery recycling and mining supply chains, *Nat. Commun.*, 2025, **16**(1), 988.
2 S. Srinivasan, S. Shanthakumar and B. Ashok, Sustainable lithium-ion battery recycling: A review on technologies, regulatory approaches and future trends, *Energy Rep.*, 2025, **13**, 789–812.
3 M. Chen, X. Ma, B. Chen, R. Arsenault, P. Karlson, N. Simon and Y. Wang, Recycling end-of-life electric vehicle lithium-ion batteries, *Joule*, 2019, **3**(11), 2622–2646.
4 R. E. Ciez and J. F. Whitacre, Examining different recycling processes for lithium-ion batteries, *Nat Sustainability*, 2019, **2**(2), 148–156.
5 G. Harper, R. Sommerville, E. Kendrick, L. Driscoll, P. Slater, R. Stolkin, A. Walton, P. Christensen, O. Heidrich, S. Lambert, A. Abbott, K. Ryder, L. Gaines and P. Anderson, Recycling lithium-ion batteries from electric vehicles, *Nature*, 2019, **575**(7781), 75–86.
6 X. Ma, Z. Meng, M. V. Bellonia, J. Spangenberger, G. Harper, E. Gratz, E. Olivetti, R. Arsenault and Y. Wang, The evolution of lithium-ion battery recycling, *Nature Reviews Clean Technology*, 2025, **1**(1), 75–94.
7 Y. Zhao, H. Du, Y. Kang, J. Zhang, B. Lan, Z. Guo, M.-M. Titirici, Y. Zhao, N. Tavajohi, F. Kang and B. Li, Spent battery regeneration for better recycling, *Nat. Rev. Mater.*, 2025, **10**(10), 722–724.
8 Z. Liang, C. Cai, G. Peng, J. Hu, H. Hou, B. Liu, S. Liang, K. Xiao, S. Yuan and J. Yang, Hydrometallurgical recovery of spent lithium ion batteries: Environmental strategies and sustainability evaluation, *ACS Sustainable Chem. Eng.*, 2021, **9**(17), 5750–5767.
9 T. A. Atia, G. Elia, R. Hahn, P. Altimari and F. Pagnanelli, Closed-loop hydrometallurgical treatment of end-of-life lithium ion batteries: Towards zero-waste process and metal recycling in advanced batteries, *J. Energy Chem.*, 2019, **35**, 220–227.
10 T. Georgi-Maschler, B. Friedrich, R. Weyhe, H. Heegn and M. Rutz, Development of a recycling process for Li-ion batteries, *J. Power Sources*, 2012, **207**, 173–182.
11 X. Ma, M. Chen, Z. Zheng, D. Bullen, J. Wang, C. Harrison, E. Gratz, Y. Lin, Z. Yang, Y. Zhang, F. Wang, D. Robertson, S.-B. Son, I. Bloom, J. Wen, M. Ge, X. Xiao, W.-K. Lee, M. Tang, Q. Wang, J. Fu, Y. Zhang, B. C. Sousa, R. Arsenault, P. Karlson, N. Simon and Y. Wang, Recycled cathode materials enabled superior performance for lithium-ion batteries, *Joule*, 2021, **5**(11), 2955–2970.
12 T. Or, S. W. D. Gourley, K. Kaliyappan, A. Yu and Z. Chen, Recycling of mixed cathode lithium-ion batteries for electric vehicles: Current status and future outlook, *Carbon Energy*, 2020, **2**(1), 6–43.
13 T. Kim, L. K. Ono and Y. Qi, Understanding the active formation of a cathode-electrolyte interphase (CEI) layer with energy level band bending for lithium-ion batteries, *J. Mater. Chem. A*, 2023, **11**(1), 221–231.
14 H. Wang, X. Li, F. Li, X. Liu, S. Yang and J. Ma, Formation and modification of cathode electrolyte interphase: A mini review, *Electrochem. Commun.*, 2021, **122**, 106870.
15 G. Zan, J. Zhang, F. Monaco, S. Gul, G. Qian, J. Li, D. J. Vine, P. Cloetens, W. Yun, P. Pianetta and Y. Liu, Understanding multi-scale battery degradation with a macro-to-nano zoom through its hierarchy, *J. Mater. Chem. A*, 2021, **9**(35), 19886–19893.
16 L. Wang, J. Qiu, X. Wang, L. Chen, G. Cao, J. Wang, H. Zhang and X. He, Insights for understanding multiscale degradation of $LiFePO_4$ cathodes, *eScience*, 2022, **2**(2), 125–137.
17 D. Li, C. Shen, Y. Zheng and J. Xu, Electrochemo-mechanical degradation and failure of active particles in high energy density batteries: A review, *Small*, 2025, **21**(8), 2407740.
18 L. Wuschke, H.-G. Jäckel, T. Leißner and U. A. Peuker, Crushing of large Li-ion battery cells, *Waste Manage.*, 2019, **85**, 317–326.
19 X. Zhong, W. Liu, J. Han, F. Jiao, W. Qin, T. Liu and C. Zhao, Pyrolysis and physical separation for the recovery of spent $LiFePO_4$ batteries, *Waste Manage.*, 2019, **89**, 83–93.
20 A. Kaas, C. Wilke and U. A. Peuker, Influence of shredder and mill settings on the material recoveries and product qualities of a two-stage mechanical recycling process of automotive lithium-ion batteries, *Waste Manage.*, 2025, **204**, 114912.

21 H. Luo, J. Zhu, E. Sahraei and Y. Xia, Adhesion strength of the cathode in lithium-ion batteries under combined tension/shear loadings, *RSC Adv.*, 2018, **8**(8), 3996–4005.
22 G. Hong, N. Li, H. Yang, H.-s. Chen, W. Song and D. Fang, Changes of adhesion properties for negative electrode and positive electrode under wet conditions and different states of charge, *Int. J. Adhes. Adhes.*, 2021, **108**, 102870.
23 Z. Shuguang, H. Wenzhi, L. Guangming, Z. Xu, H. Juwen and Z. Xiaojun, Recovering copper from spent lithium ion battery by a mechanical separation process, in *2011 International Conference on Materials for Renewable Energy & Environment*, 2011, pp. 1008–1012.
24 X. Cao, Y. Xu, L. Zou, J. Bao, Y. Chen, B. E. Matthews, J. Hu, X. He, M. H. Engelhard, C. Niu, B. W. Arey, C. Wang, J. Xiao, J. Liu, C. Wang, W. Xu and J.-G. Zhang, Stability of solid electrolyte interphases and calendar life of lithium metal batteries, *Energy Environ. Sci.*, 2023, **16**(4), 1548–1559.
25 J. Lin, E. Fan, X. Zhang, R. Chen, F. Wu and L. Li, Sustainable recycling of cathode scrap towards high-performance anode materials for Li-ion batteries, *Adv. Energy Mater.*, 2022, **12**, 2103288.
26 S. Kim, J. Bang, J. Yoo, Y. Shin, J. Bae, J. Jeong, K. Kim, P. Dong and K. Kwon, A comprehensive review on the pretreatment process in lithium-ion battery recycling, *J. Cleaner Prod.*, 2021, **294**, 126329.
27 T. Zhang, Y. He, L. Ge, R. Fu, X. Zhang and Y. Huang, Characteristics of wet and dry crushing methods in the recycling process of spent lithium-ion batteries, *J. Power Sources*, 2013, **240**, 766–771.
28 M. Bhar, S. Ghosh, S. Krishnamurthy, Y. Kaliprasad and S. K. Martha, A review on spent lithium-ion battery recycling: From collection to black mass recovery, *RSC Sustainability*, 2023, **1**(5), 1150–1167.
29 Z. Meng, X. Ma, J. Hou, Y. Zheng and Y. Wang, Impurity impacts of recycling NMC cathodes, *Adv. Energy Mater.*, 2025, **15**(46), 2405383.
30 C. Hu, H. Yi, H. Fang, B. Yang, Y. Yao, W. Ma and Y. Dai, Suppressing Li_3PO_4 impurity formation in $LiFePO_4/Fe_2P$ by a nonstoichiometry synthesis and its effect on electrochemical properties, *Mater. Lett.*, 2011, **65**(9), 1323–1326.
31 M. C. Rehwoldt, Y. Wang, F. Xu, P. Ghildiyal and M. R. Zachariah, High-temperature interactions of metal oxides and a PVDF binder, *ACS Appl. Mater. Interfaces*, 2022, **14**(7), 8938–8946.
32 S. Chen, T. He, Y. Lu, Y. Su, J. Tian, N. Li, G. Chen, L. Bao and F. Wu, Renovation of $LiCoO_2$ with outstanding cycling stability by thermal treatment with Li_2CO_3 from spent Li-ion batteries, *J. Energy Storage*, 2016, **8**, 262–273.
33 V. Gupta, M. Appleberry, W. Li and Z. Chen, Direct recycling industrialization of Li-ion batteries: The pre-processing barricade, *Next Energy*, 2024, **2**, 100091.
34 L. Zhang, H. Gao, Y. Zhu, I. Tran, W. Tang, J. Lin, A. U. Mu, J. Wu, W. Li, D. Nordlund, L. Mu and Z. Chen, Unveiling the role of critical impurities in spent $LiFePO_4$ cathodes for scalable direct regeneration, *Adv. Energy Mater.*, 2025, **15**(46), 2406084.
35 S. Bao, Z. Wang, W. Ding, Y. Zhang, C. Liu, H. Zhang, B. Chen, C. Xin and K. Xu, Emerging green recycling technologies for spent lithium-ion batteries: a comprehensive review integrating and innovating traditional methods, *Green Chem.*, 2026, **28**(8), 3394–3431.
36 A. Sen, P. Kumari and R. Kundu, Regeneration of spent LIB electrode materials: An outlook from lab-scale feasibility to industrial integration, *Energy Fuels*, 2025, **39**(29), 13879–13904.
37 W. Li, Q. Yin and Z. Chen, Managing impurities in direct battery recycling: Advancing separation and purification for high-quality feedstocks, *ACS Energy Lett.*, 2026, **11**(1), 137–147.
38 X. Zhang, Q. Xue, L. Li, E. Fan, F. Wu and R. Chen, Sustainable recycling and regeneration of cathode scraps from industrial production of lithium-ion batteries, *ACS Sustainable Chem. Eng.*, 2016, **4**(12), 7041–7049.
39 D. G. Lee, R. K. Gupta, Y. S. Cho and K. T. Hwang, Improved electrochemical properties of $Li(Ni_{0.7}Co_{0.3})O_2$ cathode for lithium ion batteries with controlled sintering conditions, *J. Appl. Electrochem.*, 2009, **39**(5), 671–679.
40 Z. Qiu, Z. Wang and S. Yuan, How sintering temperature affects the electrochemical performance of ultra-high nickel (Ni > 0.9) cathode material, *J. Colloid Interface Sci.*, 2024, **656**, 225–232.
41 H. Zhang, X. He, Z. Chen, Y. Yang, H. Xu, L. Wang and X. He, Single-crystalline Ni-rich $LiNixMnyCo_{1-x-y}O_2$ cathode materials: A perspective, *Adv. Energy Mater.*, 2022, **12**(45), 2202022.
42 M. Wang, Q. Tan, L. Liu and J. Li, A Facile, environmentally friendly, and low-temperature approach for decomposition of polyvinylidene fluoride from the cathode electrode of spent lithium-ion batteries, *ACS Sustainable Chem. Eng.*, 2019, 7(15), 12799–12806.
43 B. J. Ross, M. LeResche, D. Liu, J. L. Durham, E. U. Dahl and A. L. Lipson, Mitigating the impact of thermal binder removal for direct Li-ion battery recycling, *ACS Sustainable Chem. Eng.*, 2020, **8**(33), 12511–12515.
44 M. Wang, Q. Tan, L. Liu and J. Li, Efficient separation of aluminum foil and cathode materials from spent lithium-ion batteries using a low-temperature molten salt, *ACS Sustainable Chem. Eng.*, 2019, 7(9), 8287–8294.
45 Y. Zha, Q. Meng, P. Dong and Y. Zhang, The latest research on the pre-treatment and recovery methods of spent lithium-ion battery cathode material, *Ionics*, 2024, **30**(2), 623–645.
46 H. Gao, Y. Zhang, Y. Meng, X. Liu and F. Zhu, Regeneration of waste $LiCoO_2$ cathode materials with high energy stripping of laser, *J. Electroanal. Chem.*, 2022, **908**, 116100.
47 C. Tokoro, S. Lim, K. Teruya, M. Kondo, K. Mochidzuki, T. Namihira and Y. Kikuchi, Separation of cathode particles and aluminum current foil in Lithium-Ion battery by high-voltage pulsed discharge Part I: Experimental investigation, *Waste Manage.*, 2021, **125**, 58–66.
48 J. Zhou, X. Zhou, W. Yu, Z. Shang and S. Xu, Towards greener recycling: Direct repair of cathode materials in

spent lithium-ion batteries, *Electrochem. Energy Rev.*, 2024, **7**(1), 13.
49 N. Akhmetov, A. Manakhov and A. S. Al-Qasim, Li-ion battery cathode recycling: an emerging response to growing metal demand and accumulating battery waste, *Electronics*, 2023, **12**(5), 1152.
50 H. Bi, H. Zhu, L. Zu, Y. Gao, S. Gao and Z. Wu, Eddy current separation for recovering aluminium and lithium-iron phosphate components of spent lithium-iron phosphate batteries, *Waste Manag. Res.*, 2019, **37**(12), 1217–1228.
51 F. Yu, W. Chen and D. Zhang, The research of simulation on eddy current separation process based on MATLAB and COMSOL, *Proced. CIRP*, 2016, **56**, 520–523.
52 J. R. Nagel, An analytic model for eddy current separation, *Miner. Eng.*, 2018, **127**, 277–285.
53 H. Bi, H. Zhu, L. Zu, Y. Bai, S. Gao and Y. Gao, A new model of trajectory in eddy current separation for recovering spent lithium iron phosphate batteries, *Waste Manage.*, 2019, **100**, 1–9.
54 S. Zhang, E. Forssberg, B. Arvidson and W. Moss, Aluminum recovery from electronic scrap by High-Force® eddy-current separators, *Resour. Conserv. Recycl.*, 1998, **23**(4), 225–241.
55 W. Xue, M. Huang, Y. Li, Y. G. Zhu, R. Gao, X. Xiao, W. Zhang, S. Li, G. Xu, Y. Yu, P. Li, J. Lopez, D. Yu, Y. Dong, W. Fan, Z. Shi, R. Xiong, C.-J. Sun, I. Hwang, W.-K. Lee, Y. Shao-Horn, J. A. Johnson and J. Li, Ultra-high-voltage Ni-rich layered cathodes in practical Li metal batteries enabled by a sulfonamide-based electrolyte, *Nat. Energy*, 2021, **6**(5), 495–505.
56 R. Zhan, Z. Oldenburg and L. Pan, Recovery of active cathode materials from lithium-ion batteries using froth flotation, *Sustain. Mater. Technol.*, 2018, **17**, e00062.
57 J. Li, J. Zhang, W. Zhao, D. Lu, G. Ren and Y. Tu, Application of roasting flotation technology to enrich valuable metals from spent $LiFePO_4$ batteries, *ACS Omega*, 2022, **7**, 25590–25599.
58 G. Zhang, L. Ding, X. Yuan, Y. He, H. Wang and J. He, Recycling of electrode materials from spent lithium-ion battery by pyrolysis-assisted flotation, *J. Environ. Chem. Eng.*, 2021, **9**(6), 106777.
59 Y. He, T. Zhang, F. Wang, G. Zhang, W. Zhang and J. Wang, Recovery of $LiCoO_2$ and graphite from spent lithium-ion batteries by Fenton reagent-assisted flotation., *J. Cleaner Prod.*, 2017, **143**, 319–325.
60 Y. Miao, S. Wen, Q. Feng and R. Liao, Surface modification of ilmenite and flotation improvement using Fenton as an oxidant, *Appl. Surf. Sci.*, 2021, **555**, 149749.
61 S. C. Chelgani, M. Parian, P. S. Parapari, Y. Ghorbani and J. Rosenkranz, A comparative study on the effects of dry and wet grinding on mineral flotation separation–a review, *J. Mater. Res. Technol.*, 2019, **8**(5), 5004–5011.
62 W. J. Bruckard, G. J. Sparrow and J. T. Woodcock, A review of the effects of the grinding environment on the flotation of copper sulphides, *Int. J. Miner. Process.*, 2011, **100**(1), 1–13.
63 J. Yu, Y. He, Z. Ge, H. Li, W. Xie and S. Wang, A promising physical method for recovery of $LiCoO_2$ and graphite from spent lithium-ion batteries: Grinding flotation, *Sep. Purif. Technol.*, 2018, **190**, 45–52.
64 X. Ma, P. Ge, L. Wang, W. Sun, Y. Bu, M. Sun and Y. Yang, The recycling of spent lithium-ion batteries: Crucial flotation for the separation of cathode and anode materials, *Molecules*, 2023, **28**(10), 4081.
65 D. Garcia-Gonzalez, S. Garzon-Hernandez, A. Rusinek, R. Bernier and A. Arias, Low temperature mechanical behaviour of PVDF: cryogenic pre-treatment, quasi-static, cyclic and dynamic experimental testing and modelling, *Mech. Mater.*, 2020, **147**, 103436.
66 J. Liu, X. Bai, J. Hao, H. Wang, T. Zhang, X. Tang, S. Wang and Y. He, Efficient liberation of electrode materials in spent lithium-ion batteries using a cryogenic ball mill, *J. Environ. Chem. Eng.*, 2021, **9**(5), 106017.
67 H. Wang, J. Liu, X. Bai, S. Wang, D. Yang, Y. Fu and Y. He, Separation of the cathode materials from the Al foil in spent lithium-ion batteries by cryogenic grinding, *Waste Manage.*, 2019, **91**, 89–98.
68 J. Liu, H. Wang, T. Hu, X. Bai, S. Wang, W. Xie, J. Hao and Y. He, Recovery of $LiCoO_2$ and graphite from spent lithium-ion batteries by cryogenic grinding and froth flotation, *Miner. Eng.*, 2020, **148**, 106223.
69 B. Zhang, Y. Xu, D. S. Silvester, C. E. Banks, W. Deng, G. Zou, H. Hou and X. Ji, Direct regeneration of cathode materials in spent lithium-ion batteries toward closed-loop recycling and sustainability, *J. Power Sources*, 2024, **589**, 233728.
70 Y. Ji, C. T. Jafvert, E. E. Kpodzro and F. Zhao, Chemical-free pressure washing system as pretreatment to harvest cathode materials, *Waste Manage.*, 2022, **153**, 121–128.
71 L.-P. He, S.-Y. Sun, X.-F. Song and J.-G. Yu, Recovery of cathode materials and Al from spent lithium-ion batteries by ultrasonic cleaning, *Waste Manage.*, 2015, **46**, 523–528.
72 M. C. Shinzato and R. Hypolito, Solid waste from aluminum recycling process: characterization and reuse of its economically valuable constituents, *Waste Manage.*, 2005, **25**(1), 37–46.
73 K. P. Lee, N. C. Chromey, R. Culik, J. R. Barnes and P. W. Schneider, Toxicity of N-methyl-2-pyrrolidone (NMP): Teratogenic, subchronic, and two-year inhalation studies, *Fundam. Appl. Toxicol.*, 1987, **9**(2), 222–235.
74 Y. Bai, N. Muralidharan, J. Li, R. Essehli and I. Belharouak, Sustainable direct recycling of lithium-ion batteries via solvent recovery of electrode materials, *ChemSusChem*, 2020, **13**(21), 5664–5670.
75 S. Rose, P. Xu, H. Gao, M. Li, X. Yu and Z. Chen, Boosting the recycling efficiency of spent lithium-ion battery cathodes using a green reductant, *Adv. Energy Sustainability Res.*, 2021, **2**(8), 2100040.
76 S. Paul and P. Shrotriya, Efficient recycling processes for lithium-ion batteries, *Materials*, 2025, **18**(3), 613.
77 W. Hayduk and V. K. Malik, Density, viscosity, and carbon dioxide solubility and diffusivity in aqueous ethylene glycol solutions, *J. Chem. Eng. Data*, 1971, **16**(2), 143–146.

78 A. R. Harifi-Mood and R. Buchner, Density, viscosity, and conductivity of choline chloride+ethylene glycol as a deep eutectic solvent and its binary mixtures with dimethyl sulfoxide, *J. Mol. Liq.*, 2017, **225**, 689–695.

79 Y. Yao, M. Zhu, Z. Zhao, B. Tong, Y. Fan and Z. Hua, Hydrometallurgical processes for recycling spent lithium-ion batteries: A critical review, *ACS Sustainable Chem. Eng.*, 2018, **6**(11), 13611–13627.

80 L. Li, T. Yang and Z. Li, Parameter optimization and yield prediction of cathode coating separation process for direct recycling of end-of-life lithium-ion batteries, *RSC Adv.*, 2021, **11**(39), 24132–24136.

81 D. Song, X. Wang, E. Zhou, P. Hou, F. Guo and L. Zhang, Recovery and heat treatment of the $Li(Ni_{1/3}Co_{1/3}Mn_{1/3})O_2$ cathode scrap material for lithium ion battery, *J. Power Sources*, 2013, **232**, 348–352.

82 Y. Fu, J. Schuster, M. Petranikova and B. Ebin, Innovative recycling of organic binders from electric vehicle lithium-ion batteries by supercritical carbon dioxide extraction, *Resour., Conserv. Recycl.*, 2021, **172**, 105666.

83 Z. Qin, J. Li, T. Zhang, Z. Wen, Z. Zheng, Y. Zhang, N. Zhang, C. Jia, X. Liu and G. Chen, Effective separation of $LiNi_{0.5}Co_{0.2}Mn_{0.3}O_2$ cathode material and Al foil via digestion of PVDF enabling a closed-loop recycle, *J. Mater. Chem. A*, 2022, **10**(44), 23905–23914.

84 Y. Wang, N. An, L. Wen, L. Wang, X. Jiang, F. Hou, Y. Yin and J. Liang, Recent progress on the recycling technology of Li-ion batteries, *J. Energy Chem.*, 2021, **55**, 391–419.

85 E. Fan, L. Li, X. Zhang, Y. Bian, Q. Xue, J. Wu, F. Wu and R. Chen, Selective recovery of Li and Fe from spent lithium-ion batteries by an environmentally friendly mechanochemical approach, *ACS Sustainable Chem. Eng.*, 2018, **6**(8), 11029–11035.

86 Y. Yang, X. Zheng, H. Cao, C. Zhao, X. Lin, P. Ning, Y. Zhang, W. Jin and Z. Sun, A closed-loop process for selective metal recovery from spent lithium iron phosphate batteries through mechanochemical activation, *ACS Sustainable Chem. Eng.*, 2017, **5**(11), 9972–9980.

87 L. Li, E. Fan, Y. Guan, X. Zhang, Q. Xue, L. Wei, F. Wu and R. Chen, Sustainable recovery of cathode materials from spent lithium-ion batteries using lactic acid leaching system, *ACS Sustainable Chem. Eng.*, 2017, **5**(6), 5224–5233.

88 L. Li, Y. Bian, X. Zhang, Y. Guan, E. Fan, F. Wu and R. Chen, Process for recycling mixed-cathode materials from spent lithium-ion batteries and kinetics of leaching, *Waste Manage.*, 2018, **71**, 362–371.

89 A. P. Abbott, G. Capper, D. L. Davies, H. L. Munro, R. K. Rasheed and V. Tambyrajah, Preparation of novel, moisture-stable, Lewis-acidic ionic liquids containing quaternary ammonium salts with functional side chains, *Chem. Commun.*, 2001, (19), 2010–2011.

90 D. Yetim, L. Svecova and J.-C. Leprêtre, Lithium-Ion battery cathode recycling through a closed-loop process using a choline chloride-ethylene glycol-based deep-eutectic solvent in the presence of acid, *ChemistryOpen*, 2024, **13**(2), e202300061.

91 N. Peeters, K. Janssens, D. de Vos, K. Binnemans and S. Riaño, Choline chloride–ethylene glycol based deep-eutectic solvents as lixiviants for cobalt recovery from lithium-ion battery cathode materials: are these solvents really green in high-temperature processes?, *Green Chem.*, 2022, **24**(17), 6685–6695.

92 Y. Chen, Y. Lu, Z. Liu, L. Zhou, Z. Li, J. Jiang, L. Wei, P. Ren and T. Mu, Efficient dissolution of lithium-ion batteries cathode $LiCoO_2$ by polyethylene glycol-based deep eutectic solvents at mild temperature, *ACS Sustainable Chem. Eng.*, 2020, **8**(31), 11713–11720.

93 M. K. Tran, M.-T. F. Rodrigues, K. Kato, G. Babu and P. M. Ajayan, Deep eutectic solvents for cathode recycling of Li-ion batteries, *Nat. Energy*, 2019, **4**(4), 339–345.

94 P. Li, H. Xu, S. Luo, Y. Wang, L. Zhang, Y. Lin, Z. Li, J. Guo, Y. Xu, Y. Zhang and Y. Yue, Green and non-destructive separation of cathode materials from aluminum foil in spent lithium-ion batteries, *Sep. Purif. Technol.*, 2024, **338**, 126625.

95 M. Wang, Q. Tan, L. Liu and J. Li, A low-toxicity and high-efficiency deep eutectic solvent for the separation of aluminum foil and cathode materials from spent lithium-ion batteries, *J. Hazard. Mater.*, 2019, **380**, 120846.

96 J. Senćanski, D. Bajuk-Bogdanović, D. Majstorović, E. Tchernychova, J. Papan and M. Vujković, The synthesis of $Li(CoMnNi)O_2$ cathode material from spent-Li ion batteries and the proof of its functionality in aqueous lithium and sodium electrolytic solutions, *J. Power Sources*, 2017, **342**, 690–703.

97 H. Pinegar and Y. R. Smith, End-of-life lithium-ion battery component mechanical liberation and separation, *JOM*, 2019, **71**(12), 4447–4456.

98 F. Pagnanelli, E. Moscardini, G. Granata, S. Cerbelli, L. Agosta, A. Fieramosca and L. Toro, Acid reducing leaching of cathodic powder from spent lithium ion batteries: Glucose oxidative pathways and particle area evolution, *J. Ind. Eng. Chem.*, 2014, **20**(5), 3201–3207.

99 L. Kong, F. Liu, X. Hu, Z. Shi, A. Liu and X. Wang, An improved pretreatment method for recovering cathode materials from lithium-ion battery: ultrasonic-assisted NaOH-enhanced dissolving, *Energy Sources, Part A*, 2023, **45**(1), 877–887.

100 K. Mizushima, P. C. Jones, P. J. Wiseman and J. B. Goodenough, Li_xCoO_2 ($0<x\leqq1$): A new cathode material for batteries of high energy density, *Solid State Ionics*, 1981, **3–4**, 171–174.

101 B. Chu, Y.-J. Guo, J.-L. Shi, Y.-X. Yin, T. Huang, H. Su, A. Yu, Y.-G. Guo and Y. Li, Cobalt in high-energy-density layered cathode materials for lithium ion batteries, *J. Power Sources*, 2022, **544**, 231873.

102 R. Konar, S. Maiti, N. Shpigel and D. Aurbach, Reviewing failure mechanisms and modification strategies in stabilizing high-voltage $LiCoO_2$ cathodes beyond 4.55V, *Energy Storage Mater.*, 2023, **63**, 103001.

103 J. Qian, L. Liu, J. Yang, S. Li, X. Wang, H. L. Zhuang and Y. Lu, Electrochemical surface passivation of $LiCoO_2$

particles at ultrahigh voltage and its applications in lithium-based batteries, *Nat. Commun.*, 2018, **9**(1), 4918.

104 Y. Yao, Z. Xue, C. Li, J. Li, J. He, X. Zhang and Y. Xiang, Progress and perspective of doping strategies for lithium cobalt oxide materials in lithium-ion batteries, *Energy Storage Mater.*, 2024, **71**, 103666.

105 X. Ma, J. Wang, Z. Wang, L. Wang, H. Xu and X. He, Engineering strategies for high-voltage $LiCoO_2$ based high-energy Li-ion batteries, *Electron*, 2024, **2**(3), e33.

106 S. Li, K. Li, J. Zheng, Q. Zhang, B. Wei and X. Lu, Structural distortion-induced charge gradient distribution of co ions in delithiated $LiCoO_2$ cathode, *J. Phys. Chem. Lett.*, 2019, **10**(24), 7537–7546.

107 C. Sun, X. Liao, F. Xia, Y. Zhao, L. Zhang, S. Mu, S. Shi, Y. Li, H. Peng, G. Van Tendeloo, K. Zhao and J. Wu, High-voltage cycling induced thermal vulnerability in $LiCoO_2$ cathode: Cation loss and oxygen release driven by oxygen vacancy migration, *ACS Nano*, 2020, **14**(5), 6181–6190.

108 M. Duffiet, D. Goonetilleke, F. Fauth, T. Brezesinski, J. Janek and M. Bianchini, Real-time crystallization of $LiCoO_2$ from β-$Co(OH)_2$ and Co_3O_4: Synthetic pathways and structural evolution, *Chem. Mater.*, 2022, **34**(22), 9955–9969.

109 C. Weng, M. Qiu, B. Wang, J. Yang, W. Mai, L. Pan, S. Huang and J. Li, Organic cathode electrolyte interphase achieving 4.8 V $LiCoO_2$, *Angew. Chem., Int. Ed.*, 2025, **64**(7), e202419539.

110 J. Xu, Critical review on cathode-electrolyte interphase toward high-voltage cathodes for Li-ion batteries, *Nano-Micro Lett.*, 2022, **14**(1), 166.

111 X. Yang, Y. Lin, S. Tang, Y. Zhou, X. Huang, W. Song, W. Yang and Y. Yang, Interplay of interfacial and structural cracking degradation modes for the high-voltage $LiCoO_2$ cathode at particle's level, *Energy Storage Mater.*, 2025, **81**, 104473.

112 P. Xu, D. H. S. Tan, B. Jiao, H. Gao, X. Yu and Z. Chen, A materials perspective on direct recycling of lithium-ion batteries: Principles, challenges and opportunities, *Adv. Funct. Mater.*, 2023, **33**(14), 2213168.

113 H.-J. Noh, S. Youn, C. S. Yoon and Y.-K. Sun, Comparison of the structural and electrochemical properties of layered Li $[Ni_xCo_yMn_z]O_2$ (x = 1/3, 0.5, 0.6, 0.7, 0.8 and 0.85) cathode material for lithium-ion batteries, *J. Power Sources*, 2013, **233**, 121–130.

114 A. Chakraborty, S. Kunnikuruvan, S. Kumar, B. Markovsky, D. Aurbach, M. Dixit and D. T. Major, Layered Cathode Materials for Lithium-Ion Batteries: Review of Computational Studies on LiNi1–x–yCoxMnyO2 and LiNi1–x–yCoxAlyO2, *Chem. Mater.*, 2020, **32**(3), 915–952.

115 M. Zheng, Y. You and J. Lu, Understanding materials failure mechanisms for the optimization of lithium-ion battery recycling, *Nat. Rev. Mater.*, 2025, **10**(5), 355–368.

116 S. S. Zhang, Problems and their origins of Ni-rich layered oxide cathode materials, *Energy Storage Mater.*, 2020, **24**, 247–254.

117 Z. Dai, Z. Li, R. Chen, F. Wu and L. Li, Defective oxygen inert phase stabilized high-voltage nickel-rich cathode for high-energy lithium-ion batteries, *Nat. Commun.*, 2023, **14**(1), 8087.

118 Y. Zhu, Y. Huang, R. Du, M. Tang, B. Wang and J. Zhang, Effect of Ni^{2+} on lithium-ion diffusion in layered $LiNi_{1-x-y}Mn_xCo_yO_2$ materials, *Crystals*, 2021, **11**(5), 465.

119 F. Zhang, S. Lou, S. Li, Z. Yu, Q. Liu, A. Dai, C. Cao, M. F. Toney, M. Ge, X. Xiao, W.-K. Lee, Y. Yao, J. Deng, T. Liu, Y. Tang, G. Yin, J. Lu, D. Su and J. Wang, Surface regulation enables high stability of single-crystal lithium-ion cathodes at high voltage, *Nat. Commun.*, 2020, **11**(1), 3050.

120 W. Zeng, F. Liu, J. Yang, B. Zhang, F. Cao, W. Tian, J. Wang, R. Yu, F. Xia, H. Peng, J. Ma, Z. Wang, S. Mu and J. Wu, Single-crystal Li-rich layered cathodes with suppressed voltage decay by double-layer interface engineering, *Energy Storage Mater.*, 2023, **54**, 651–660.

121 Y. Chu, Y. Mu, L. Zou, F. Wu, L. Yang, Y. Feng and L. Zeng, Oxygen release in Ni-rich layered cathode for lithium-ion batteries: Mechanisms and mitigating strategies, *ChemElectroChem*, 2024, **11**(14), e202300653.

122 W. M. Dose, I. Temprano, J. P. Allen, E. Björklund, C. A. O'Keefe, W. Li, B. L. Mehdi, R. S. Weatherup, M. F. L. De Volder and C. P. Grey, Electrolyte reactivity at the charged Ni-rich cathode interface and degradation in Li-ion batteries, *ACS Appl. Mater. Interfaces*, 2022, **14**(11), 13206–13222.

123 Y. Bi, J. Tao, Y. Wu, L. Li, Y. Xu, E. Hu, B. Wu, J. Hu, C. Wang, J.-G. Zhang, Y. Qi and J. Xiao, Reversible planar gliding and microcracking in a single-crystalline Ni-rich cathode, *Science*, 2020, **370**(6522), 1313–1317.

124 A. K. Padhi, K. S. Nanjundaswamy and J. B. Goodenough, Phospho-olivines as positive-electrode materials for rechargeable lithium batteries, *J. Electrochem. Soc.*, 1997, **144**(4), 1188.

125 Y. Guo, Y. Yao, C. Guo, Y. Song, P. Huang, X. Liao, K. He, H. Zhang, H. Liu, R. Hu, W. Wang, C. Li, S. Wang, A. Nie, Y. Yuan and Y. Huang, Atomistic observation and transient reordering of antisite Li/Fe defects toward sustainable $LiFePO_4$, *Energy Environ. Sci.*, 2024, **17**(20), 7749–7761.

126 M. S. Islam, D. J. Driscoll, C. A. J. Fisher and P. R. Slater, Atomic-scale investigation of defects, dopants, and lithium transport in the $LiFePO_4$ olivine-type battery material, *Chem. Mater.*, 2005, **17**(20), 5085–5092.

127 D. Wang, X. Wu, Z. Wang and L. Chen, Cracking causing cyclic instability of $LiFePO_4$ cathode material, *J. Power Sources*, 2005, **140**(1), 125–128.

128 H. Nie, L. Xu, D. Song, J. Song, X. Shi, X. Wang, L. Zhang and Z. Yuan, $LiCoO_2$: recycling from spent batteries and regeneration with solid state synthesis, *Green Chem.*, 2015, **17**(2), 1276–1280.

129 X. Meng, J. Hao, H. Cao, X. Lin, P. Ning, X. Zheng, J. Chang, X. Zhang, B. Wang and Z. Sun, Recycling of $LiNi_{1/3}Co_{1/3}Mn_{1/3}O_2$ cathode materials from spent lithium-ion batteries using mechanochemical activation and solid-state sintering, *Waste Manage.*, 2019, **84**, 54–63.

130 A. T. Montoya, Z. Yang, E. U. Dahl, K. Z. Pupek, B. Polzin, A. Dunlop and J. T. Vaughey, Direct recycling of lithium-ion battery cathodes: A multi-stage annealing process to recover the pristine structure and performance, *ACS Sustainable Chem. Eng.*, 2022, **10**(40), 13319–13324.

131 Y. Shi, G. Chen, F. Liu, X. Yue and Z. Chen, Resolving the compositional and structural defects of degraded $LiNi_xCo_yMn_zO_2$ particles to directly regenerate high-performance lithium-ion battery cathodes, *ACS Energy Lett.*, 2018, **3**(7), 1683–1692.

132 X. Song, T. Hu, C. Liang, H. L. Long, L. Zhou, W. Song, L. You, Z. S. Wu and J. W. Liu, Direct regeneration of cathode materials from spent lithium iron phosphate batteries using a solid phase sintering method, *RSC Adv.*, 2017, **7**(8), 4783–4790.

133 Q. Liang, H. Yue, S. Wang, S. Yang, K.-h. Lam and X. Hou, Recycling and crystal regeneration of commercial used $LiFePO_4$ cathode materials, *Electrochim. Acta*, 2020, **330**, 135323.

134 C. Xu, K. Märker, J. Lee, A. Mahadevegowda, P. J. Reeves, S. J. Day, M. F. Groh, S. P. Emge, C. Ducati, B. Layla Mehdi, C. C. Tang and C. P. Grey, Bulk fatigue induced by surface reconstruction in layered Ni-rich cathodes for Li-ion batteries, *Nat. Mater.*, 2021, **20**(1), 84–92.

135 M. Guan, P. Lou, G. Xu, K. Zhou, W. Zhang and Q. Cheng, Regeneration for single crystal $LiNi_{0.6}Co_{0.1}Mn_{0.3}O_2$ from spent lithium ion batteries via an innovative approach, *Ionics*, 2023, **29**(1), 97–103.

136 H. Dong, H. Wang, J. Qi, J. Wang, W. Ji, J. Pan, X. Li, Y. Yin and S. Yang, Single-crystal materials regenerated and modified by spent NCM523 as a high-voltage stable cycling cathode material, *ACS Sustainable Chem. Eng.*, 2022, **10**(35), 11587–11596.

137 J. Wang, K. Jia, J. Ma, Z. Liang, Z. Zhuang, Y. Zhao, B. Li, G. Zhou and H.-M. Cheng, Sustainable upcycling of spent $LiCoO_2$ to an ultra-stable battery cathode at high voltage, *Nat Sustainability*, 2023, **6**(7), 797–805.

138 H. Lei, X. Cui, Z. Zeng, C. Zhu, W. Sun, Y. Yang and P. Ge, Directly regenerating of spent $LiCoO_2$ with gradient f-doped subsurface towards ultra-stable storage properties, *Angew. Chem., Int. Ed.*, 2025, **64**(2), e202414918.

139 X. Fan, C. Tan, Y. Li, Z. Chen, Y. Li, Y. Huang, Q. Pan, F. Zheng, H. Wang and Q. Li, A green, efficient, closed-loop direct regeneration technology for reconstructing of the $LiNi_{0.5}Co_{0.2}Mn_{0.3}O_2$ cathode material from spent lithium-ion batteries, *J. Hazard. Mater.*, 2021, **410**, 124610.

140 Y. Cao, J. Li, D. Tang, F. Zhou, M. Yuan, Y. Zhu, C. Feng, R. Shi, X. Wei, B. Wang, Y. Song, H.-M. Cheng and G. Zhou, Targeted defect repair and multi-functional interface construction for the direct regeneration of spent $LiFePO_4$ cathodes, *Adv. Mater.*, 2024, **36**(48), 2414048.

141 G. Ji, J. Wang, Z. Liang, K. Jia, J. Ma, Z. Zhuang, G. Zhou and H.-M. Cheng, Direct regeneration of degraded lithium-ion battery cathodes with a multifunctional organic lithium salt, *Nat. Commun.*, 2023, **14**(1), 584.

142 H. Zhang, Y. Song, J. Zhao, Z. Cheng, J. Guo, M. Cao, H. Yu, H. Wang, L. Qie, L. Yuan, Y. Yao and Y. Huang, Kinetics dominated, interface targeted rapid heating for battery material rejuvenation, *Adv. Energy Mater.*, 2025, **15**(13), 2404838.

143 W. Chen, Y. Cheng, J. Chen, K. V. Bets, R. V. Salvatierra, C. Ge, J. T. Li, D. X. Luong, C. Kittrell, Z. Wang, E. A. McHugh, G. Gao, B. Deng, Y. Han, B. I. Yakobson and J. M. Tour, Nondestructive flash cathode recycling, *Nat. Commun.*, 2024, **15**(1), 6250.

144 Y.-C. Yin, C. Li, X. Hu, D. Zuo, L. Yang, L. Zhou, J. Yang and J. Wan, Rapid, direct regeneration of spent $LiCoO_2$ cathodes for Li-ion batteries, *ACS Energy Lett.*, 2023, **8**(7), 3005–3012.

145 G. Ji, H. Ji, J. Wang, J. Li, N. Zheng, J. Zhao, Y. Zhu, S. Liu, J. Tang, Z. Liang, H.-M. Cheng and G. Zhou, Solid-solution phase engineering enables ultrahigh-rate $LiFePO_4$ regeneration from spent batteries, *Joule*, 2026, **10**(4), 102312.

146 Y. Luo, F. Hu, L. Tian, Q. Liu, Y. Fan, Y. Zhang, Z. Fei, Q. Meng and P. Dong, Efficient direct regeneration of spent $LiFePO_4$ cathodes via molecular fencing and vapor deposition, *Adv. Funct. Mater.*, 2026, **36**(13), e12637.

147 Z. Fei, S. Zhou, Y. Zhang, Q. Meng, P. Dong, Y. Li, J. Fei, H. Qi, J. Yan and X. Zhao, Toward high voltage performance of $LiCoO_2$ cathode materials directly regenerated with a bulk and surface synergistic approach from spent lithium-ion batteries, *ACS Sustainable Chem. Eng.*, 2022, **10**(20), 6853–6862.

148 Y. Han, Y. Fang, M. Yan, H. Qiu, Y. Han, Y. Chen, L. Lin, J. Qian, T. Mei and X. Wang, Direct regeneration of fluorine-doped carbon-coated $LiFePO_4$ cathode materials from spent lithium-ion batteries, *Green Chem.*, 2024, **26**(18), 9791–9801.

149 D. Fang, F. Wu, X. Zhang, X. Zhang, Y. Ye, R. Chen and L. Li, Direct upcycling of degraded $LiCoO_2$ towards high-performance cathodes via a multifunctional organic lithium salt, *Angew. Chem., Int. Ed.*, 2025, **64**(17), e202502176.

150 J. Wu, L. Xiao, P. Liu, Y. Zhu and J. Li, Direct regeneration and upcycling of cathode material from spent lithium ion batteries: Recent advances and perspectives, *Sep. Purif. Technol.*, 2025, **355**, 129574.

151 V. Gupta, X. Yu, H. Gao, C. Brooks, W. Li and Z. Chen, Scalable direct recycling of cathode black mass from spent lithium-ion batteries, *Adv. Energy Mater.*, 2023, **13**(6), 2203093.

152 D.-S. Kim, J.-S. Sohn, C.-K. Lee, J.-H. Lee, K.-S. Han and Y.-I. Lee, Simultaneous separation and renovation of lithium cobalt oxide from the cathode of spent lithium ion rechargeable batteries, *J. Power Sources*, 2004, **132**(1), 145–149.

153 Z. Zhang, W. He, G. Li, J. Xia, H. Hu, J. Huang and S. Zhang, Recovery of lithium cobalt oxide material from the cathode of spent lithium-ion batteries, *ECS Electrochem. Lett.*, 2014, **3**(6), A58.

154 Y. Shi, G. Chen and Z. Chen, Effective regeneration of $LiCoO_2$ from spent lithium-ion batteries: a direct

approach towards high-performance active particles, *Green Chem.*, 2018, **20**(4), 851–862.
155 Y. Wang, H. Yu, Y. Liu, Y. Wang, Z. Chen, D. Tang, W. Li and J. Li, Sustainable regenerating of high-voltage performance $LiCoO_2$ from spent lithium-ion batteries by interface engineering, *Electrochim. Acta*, 2022, **407**, 139863.
156 F. Wu, M. Wang, Y. Su, L. Bao and S. Chen, A novel method for synthesis of layered $LiNi_{1/3}Mn_{1/3}Co_{1/3}O_2$ as cathode material for lithium-ion battery, *J. Power Sources*, 2010, **195**(8), 2362–2367.
157 K. H. Chan, M. Malik and G. Azimi, Direct recycling of degraded lithium-ion batteries of an electric vehicle using hydrothermal relithiation, *Mater. Today Energy*, 2023, **37**, 101374.
158 K. Jia, J. Wang, Z. Zhuang, Z. Piao, M. Zhang, Z. Liang, G. Ji, J. Ma, H. Ji, W. Yao, G. Zhou and H.-M. Cheng, Topotactic transformation of surface structure enabling direct regeneration of spent lithium-ion battery cathodes, *J. Am. Chem. Soc.*, 2023, **145**(13), 7288–7300.
159 P. Xu, Z. Yang, X. Yu, J. Holoubek, H. Gao, M. Li, G. Cai, I. Bloom, H. Liu, Y. Chen, K. An, K. Z. Pupek, P. Liu and Z. Chen, Design and optimization of the direct recycling of spent Li-ion battery cathode materials, *ACS Sustainable Chem. Eng.*, 2021, **9**(12), 4543–4553.
160 H. Liu, M.-J. Choe, R. A. Enrique, B. Orvañanos, L. Zhou, T. Liu, K. Thornton and C. P. Grey, Effects of antisite defects on li diffusion in $LiFePO_4$ revealed by Li isotope exchange, *J. Phys. Chem. C*, 2017, **121**(22), 12025–12036.
161 K.-Y. Park, I. Park, H. Kim, H.-d. Lim, J. Hong, J. Kim and K. Kang, Anti-site reordering in $LiFePO_4$: Defect annihilation on charge carrier injection, *Chem. Mater.*, 2014, **26**(18), 5345–5351.
162 Q. Jing, J. Zhang, Y. Liu, W. Zhang, Y. Chen and C. Wang, Direct regeneration of spent $LiFePO_4$ cathode material by a green and efficient one-step hydrothermal method, *ACS Sustainable Chem. Eng.*, 2020, **8**(48), 17622–17628.
163 B. Chen, M. Liu, S. Cao, H. Hu, G. Chen, X. Guo and X. Wang, Direct regeneration and performance of spent $LiFePO_4$ via a green efficient hydrothermal technique, *J. Alloys Compd.*, 2022, **924**, 166487.
164 P. Xu, Q. Dai, H. Gao, H. Liu, M. Zhang, M. Li, Y. Chen, K. An, Y. S. Meng, P. Liu, Y. Li, J. S. Spangenberger, L. Gaines, J. Lu and Z. Chen, Efficient direct recycling of lithium-ion battery cathodes by targeted healing, *Joule*, 2020, **4**(12), 2609–2626.
165 X. Tang, R. Wang, Y. Ren, J. Duan, J. Li and P. Li, Effective regeneration of scrapped $LiFePO_4$ material from spent lithium-ion batteries, *J. Mater. Sci.*, 2020, **55**(27), 13036–13048.
166 Y. Yang, Z. Liu, J. Zhang, Y. Chen and C. Wang, Economical and low-carbon regeneration of spent $LiFePO_4$ materials by hydrothermal relithiation, *J. Alloys Compd.*, 2023, **947**, 169660.
167 K. Jia, J. Ma, J. Wang, Z. Liang, G. Ji, Z. Piao, R. Gao, Y. Zhu, Z. Zhuang, G. Zhou and H.-M. Cheng, Long-Life regenerated $LiFePO_4$ from spent cathode by elevating the d-band center of Fe, *Adv. Mater.*, 2023, **35**(5), 2208034.
168 X.-X. Zhao, X.-T. Wang, J.-Z. Guo, Z.-Y. Gu, J.-M. Cao, J.-L. Yang, F.-Q. Lu, J.-P. Zhang and X.-L. Wu, Dynamic Li^+ capture through ligand-chain interaction for the regeneration of depleted $LiFePO_4$ cathode, *Adv. Mater.*, 2024, **36**(14), 2308927.
169 T. Wang, H. Luo, Y. Bai, J. Li, I. Belharouak and S. Dai, Direct recycling of spent NCM cathodes through ionothermal lithiation, *Adv. Energy Mater.*, 2020, **10**(30), 2001204.
170 K. Park, J. Yu, J. Coyle, Q. Dai, S. Frisco, M. Zhou and A. Burrell, Direct cathode recycling of end-of-life Li-ion batteries enabled by redox mediation, *ACS Sustainable Chem. Eng.*, 2021, **9**(24), 8214–8221.
171 C. Wu, J. Hu, L. Ye, Z. Su, X. Fang, X. Zhu, L. Zhuang, X. Ai, H. Yang and J. Qian, Direct regeneration of spent Li-ion battery cathodes via chemical relithiation reaction, *ACS Sustainable Chem. Eng.*, 2021, **9**(48), 16384–16393.
172 Y. Liu, H. Yu, Y. Wang, D. Tang, W. Qiu, W. Li and J. Li, Microwave hydrothermal renovating and reassembling spent lithium cobalt oxide for lithium-ion battery, *Waste Manage.*, 2022, **143**, 186–194.
173 N. Zhang, W. Deng, Z. Xu and X. Wang, Upcycling of spent $LiCoO_2$ cathodes via nickel- and manganese-doping, *Carbon Energy*, 2023, **5**(1), e231.
174 S. E. Sloop, L. Crandon, M. Allen, M. M. Lerner, H. Zhang, W. Sirisaksoontorn, L. Gaines, J. Kim and M. Lee, Cathode healing methods for recycling of lithium-ion batteries, *Sustainable Mater. Technol.*, 2019, **22**, e00113.
175 P. Lou, M. Guan, G. Wu, J. Wu, H. Yu, W. Zhang and Q. Cheng, Recycle cathode materials from spent lithium-ion batteries by an innovative method, *Ionics*, 2022, **28**(5), 2135–2141.
176 F. Gao, C. Gou, Z. Geng, M. Yang and J. Zhang, Direct regeneration of spent $LiNi_{0.5}Co_{0.2}Mn_{0.3}O_2$ cathodes with Nb-doped for high-performance lithium-ion batteries, *J. Energy Storage*, 2026, **155**, 121464.
177 Y. Lan, J. Wen, Y. Zhang, X. Lan, T. Song, J. Zhu, J. Peng, W. Yao, Y. Tang and H.-M. Cheng, Direct repair of the crystal structure and coating surface of spent $LiFePO_4$ materials enables superfast Li-ion migration, *Nano-Micro Lett.*, 2026, **18**(1), 137.
178 Z. Jiang, J. Sun, P. Jia, W. Wang, Z. Song, X. Zhao and Y. Mao, A sustainable strategy for spent Li-ion battery regeneration: microwave-hydrothermal relithiation complemented with anode-revived graphene to construct a $LiFePO_4$/MWrGO cathode material, *Sustainable Energy Fuels*, 2022, **6**(9), 2207–2222.
179 W. Song, J. Liu, L. You, S. Wang, Q. Zhou, Y. Gao, R. Yin, W. Xu and Z. Guo, Re-synthesis of nano-structured $LiFePO_4$/graphene composite derived from spent lithium-ion battery for booming electric vehicle application, *J. Power Sources*, 2019, **419**, 192–202.
180 Y. Liu, J. Bai, R. Shi, P. Wang, K. Xiao, S. Wang, S. Qiu, X. Wang, X. Zhu, K. Yang, G. Zhou, B. Zhao and Y. Sun, Direct recycling of degraded $LiFePO_4$ cathode material via natural electron donors healing and targeted surface reconstruction, *Adv. Mater.*, 2026, **38**(1), e11246.

181 X. Li, J. Li, M. Wu, Y. Chen, J. Zhang and M. Tian, Direct regeneration of spent $LiFePO_4$ cathode material via ionic liquids as efficient ion transport media, *Nano Energy*, 2025, **140**, 111014.

182 C. Li, R. Gong, Y. Zhang, Q. Meng and P. Dong, Direct regeneration of degraded $LiFePO_4$ cathode via reductive solution relithiation regeneration process, *Molecules*, 2024, **29**(14), 3340.

183 X. Wu, J. Ma, J. Wang, X. Zhang, G. Zhou and Z. Liang, Progress, key issues, and future prospects for Li-ion battery recycling, *Glob. Chall.*, 2022, **6**(12), 2200067.

184 J. Yang, W. Wang, H. Yang and D. Wang, One-pot compositional and structural regeneration of degraded $LiCoO_2$ for directly reusing it as a high-performance lithium-ion battery cathode, *Green Chem.*, 2020, **22**(19), 6489–6496.

185 G. Gao, Y. Zhu, S. Di, J. Zhao, C. Liu, S. Wang and L. Li, Direct regeneration of spent $LiCoO_2$ cathodes with Ca^{2+}-assisted molten salt strategy, *Acta Mater.*, 2024, **273**, 119969.

186 S. Yan, N. Yao, H. Liu, Z. Zhang, Y. Lu, Z. Liu, W. Hou, P. Zhou, H. Zhou, X. Chen, K. Liu and Q. Zhang, Molten salt electrolytes with enhanced Li^+-transport kinetics for fast-cycling of high-temperature lithium metal batteries, *Energy Environ. Sci.*, 2025, **18**(4), 1696–1706.

187 X. Chen, Y. Feng, S. Zhang, W. Kou, H. Ji and G. Yang, Comparison study on regeneration of spent ternary materials by molten salt solid-liquid method and traditional solid-solid method, *J. Alloys Compd.*, 2022, **900**, 163308.

188 Z. Qin, T. Zhang, X. Gao, W. Luo, J. Han, B. Lu, J. Zhou and G. Chen, Self-reconstruction of highly degraded $LiNi_{0.8}Co_{0.1}Mn_{0.1}O_2$ toward stable single-crystalline cathode, *Adv. Mater.*, 2024, **36**(5), 2307091.

189 G. G. Eshetu, H. Zhang, X. Judez, H. Adenusi, M. Armand, S. Passerini and E. Figgemeier, Production of high-energy Li-ion batteries comprising silicon-containing anodes and insertion-type cathodes, *Nat. Commun.*, 2021, **12**(1), 5459.

190 G. Qian, Z. Li, Y. Wang, X. Xie, Y. He, J. Li, Y. Zhu, S. Xie, Z. Cheng, H. Che, Y. Shen, L. Chen, X. Huang, P. Pianetta, Z.-F. Ma, Y. Liu and L. Li, Value-creating upcycling of retired electric vehicle battery cathodes, *Cell Rep. Phys. Sci.*, 2022, **3**(2), 100741.

191 X. Liu, M. Wang, L. Deng, Y.-J. Cheng, J. Gao and Y. Xia, Direct regeneration of spent lithium iron phosphate via a low-temperature molten salt process coupled with a reductive environment, *Ind. Eng. Chem. Res.*, 2022, **61**(11), 3831–3839.

192 Y. Shi, M. Zhang, Y. S. Meng and Z. Chen, Ambient-pressure relithiation of degraded $Li_xNi_{0.5}Co_{0.2}Mn_{0.3}O_2$ ($0<x<1$) via eutectic solutions for direct regeneration of lithium-ion battery cathodes, *Adv. Energy Mater.*, 2019, **9**(20), 1900454.

193 S. Jayaraman, A. P. Thompson and O. A. von Lilienfeld, Molten salt eutectics from atomistic simulations, *Phys. Rev. E:Stat., Nonlinear, Soft Matter Phys.*, 2011, **84**(3), 030201.

194 J. Ma, J. Wang, K. Jia, Z. Liang, G. Ji, Z. Zhuang, G. Zhou and H.-M. Cheng, Adaptable eutectic salt for the direct recycling of highly degraded layer cathodes, *J. Am. Chem. Soc.*, 2022, **144**(44), 20306–20314.

195 H. Yang, B. Deng, X. Jing, W. Li and D. Wang, Direct recovery of degraded $LiCoO_2$ cathode material from spent lithium-ion batteries: Efficient impurity removal toward practical applications, *Waste Manage.*, 2021, **129**, 85–94.

196 B. Deng, Z. Zhou, W. Wang and D. Wang, Direct recovery and efficient reutilization of degraded ternary cathode materials from spent lithium-ion batteries via a homogeneous thermochemical process, *ACS Sustainable Chem. Eng.*, 2020, **8**(37), 14022–14029.

197 G. Jiang, Y. Zhang, Q. Meng, Y. Zhang, P. Dong, M. Zhang and X. Yang, Direct regeneration of $LiNi_{0.5}Co_{0.2}Mn_{0.3}O_2$ cathode from spent lithium-ion batteries by the molten salts method, *ACS Sustainable Chem. Eng.*, 2020, **8**(49), 18138–18147.

198 J. Yan, Y. Xia, S. Lin, Y. Du, Z. Zhou, J. Li and G. Yue, Direct regeneration of spent $LiNi_{0.5}Co_{0.2}Mn_{0.3}O_2$ cathodes by utilizing eutectic lithium salts for high-performance lithium-ion batteries, *Coatings*, 2026, **16**(1), 107.

199 Z. Qin, Z. Wen, Y. Xu, Z. Zheng, M. Bai, N. Zhang, C. Jia, H. B. Wu and G. Chen, A ternary molten salt approach for direct regeneration of $LiNi_{0.5}Co_{0.2}Mn_{0.3}O_2$ cathode, *Small*, 2022, **18**(43), 2106719.

200 T. Wang, H. Luo, J. Fan, B. P. Thapaliya, Y. Bai, I. Belharouak and S. Dai, Flux upcycling of spent NMC 111 to nickel-rich NMC cathodes in reciprocal ternary molten salts, *iScience*, 2022, **25**(2), 103801.

201 X. Ma, J. Hou, P. Vanaphuti, Z. Yao, J. Fu, L. Azhari, Y. Liu and Y. Wang, Direct upcycling of mixed Ni-lean polycrystals to single-crystal Ni-rich cathode materials, *Chem*, 2022, **8**(7), 1944–1955.

202 C. Xing, H. Da, P. Yang, J. Huang, M. Gan, J. Zhou, Y. Li, H. Zhang, B. Ge and L. Fei, Aluminum impurity from current collectors reactivates degraded ncm cathode materials toward superior electrochemical performance, *ACS Nano*, 2023, **17**(3), 3194–3203.

203 X. Liu, R. Wang, S. Liu, J. Pu, H. Xie, M. Wu, D. Liu, Y. Li and J. Liu, Organic eutectic salts-assisted direct lithium regeneration for extremely low state of health Ni-rich cathodes, *Adv. Energy Mater.*, 2023, **13**(44), 2302987.

204 Y. He, K. Jia, Z. Piao, Z. Cao, M. Zhang, P. Li, Z. Li, Z. Jiang, G. Yang, H. Xi, G. Zhou, W. Tang, Z. Qu, R. V. Kumar, S. Ding and K. Xi, Li^+ quasi-Grotthuss topochemistry transport enables direct regeneration of spent lithium-ion battery cathodes, *Angew. Chem., Int. Ed.*, 2025, **64**(13), e202422610.

205 J. Asenbauer, T. Eisenmann, M. Kuenzel, A. Kazzazi, Z. Chen and D. Bresser, The success story of graphite as a lithium-ion anode material–fundamentals, remaining challenges, and recent developments including silicon (oxide) composites, *Sustainable Energy Fuels*, 2020, **4**(11), 5387–5416.

206 R. J. Robin, Viability and eco-consequences of synthetic and natural graphite for li-ion battery anodes in the US, *IEEE Eng. Manag. Rev.*, 2024, 1–16.
207 S. Natarajan and V. Aravindan, Burgeoning prospects of spent lithium-ion batteries in multifarious applications, *Adv. Energy Mater.*, 2018, **8**(33), 1802303.
208 J. Wang, J. Ma, K. Jia, Z. Liang, G. Ji, Y. Zhao, B. Li, G. Zhou and H.-M. Cheng, Efficient extraction of lithium from anode for direct regeneration of cathode materials of spent Li-ion batteries, *ACS Energy Lett.*, 2022, **7**(8), 2816–2824.
209 W. Chen, R. V. Salvatierra, J. T. Li, C. Kittrell, J. L. Beckham, K. M. Wyss, N. La, P. E. Savas, C. Ge, P. A. Advincula, P. Scotland, L. Eddy, B. Deng, Z. Yuan and J. M. Tour, Flash recycling of graphite anodes, *Adv. Mater.*, 2023, **35**(8), 2207303.
210 Q. Chen, L. Huang, J. Liu, Y. Luo and Y. Chen, A new approach to regenerate high-performance graphite from spent lithium-ion batteries, *Carbon*, 2022, **189**, 293–304.
211 H. Da, M. Gan, D. Jiang, C. Xing, Z. Zhang, L. Fei, Y. Cai, H. Zhang and S. Zhang, Epitaxial regeneration of spent graphite anode material by an eco-friendly in-depth purification route, *ACS Sustainable Chem. Eng.*, 2021, **9**(48), 16192–16202.
212 D. Liu, X. Qu, B. Zhang, J. Zhao, H. Xie and H. Yin, Alkaline roasting approach to reclaiming lithium and graphite from spent lithium-ion batteries, *ACS Sustainable Chem. Eng.*, 2022, **10**(18), 5739–5747.
213 C. Yuwen, B. Liu, H. Zhang, S. Tian, L. Zhang, S. Guo and B. Zhou, Efficient recovery and regeneration of waste graphite through microwave stripping from spent batteries anode for high-performance lithium-ion batteries, *J. Clean. Prod.*, 2022, **333**, 130197.
214 X. Ma, M. Chen, B. Chen, Z. Meng and Y. Wang, High-performance graphite recovered from spent lithium-ion batteries, *ACS Sustainable Chem. Eng.*, 2019, **7**(24), 19732–19738.
215 B. Markey, M. Zhang, I. Robb, P. Xu, H. Gao, D. Zhang, J. Holoubek, D. Xia, Y. Zhao, J. Guo, M. Cai, Y. S. Meng and Z. Chen, Effective upcycling of graphite anode: healing and doping enabled direct regeneration, *J. Electrochem. Soc.*, 2020, **167**(16), 160511.
216 M. Bhar, S. Ghosh, S. Krishnamurthy, K. Yalamanchili and S. K. Martha, Electrochemical compatibility of graphite anode from spent li-ion batteries: recycled via a greener and sustainable approach, *ACS Sustainable Chem. Eng.*, 2022, **10**(23), 7515–7525.
217 N. Cao, Y. Zhang, L. Chen, W. Chu, Y. Huang, Y. Jia and M. Wang, An innovative approach to recover anode from spent lithium-ion battery, *J. Power Sources*, 2021, **483**, 229163.
218 Y. Gao, C. Wang, J. Zhang, Q. Jing, B. Ma, Y. Chen and W. Zhang, Graphite recycling from the spent lithium-ion batteries by sulfuric acid curing–leaching combined with high-temperature calcination, *ACS Sustainable Chem. Eng.*, 2020, **8**(25), 9447–9455.
219 F. Hanna, C. Somers and A. Anctil, Life cycle assessment of lithium-ion battery recycling: Evaluating the impact of recycling methods and location, *Environ. Sci. Technol.*, 2025, **59**(28), 14432–14443.
220 S. Sharifian, S. Nikfar, C. Subasinghe, Z. Iranmanesh, M. Rezaee and E. Vahidi, Conventional vs. direct vs. electrochemical lithium extraction: A holistic TEA-LCA of lithium carbonate production from spodumene, *Green Chem.*, 2026, **28**(2), 1144–1157.
221 J. Lin, W. Li and Z. Chen, Scaling direct recycling of lithium-ion batteries toward industrialization: Challenges and opportunities, *ACS Energy Lett.*, 2025, **10**(2), 947–957.